Lithospheric Structure of the West and Central African Rift Zone

Dissertation

zur Erlangung des akademischen Grades
eines Doktors der Naturwissenschaften (Dr. rer. nat.)
der Mathematisch-Naturwissenschaftlichen Fakultät
der Christian-Albrechts-Universitat zu Kiel

vorgelegt von

Estelle Eric Fosso Téguia Moussé

Kiel, January 2024

Erster Gutachter: Prof. Dr. Jörg Ebbing
Zweiter Gutachter: Prof. Dr. Carla Braitenberg
Tag der mundlichen Prufung: 28.02.2025
Zum Druck genehmigt:

Der Dekan

Erklärung

Diese Arbeit ist, abgesehen von der Beratung durch meinen Betreuer und die Zuhilfenahme der angegebenen Mittel, nach Inhalt und Form meine eigene. Die Arbeit hat weder ganz noch zum Teil bereits an anderer Stelle im Rahmen eines Prüfungsverfahrens vorgelegen. Die Arbeit wurde weder veröffentlicht noch zur Veröffentlichung eingereicht. Die Arbeit ist unter Einhaltung der Regeln guter wissenschaftlicher Praxis der Deutschen Forschungsgemeinschaft entstanden. Ich versichere, dass mir noch kein akademischer Grad entzogen wurde. Mit dieser Arbeit strebe ich die Erlangung des akademischen Grades Doktor der Naturwissenschaften (Dr. rer. nat.) an.

Ort, Datum

Estelle Eric Fosso Téguia Moussé

"If you differ from me, my brother, far from harming me, you enrich me." Antoine de Saint-Exupéry

Abstract

The West and Central African Rift System (WCARS) is a geologically complex and dynamic region that provides unique opportunities to investigate the processes of continental rifting, magmatism, and lithosphere evolution. This thesis aims to unravel key aspects of the WCARS by integrating geophysical, petrological, and thermal datasets to examine its lithospheric architecture, crustal structure, and thermal regime. Four primary research questions guide this work: (1) The key lithospheric and crustal structures that define the WCARS, and the how do these structures reflect the interplay of tectonic inheritance, rifting, and magmatism, (2) the question of the origin of the Cameroon Volcanic Line (CVL), (3) the question of the origin of the Bangui Magnetic Anomaly (BMA), and the how are these two structure linked to regional tectonic and magmatic evolution, and (4) how do surface heat flow variations across the WCARS relate to crustal composition, radiogenic heat production, and magmatic processes?

The study begins by constructing a comprehensive 3D lithospheric model of the WCARS, utilizing gravity, seismic, and petrological data to delineate variations in lithospheric thickness and composition. The results confirm the passive origin of the WCARS, reveal significant heterogeneity in lithospheric architecture, with crustal thickness ranging from 25 km in rift zones to over 50 km beneath cratonic regions, and lithospheric thickness varying from 70 km in the Benue trough to 250 km beneath the cratons. Transitional zones between Phanerozoic and Proterozoic lithosphere are identified, underscoring the role of tectonic inheritance in guiding rift development and lithospheric evolution.

Based on my model results, I attribute the origin of the CVL to edge-driven convection beneath the lithospheric mantle caused by the V-shaped opening of the WCARS. This process likely created magma chambers aligned with pre-existing lithospheric weaknesses, highlighting the critical interplay between mantle dynamics and tectonic inheritance in shaping these features. The origin of the BMA is explored through detailed crustal modeling based on gravity and magnetic field data. The findings suggest that the BMA results from felsic and plutonic intrusions created during Mesozoic rifting, that carry strong remnant magnetization.

Surface heat flow variations across the WCARS are investigated by integrating radiogenic heat production data into thermal models. The results demonstrate that heat flow anomalies are closely linked to lithospheric thinning, magmatic intrusions, and crustal heterogeneity. Elevated heat flow values are measured in rift zones such as the Benue trough and CVL, where magmatic processes and radiogenic heat production contribute to the thermal regime.

In contrast, lower heat flow values are associated with stable cratonic regions, reflecting their thick and thermally insulating lithospheric roots. These findings provide critical insights into the region's thermal structure.

This thesis makes significant contributions to the understanding of the WCARS by elucidating its lithospheric and crustal architecture, identifying the origins of major geophysical anomalies, and refining the thermal model of the region. The results underscore the importance of integrating geophysical and petrological datasets to address complex geodynamic questions. Furthermore, the findings have broader implications for the study of rift systems worldwide, offering new perspectives on the processes governing lithospheric modification, intra-plate volcanism, and continental rifting.

Zusammenfassung

Das West- und Zentralafrikanische Riftsystem (WCARS) ist eine geologisch komplexe und dynamische Region, die eine einzigartige Gelegenheit bietet, die Prozesse der kontinentalen Riftbildung, des Magmatismus und der Lithosphärenentwicklung zu untersuchen. Diese Dissertation zielt darauf ab, zentrale Aspekte des WCARS zu entschlüsseln, indem geophysikalische, petrologische und thermische Datensätze integriert werden, um dessen litho–sphärische Architektur, Krustenstruktur und thermisches Regime zu analysieren. Vier zentrale Forschungsfragen leiten diese Arbeit: (1) Welche wichtigen litho–sphärischen und krustalen Strukturen definieren das WCARS, und wie spiegeln diese Strukturen das Zusammenspiel von tektonischem Erbe, Riftbildung und Magmatismus wider? (2) Was ist der Ursprung der 'Cameroon Volcanic Line' (CVL)? (3) Was ist der Ursprung der "Bangui Magnetic Anomaly" (BMA), und wie sind diese beiden Strukturen mit der regionalen tektonischen und magmatischen Entwicklung verbunden? (4) Wie hängen Schwankungen des geothermischen Wärme–fluss im WCARS mit der Krusten–zusammensetzung, der radiogenen Wärmeproduktion und magmatischen Prozessen zusammen?

Die Untersuchung beginnt mit der Konstruktion eines umfassenden 3D-Lithosphärenmodells des WCARS, das Schwerefeld-, seismische und petrologische Daten verwendet, um Variationen in der Dicke und Zusammensetzung der Lithosphäre vorherzusagen. Die Ergebnisse bestätigen, dass das WCARS passiven Ursprungs ist und zeigen eine erhebliche Heterogenität der Lithosphäre: Die Mächtigkeit der Kruste reicht von 25 km in Riftzonen bis zu über 50 km unter kratonischen Regionen, während die Tiefe der Lithosphären-Asthenosphärengrenze zwischen 70 km im Benue-Trog 250 km unter den Kratonen schwankt. Übergangszonen zwischen phanerozoischer und proterozoischer Lithosphäre konnten mithilfe der Modellierung identifiziert werden, was die Rolle des tektonischen Erbes bei der Steuerung der Rift- und Lithosphärenentwicklung unterstreicht.

M.E. wurde die CVL durch 'edge-driven convection' ("randgetriebene Konvektion") erzeugt, die durch die V-förmige Öffnung des WCARS verursacht hervorgerufen wurde. Dieser Prozess führte wahrscheinlich zur Bildung von Magmakammern entlang bestehender litho–sphärischer Schwächezonen, was wiederum das Zusammenspiel von Manteldynamik und tektonischem Erbe für die Ausprägung der Strukturen im Gebiet des WCARS unterstreicht. Ich untersuche den Ursprung der BMA mithilfe detaillierter Krustenmodelle, die auf Daten des Schwere- und Magnetfeldes basieren. Die Ergebnisse legen nahe, dass die BMA aus felsischen

und plutonischen Intrusionen während des Riftings im Mesozoikum resultiert, wobei diese Intrusionen wahrscheinlich stark remanent magnetisiert sind.

Die Verteilung des geothermischen Wärmefluss im WCARS wurde mit thermischen Modellen untersucht, wobei Daten über die Verteilung radiogener Wärmeproduktion in die Analyse einbezogen wurden. Die Ergebnisse zeigen, dass Wärmeflussanomalien eng mit Schwankungen der Lithosphärenmächtigkeit, magmatischen Intrusionen und krustaler Heterogenität verbunden sind. Erhöhte Wärmeflusswerte wurden in Riftzonen wie dem Benue-Trog und der CVL beobachtet, wo magmatische Prozesse und radiogene Wärmeerzeugung zum thermischen Regime beitragen. Im Gegensatz dazu tritt reduzierter Wärmefluss in stabilen kratonischen Regionen auf, da die lithosphärische Wurzel eine isolierende Wirkung hat. Diese Ergebnisse liefern wichtige Einblicke in die thermische Struktur der Region.

Diese Dissertation leistet einen bedeutenden Beitrag zum Verständnis des WCARS, indem sie dessen lithosphärische und krustale Architektur entschlüsselt, die Ursprünge bedeutender geophysikalischer Anomalien identifiziert und das thermische Modell der Region verfeinert. Die Ergebnisse unterstreichen die Bedeutung der Integration geophysikalischer und petrologischer Datensätze, um komplexe geodynamische Fragestellungen zu beantworten. Darüber hinaus haben die Ergebnisse weitreichendere Implikationen für das Studium von Riftsystemen weltweit, da sie neue Perspektiven auf die Prozesse bieten, die die Modifikation der Lithosphäre, intrakontinentalen Vulkanismus und kontinentale Riftbildung steuern.

Contents

1 Introduction

The West and Central African Rift System (WCARS) is a geologically significant region that exemplifies the complex interplay of tectonic, magmatic, and thermal processes involved in continental rifting. Spanning from the Gulf of Guinea to the Central African Republic, the WCARS encompasses diverse geological structures, including the Benue Trough, the Cameroon Volcanic Line (CVL), and the enigmatic Bangui Magnetic Anomaly (BMA) (Guiraud et al. 1992, Fairhead 2023). Bordered by the stable West African Craton to the west and the Congo Craton to the south, the WCARS provides a unique natural laboratory for investigating lithospheric deformation, magmatic processes, and the thermal evolution of rift systems.

The WCARS's formation and evolution are closely tied to the breakup of the Gondwana supercontinent during the Late Jurassic to Early Cretaceous. This tectonic event initiated extensional forces that led to the development of sedimentary basins, volcanic chains, and shear zones, creating a geodynamically complex region. Key rift segments include the Benue Trough, the Chad Basin, and the shear zones such as the Central African Shear Zone (CASZ) and Kandi Shear Zone (KSZ). The sedimentary basins within the WCARS are primarily filled with Mesozoic to Cenozoic sediments, deposited during periods of rifting and subsidence, further underscoring the region's dynamic history (Burke 1976; Fairhead & Green 1989).

The CVL, a linear volcanic chain extending from the Atlantic Ocean to the continental interior, is a prominent feature of the WCARS. It represents an exceptional geological phenomenon whose origin remains a subject of debate. Similarly, the BMA, one of the world's most prominent magnetic anomalies, has been linked to deep-seated tectono-magmatic processes and ancient lithospheric structures (Fairhead & Binks 1991, Girdler et al. 1992).

The rifting processes that shaped the WCARS were heavily influenced by pre-existing structural weaknesses in the Precambrian basement. These inherited structures localized the development of rift zones, facilitating the formation of deep basins and widespread volcanic activity during the Cretaceous (Fairhead & Green 1989, Guiraud et al. 1992). The extensional tectonics accompanying the breakup of Gondwana resulted in significant lithospheric thinning, crustal deformation, and magmatic intrusions. These processes have left a lasting imprint on the thermal and mechanical properties of the lithosphere, as evidenced by high

heat flow and crustal thinning in the rift basins (Djomani et al. 1995).
Geophysical studies using seismic, gravity, and magnetic datasets have revealed the WCARS's intricate crustal and lithospheric architecture. These investigations have highlighted lateral heterogeneities in crustal thickness, density, and magnetic susceptibility, underscoring the complexity of the region's tectonic and magmatic history (Tokam et al. 2010, Eyike & Ebbing 2015, Ghomsi et al. (2022)).

Despite the wealth of research on the WCARS, significant knowledge gaps remain regarding its origin, its evolution and its current architecture. For instance, the origin and evolution of the enigmatic CVL remain topics of ongoing debate, while the origin of the BMA is still uncertain between hypotheses ranging from meteoric impact, ancient tectonic processes to Mesozoic rifting-related magmatism.
Another critical aspect of the WCARS that warrants further investigation in surface heat flow. The spatial distribution of heat flow across tectonic units provides valuable insights into the lithospheric structure, thermal evolution, and geodynamic processes. However, the West and Central African region remains underexplored in terms of heat flow studies, limiting our understanding of its geothermal potential and magmatic activity.

Understanding the WCARS requires a multidisciplinary approach, as its geological complexity cannot be captured by a single method. Previous studies, as I will outline in Chapter 3 and 4, have employed geophysical techniques, such as gravity, magnetic, and seismic surveys, to investigate its crustal and lithospheric structure. However, these efforts have often been limited in scope, failing to integrate datasets at a regional scale. This thesis addresses this gap combining geophysical and petrological data to build detailed 3D models, at the lithospheric then at the crustal scales, that elucidate the region's tectonic and geodynamic history.

2 Motivation, Research Questions and Structure of the Thesis

2.1 Motivations

The West and Central African Rift System (WCARS) is a fascinating geological domain where the interplay of tectonic inheritance, magmatic processes, and lithospheric dynamics can be studied in detail. Despite its geological significance, this region remains underexplored compared to other major rift systems like the East African Rift. The WCARS is characterized by unique features such as the Cameroon Volcanic Line (CVL), the Benue Trough, and the enigmatic Bangui Magnetic Anomaly (BMA). These structures offer unparalleled opportunities to study the processes of continental rifting, mantle dynamics, and crustal evolution.

Understanding Lithospheric and Crustal Structure: While prior studies have highlighted the role of pre-existing structures in guiding rift development, the detailed composition and density variations within the lithosphere and crust remain poorly known. Investigating these parameters is essential for understanding the forces driving rift propagation and magmatism.

Unraveling Origins of the CVL and the BMA: The BMA is one of the most prominent magnetic anomalies globally. Despite its significance, its origin as well as the CVL origin remain ambiguous, then still debated. Addressing this uncertainty is critical for understanding the region's tectonic history.

Exploring Surface Heat Flow Variations: Surface heat flow is a key indicator of lithospheric thermal state and magmatic activity. However, the WCARS remains underexplored in terms of heat flow measurements and modeling. Refining our understanding of heat flow distributions will shed light on regional geothermal gradients and magmatic processes.

2.2 Research Questions

This thesis is guided by four primary research questions:

What are the key lithospheric and crustal structures that define the WCARS, and how do

these structures reflect the interplay of tectonic inheritance, rifting, and magmatism?
Approach to Answer: This question will be addressed by integrating gravity, seismic, and petrological datasets to develop a 3D lithospheric model. The focus will be on identifying lateral variations in density, compositional heterogeneity, and crustal thickness.

What is the origin of the CVL, and how is it linked to the tectonic and magmatic evolution of the region? Approach to Answer: This question will be also addressed after integrating gravity, seismic, and petrological datasets to develop a 3D lithospheric model. The focus will be on identifying interactions between geological structure and the role plays by each of them.

What is the origin of the Bangui Magnetic Anomaly, and how is it linked to the tectonic and magmatic evolution of the region?
Approach to Answer: This question will be answered by constructing a detailed crustal model using magnetic and gravity data. Density and magnetic susceptibility distributions will be analyzed to characterize the anomaly's source and its relationship with regional tectonic structures.

How do surface heat flow variations across the WCARS relate to crustal composition, radiogenic heat production, and magmatic processes?
Approach to Answer: This question will be explored by integrating radiogenic heat production data with thermal models. Surface heat flow variations will be correlated with crustal heterogeneity and geological structures to enhance our understanding of the regional evolution.

2.3 Structure of the Thesis

The research question will be addressed in the following three chapters, each contributing to a cohesive exploration of the WCARS: Chapter 3 is already published, Chapter 4 is submitted for publication, and Chapter 5 is in a draft manuscript.
Chapter 3, focuses on lithospheric modeling by integrating seismic, gravity, and petrological data to develop a comprehensive 3D model of the WCARS. My contribution to this paper includes codes writing, data curation, investigation, formal analysis, writing original draft and editing.
Fosso Téguia M, E. E., Ebbing, J., Haas, P., and Szwillus, W. (2024). Integrated Geophysical-Petrological 3D Modeling of the West and Central African Rift System and Its Adjoining Areas. Journal of Geophysical Research: Solid Earth, 129(7), e2024JB029226. https://doi.org/10.1029/2024JB029226

Chapter 4: Investigates the crustal architecture, with a particular emphasis on understanding the origin of the BMA through density and magnetic susceptibility modeling. My contri-

bution to this paper includes codes writing, data curation, investigation, formal analysis, writing original draft and editing.

Fosso Téguia M, E. E., Ebbing, J., Eyike A., Tokam A., Nana, G. V., Tankersley M. Crustal modelling across the west and central African rift system, based on gravity, magnetic and seismic data - Implications for the origin of the Bangui magnetic anomaly. Submitted in Tectonophysics Journal

Chapter 5: Explores surface heat flow variations across the WCARS, linking thermal anomalies to crustal heterogeneity, magmatic processes, and radiogenic heat production. Title: Surface Heat Flow Variations across the West and Central African Rift System.

3 Integrated geophysical-petrological 3D-modelling of the West and Central African Rift System and its adjoining areas

Estelle Eric Fosso Téguia M.; Jörg Ebbing; Peter Haas; Wolfgang, Szwillus
Journal of Geophysical Research: Solid Earth, 129, e2024JB029226.
https://doi.org/10.1029/2024JB029226

Abstract

This study addresses the lithospheric structure of the West and Central African rift system (WCARS) and explores its origin and development in relation to the enigmatic Cameroon volcanic line (CVL). Based on a recent seismic tomography model, we subdivide the areas in tectonic domains. We perform integrated 3D geophysical and petrological forward modeling. By exploring the thickness and composition of different domains, we compare the model response to the observed topography and gravity anomalies, under consideration of the available seismic Moho depth points.

Our model reveals three distinct domains within the study area: The WCARS is predominantly underlain by a Phanerozoic-type lithospheric mantle, surrounded by the West African and the Congo Cratons, where the lithospheric mantle has a Proterozoic-type signature. Between these domains, we identify a transition area where lithospheric thickness changes

rapidly. Our preferred model shows significant variability of crustal thickness from 20 km in the rift area to 50 km beneath the cratons accompanied by thin lithosphere of 80 km in the rift area to thick lithosphere of up to 240 km beneath the cratons.
The final model confirms that the WCARS' origin is passive, and suggests that the origin of the CVL, particularly its continental part, is the result of two tectonic events: (1) V-shaped opening of the lithospheric mantle beneath the West and Central African rift system, resulting in (2) a strong variation of the lithosphere thickness at the transition between the rift zone and the northwestern part of the Congo craton.

Plain Language Summary

In this study, we describe the current structure of the subsurface (from the surface to a depth of 300 km) in Central and Western Africa. The aim is to understand the formation of the Central African Rift zone during the opening of the Atlantic Ocean, and how this relates to the linear chain of volcanoes that cross Cameroon, known as the Cameroon Volcanic Line.
To achieve these objectives, we divide the study area into tectonic domains reflecting their seismological signature, and then, establish a three-dimensional representation of the subsurface structure, based on fitting topography and gravity data. Our model confirms the geological subdivision of the study area into three blocks corresponding to two cratons and a rift zone, with transitional areas between them.
Our model is compatible with a passive origin of the rifts in the region. We propose that the origin of the volcanic line of Cameroon is related to magma ascent during the separation of the African and South American plate in connection with the opening of the Atlantic and channeled by the lithospheric architecture.

3.1 Introduction

Since the Proterozoic, the African continent has experienced a long and complex geodynamic history with various geological processes contributing to the current lithospheric architecture. The tectonic activity has been centered around three major rift systems: the East African Rift System (EARS), the West African Rift System (WARS), and the Central African Rift System (CARS). Although there is a junction area between the CARS and the EARS at the Gregory Rift in eastern Africa, the EARS seems not to be connected to the two others: The Cenozoic EARS is a younger and less mature rift system compared to the Mesozoic CARS and WARS (Globig et al. 2016), and it is also well known as an active rift system resulting from the ongoing separation of the African and Arabian plates. For the CARS and WARS, the origin after the break-up of the Gondwana supercontinent during Jurassic-Cretaceous times is still debated (Schull 1988; Bosworth 1992; Fairhead 2023; etc.). These are often

jointly referred to as the West and Central African Rift System (WCARS), a large scale tectonic feature distinctive in the sense that it traverses the entire continent from west to the east and from the centre to the north of the continent. It adjoins the northern border of the Congo craton, the eastern border of the West African craton, and spans across parts of the Sahara meta craton (SMC). Consequently, unveiling the lithospheric strcture of the WCARS (Figure 1) is a key element in understanding the geodynamic history of the African continent since the Mesozoic. How the WCARS relates to the Cameroon volcanic line (CVL) also remains enigmatic, despite multiple studies dedicated to its origin (Elsheikh et al. 2014; Koch et al. 2012; Milelli et al. 2012; King & Ritsema 2000; etc.).
Our study examines the origin and evolution of the WCARS and the CVL. For that we investigate the lithospheric structure of the WCARS by applying integrated geophysical and petrological 3D modeling. Hereby, several existing regional and local data sets are utilized. As preparation for the modeling, seismic tomography data is used in a cluster analysis to define tectonic domains in the lithospheric mantle. These tectonic domains are considered in the 3D forward modelling to define composition and temperature of the lithospheric mantle.

3.2 Earlier geophysical studies

In the past, a number of geophysical and geodynamic studies have been addressing the origin and the evolution of the WCARS (Schull 1988; Bosworth 1992; Fairhead 2023; etc.). In one of the earliest studies, based on the interpretation of gravity and seismological data, Fairhead (1986) showed that although both WCARS and EARS have appeared after extensional tectonics, they exhibit significant tectonic disparities: the EARS experiences uplift and is characterized by volcanic activity, while the WCARS underwent subsidence and is marked by sediment deposition.
Most of the subsequent studies agreed that the WCARS is a passive rift system, closely related to the extensional rift basin model of McKenzie (1978). Taking into consideration the thinning of its crust and its early geological development, it seems that the WCARS shows a closer association with the breakup of the Gondwana supercontinent rather than the EARS (Fairhead 1988). In support of that concept, Guiraud et al. (1992) concluded that the Early Cretaceous to Paleogene development of the WCARS is linked to the build-up of intraplate extensional stresses during the break-up of Gondwana, which caused reactivation of pre-existing zones of lithospheric weakness. A recent study by Fairhead (2023) confirms this idea, since there is no active upper mantle process detected so far beneath the region.
But even though most of these studies describe the WCARS as a passive rift in contrast to the active EARS, the question of its origin and evolution remains challenging due to the presence of the enigmatic CVL. Somewhat contradictory to the statement by Fairhead (2023), others studies like Plomerova et al. (1993) based on seismology, Burke (2001) and Asaah et al. (2015) based on geochemistry, suggest that parts of the WCARS have been affected by active asthenospheric processes, particular in the area of the CVL. This is sup-

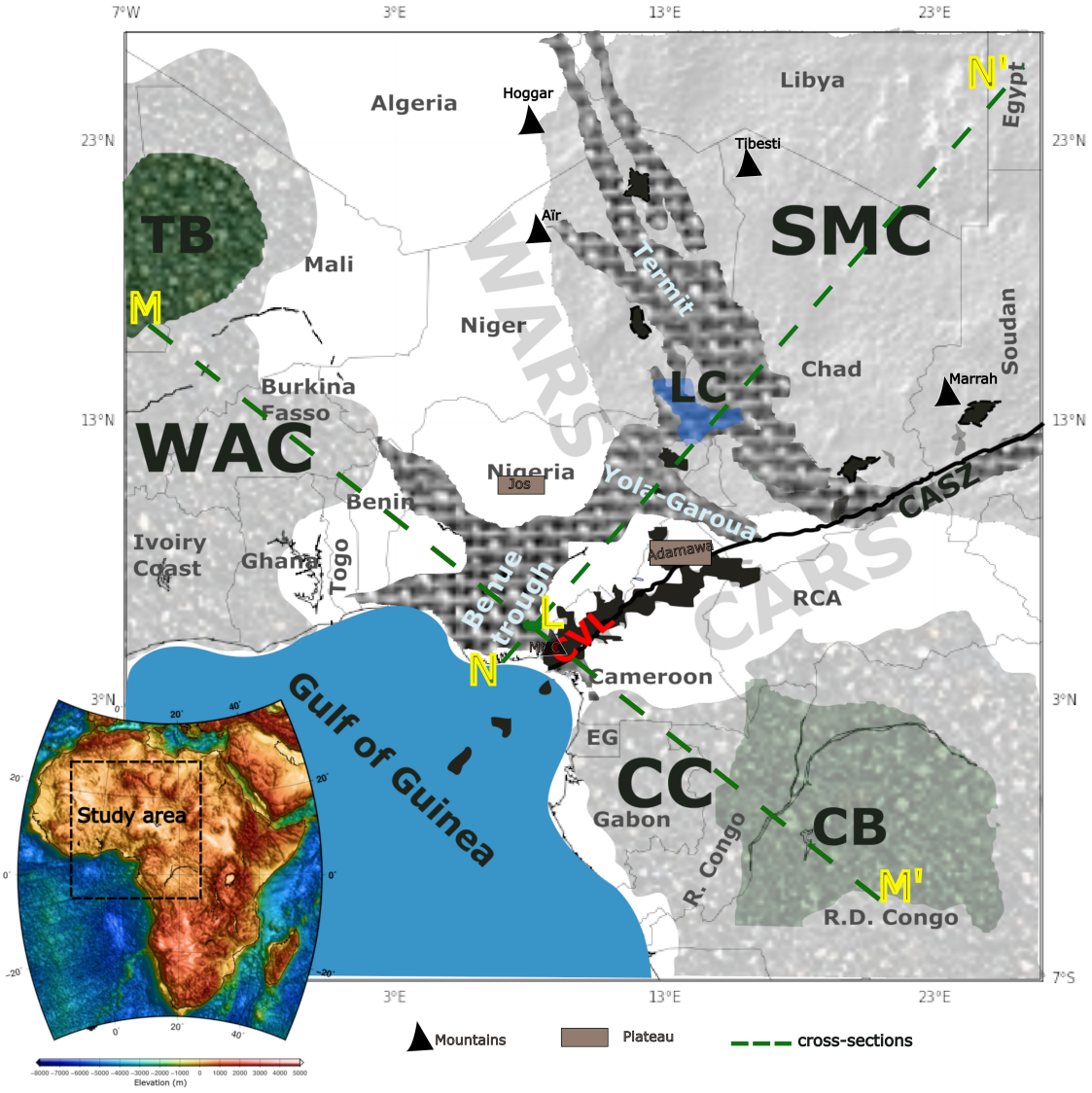

Figure **3-1**: Simplified tectonic map of the study area. WAC: West African craton, CC: Congo craton, CB: Congo basin, TB: Taoudeni basin, SMC: Sahara meta craton, LC: Lake Chad, CASZ: Central African shear zone, CVL: Cameroon volcanic line, WARS: West African rift system, CARS: Central African rift system. MM' and NN' are the cross sections we will display from the final model, and L their intersection.

ported by three observations: First, 140 Ma ago the CVL was positioned directly above the "711" plume (711 indicates latitude 7°N and longitude 11.5°E); second, the site moved at a right angle to the continental margin and remained in this position for almost 125 Ma, and third, a new plate-wide pattern of shallow-mantle convection was established when the African plate came to rest, as suggested as well from seismic anisotropy (Koch et al. 2012). However, the absence of a discernible chronological pattern of volcanism (De Plaen et al. 2014) would rule out a simple stationary mantle plume. Furthermore, the CVL exhibited active volcanism occurring over an extended period of time (66 Ma), but with a relatively low plume volume flux, indeed much smaller than for any of the accepted plumes (e.g., Hawaii) (Kolínskỳ et al. 2020). Hence, there is still no ultimate agreement on the mechanisms responsible for the formation of the CVL.

Precise knowledge of the lithospheric structure would help to understand the formation of the WCARS and deduce the origin of the CVL. Several studies based on different seismic techniques were conducted to describe the current condition of the lithospheric structure over the WCARS. Fitton (1980) suggested a connection between the CVL and the Benue trough, while Stuart et al. (1985) presented seismic crustal depth variations between the CVL and the Benue trough and deduced that the differences over the WCARS could be attributed to substantial crustal extension. Moreover, an examination of the crustal composition beneath the CVL and adjoining areas, utilizing models based on shear wave velocity, reveals interesting insights. It appears that the crustal thickness is comparable (ranging from 35 to 39 km) beneath both the CVL and the Pan African Oubanguides Belt in the south. However, a notable variation occurs in the northern margin of the Congo Craton, where the crust is significantly thicker (measuring between 43 and 48 km) and characterized by shear wave velocities greater than 4.0 km s^{-1} in the lower crust. In contrast, the Garoua rift at the northern border of the CVL and the coastal plain exhibit a thinner crust, measuring between 26 and 31 km (Tokam et al. 2010). Unfortunately, the region is still lacking complete seismic data coverage (Szwillus et al. (2019)), making these conclusions somewhat incomplete.
Various studies based on potential methods have also been done to describe the structure of the WCARS, notably, gravity data constrained by available seismic Moho depths have been used to determine crustal thickness (Eyike & Ebbing 2015; Ghomsi et al. 2022). However, the studies mentioned above solely focused on the crustal structure of the WCARS but do not consider the influence of the lithospheric mantle, which plays a crucial role in affecting observable signals such as the gravity field (Afonso et al. 2008).
On the scale of the African continent, Globig et al. (2016) combined elevation, geoid, and thermal analysis to address the crustal and the lithospheric structure. They propose a lithospheric thickness model with large variability with deeper LAB related to cratonic domains (up to 230 km) adjoining the WCARS and shallower LAB (ca. 90 km) related to Mesozoic WCARS rifting domains in agreement with tomography models, and stating that the most striking result for the crust was the crustal thinning (28–30 km thickness) imaged along the

Table **3-1**: Data and models used during the modeling process.

data	**Description**	**Reference**
Elevation: ETOPO1	Model geometry & gravity reduction	Amante & Eakins 2008
Gravity: Spherical harmonic global earth model XGM2019e	Observable to calculate gravity and gravity gradients	Zingerle et al. 2020
Seismic Moho depths	Initial Moho depth and local constraints	Mooney et al. (2010) and Globig et al. (2016)
Seismic tomography model AF2019	Input for cluster analysis	Celli et al. 2020
Global model Crust1.0	Geometry of sedimentary thickness	Laske et al. 2013
Continental model WINTERC-G	Geometry of initial LAB	Fullea et al. 2021
Heat flow	Observable used for discussion only	Lucazeau (2019)

Mesozoic West and Central African Rift Systems. But although on a large scale the WCARS appears to be a simple area of major shear zones terminated by orthogonal extensional basins and surrounded by cratons, it remains complicated in terms of understanding the multiphase evolution of rifting (Fairhead 2023).

3.3 Data

Table 2 provides an overview of the data sets, which are described in detail below.

3.3.1 Elevation and gravity data

Figure 2 shows the topography and gravity data for the study area. Topography data was obtained from the ETOPO1 model (Amante & Eakins 2008).

To investigate the lithospheric structure, we analyze both the Bouguer anomaly at a height of 10 km and gravity gradients at satellite height of 225 km. Both these fields are used as they offer a complimentary sensitivity, with the Bouguer anomaly being more suitable for identifying sources at crustal level, while satellite gravity gradients are better suited for

lithospheric sources (Bouman et al. 2016).

The Bouguer anomaly (Figure 2d) is calculated from the free air anomaly, which is derived using the spherical harmonic global earth model XGM2019e (Zingerle et al. 2020), with a maximum degree set to 720 (Figure 2b). The gravitational effect of topography (Figure 2c) was calculated with the 'tesseroids' software package (Uieda et al. 2016).
Hereby, the calculation areas was extended by 3° to avoid boundary effects.
The same procedure was applied to the satellite gravity gradient components, with adjustment of the window of spherical harmonic degree, to address particularly deeper structures of our model. The satellite gravity gradient components were taken up to a maximum degree of 300 from XGM2019e, limiting the data to the longer wavelengths, which satellite data are sensitive to. The topographic effect for each gradient component was then calculated and applied to the measured gradient data as illustrated in Figure 3.

For the topographic correction, densities of $\rho_{\text{topo}} = 2670$ kg.m^{-3} and $\rho_{\text{water}} = 1030$ kg.m^{-3} were applied to the topography and bathymetry, respectively.

3.3.2 Seismic and seismological data

The seismic Moho depths shown in Figure 4a are compiled from a combination of active and passive seismic data sources, specifically the datasets of Mooney et al. (2010) and Globig et al. (2016). By utilizing the kriging interpolation technique (Szwillus et al. 2019), we generate a preliminary gridded Moho depth (Figure 4b) and its uncertainty (Figure 4c) as starting point for the modelling. Additionally, these seismic data points were used to validate the results of our final 3D modeling study although the distribution of these data points is irregular throughout the study area, with a concentration along the Cameroon Volcanic Line.
In order to define different lithospheric domains, we use the shear wave tomography model AF2019 (Celli et al. 2020) (Figure 5). The deviations dVs of each model's point have been determined by subtracting to the mean value from the values of the corresponding horizontal layer. The model is defined from the surface to the asthenosphere. Here, we use the model only in the lithospheric extension, up to 300 km depth.

3.3.3 Additional data

In addition to the interpolated Moho depths, the global models Crust1.0 (Laske et al. 2013) and WINTERC-G (Fullea et al. 2021) serve as an initial reference for the model's geometry. Crust1.0 provides sediment thickness with a 1- degree resolution (Figure 6a). In absence of a more detailed data set, we use this model, which is not bad at the lithospheric scale, as at that scale the model is not very sensitive to the sedimentary layer. WINTERC-G provides

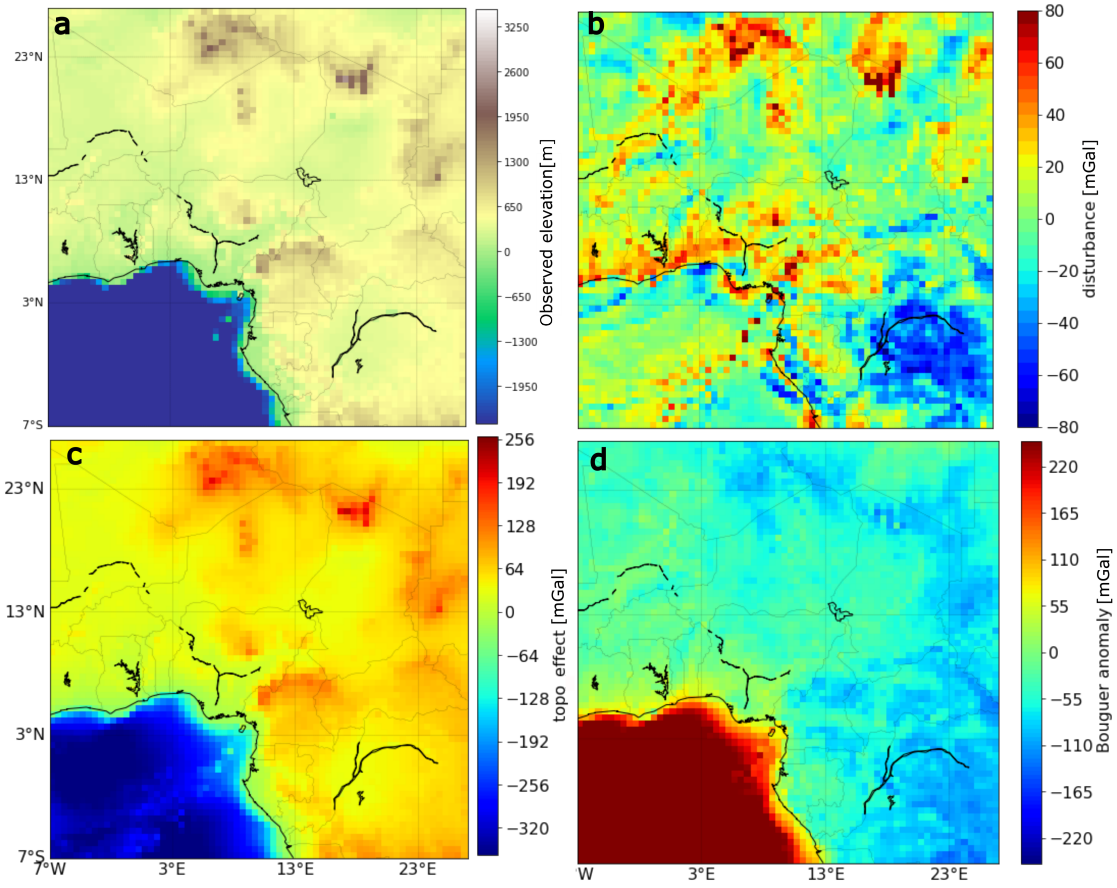

Figure **3-2**: **a** Topography of the study area after ETOPO1 (Amante & Eakins (2008)), **b** Free-air anomaly (XGM2019e, Zingerle et al. (2020)), **c** Gravity effect of topography , **d** Bouguer anomaly. See text for more details.

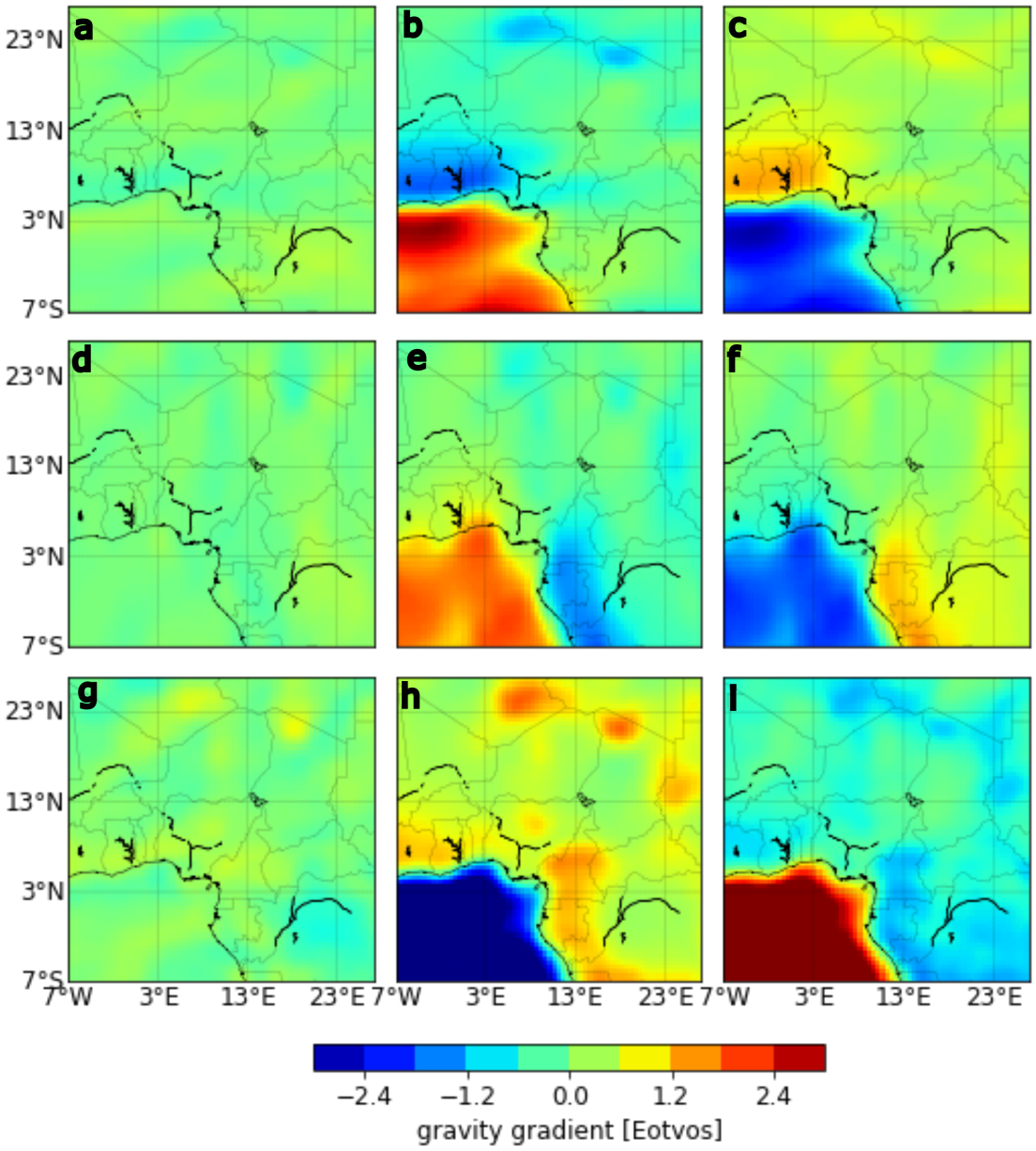

Figure **3-3**: Satellite gravity gradient at the satellite height of 225 km; **a**, **d** and **g** are the xx, yy and zz components of the observed field, respectively. **b**, **e** and **h** are the xx, yy and zz components of the topographic effect and **c**, **f** and **i** are the xx, yy and zz components of the topographic corrected gravity gradient

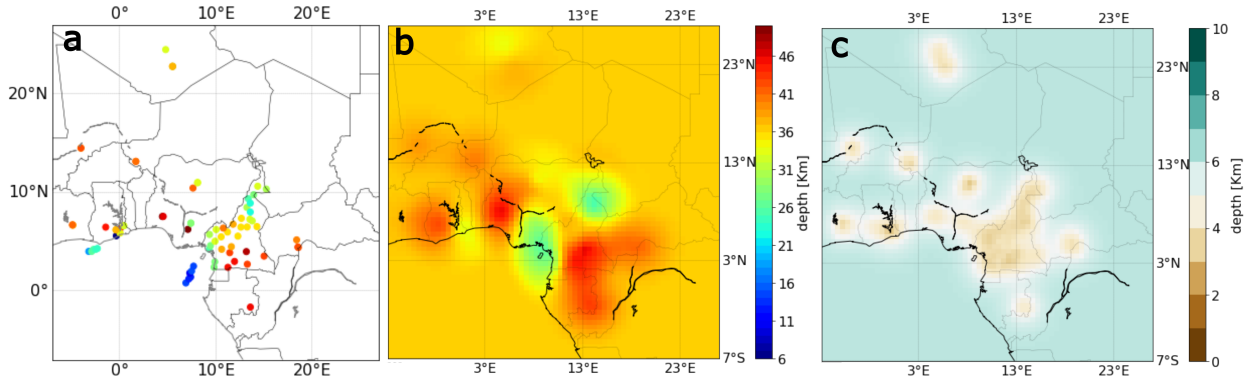

Figure **3-4**: **a** Represents the combination of available passive and active seismic Moho depth (Mooney et al. 2010 and Globig et al. 2016) in the area. **b** Is the interpolated Moho depth deduced from **a**, and **c** the associated uncertainty following the methodology of Szwillus et al. (2019).

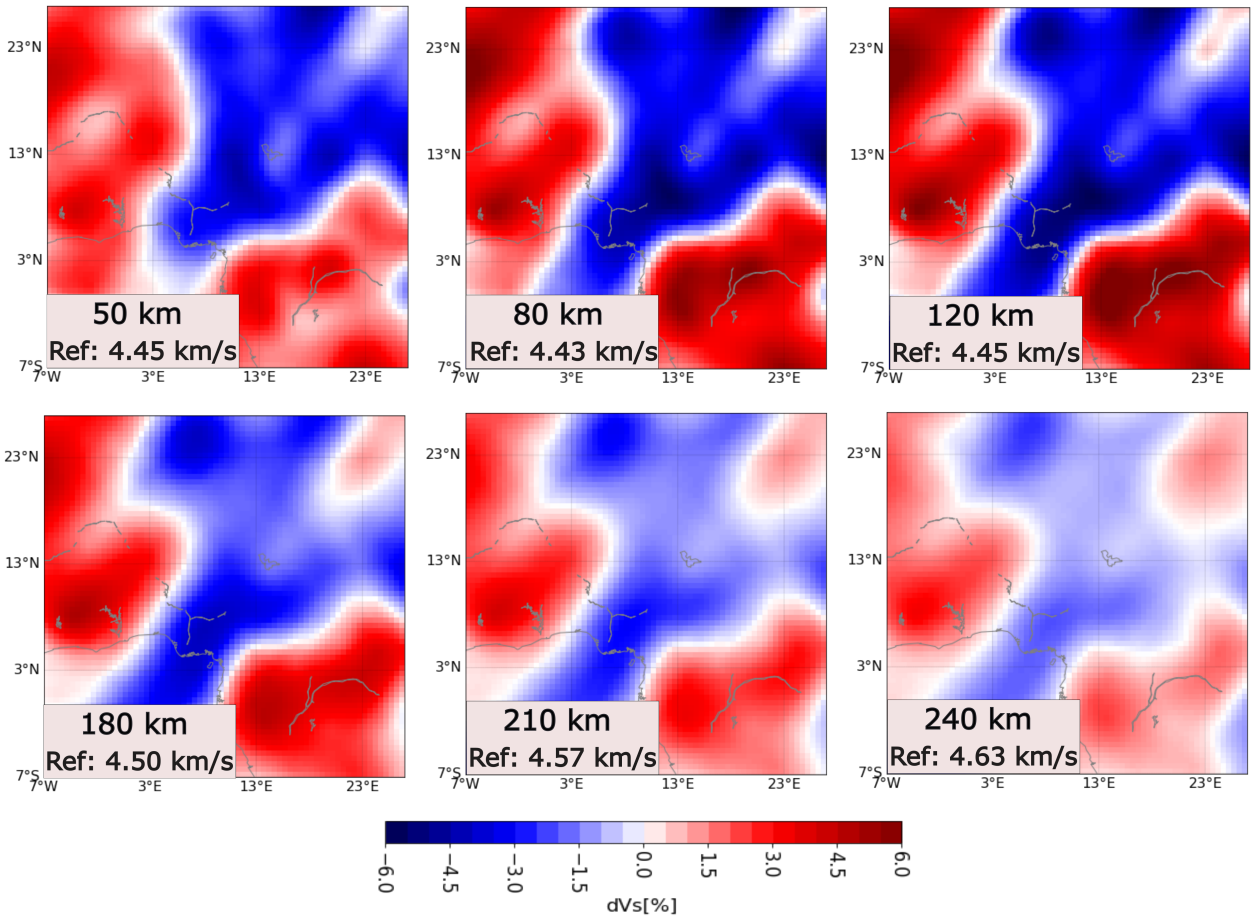

Figure **3-5**: Deviation of the seismic tomography calculated at different depths. Each slice represents the mean value of Vs for the respective depth. The seismic tomography is taken from the model AF2019 (Celli et al. 2020)

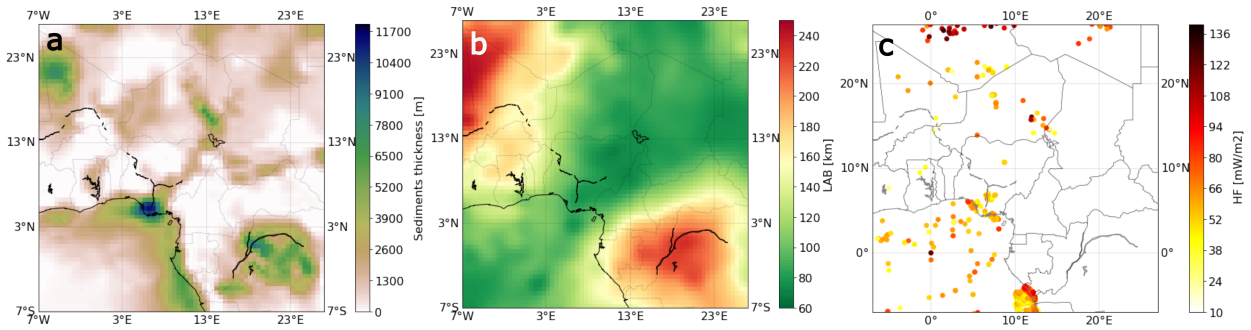

Figure **3-6**: **a** Sediment thickness (Laske et al. 2013). **b** Initial LAB from WINTERC-G (Fullea et al. 2021). **c** Heat flow data points (Lucazeau 2019).

the initial lithosphere-asthenosphere boundary in 2 degree resolution (Figure 6b).
Figure 6c shows available heat flow data over the study area, taken from Lucazeau (2019). Similar as for seismic Moho depths, data coverage is sparse. These heat flow data are only used for comparison to our model outputs.

3.4 Method

To address the structure of the WCARS and its surroundings, we first perform cluster analysis to identify different tectonic domains. Secondly, we perform the 3D modelling of the lithosphere, taking into account the lateral variability of the mantle composition, based on tectonic domains previously determined. Figure 7 shows a flowchart of the modelling steps.

3.4.1 Cluster analysis

The K-means clustering algorithm is used to cluster vertical velocity profiles from regional seismic tomography. That algorithm follows an iterative process which can be subdivided into three steps: 1) Data are initially partitioned into K groups around k random centroids. 2) Centroid positions are recalculated by using the simple Euclidean distance (given by equation (1)), and new links are made to generate new groups, by minimizing the mean value (given by equation (2)) of the previous distances between objects and their associated centroid. 3) Step 2) is repeated until no more transfer of objects between groups (Weatherill & Burton 2009, Novianti et al. 2017).
(1)

$$d(x,y) = \sqrt{(x_1 - y_1)^2 + (x_2 - y_2)^2 + ... + (x_p - y_p)^2}$$

where x and y, represent velocity-depth profiles

(2)

$$C_{kj} = \frac{x_{kj} + x_{2kj} + ... + x_{akj}}{a}, j = 1, 2, ..., p$$

where C_{kj} is centroid of group-k, variable-j, and a the number of members in the group k
(3)

$$E(m_1, m_2, ..., m_k) = \sum_{i=1}^{N} \sum_{k=1}^{K} I(x_i \in C_k) \|x_i - m_k\|^2$$

where m_k is the mean of cluster C_k and $I(x)$ is 1 if statement x is true, 0 otherwise.
Furthermore, assessing the adequacy of a partition is highly significant in the context of cluster analysis in geophysics. The predominant measure utilized to gauge cluster quality (given a known K) is the total within-cluster sum of squares, also denoted as squared error or clustering error (E, given by equation (3)) (Likas et al. 2003). In our case, this unsupervised machine learning technique groups the velocity-depth profiles derived from seismic tomography, delineating lithospheric domains and the transitional regions connecting them, on the base of the proximity of velocity-depth profiles to the determined centroids. This approach has already been successfully applied on a global (Lekic & Romanowicz 2011; Schaeffer & Lebedev 2015) and continental (Haas et al. 2021) scale.

3.4.2 3D modelling

We use a lithospheric forward modelling approach based on Litmod3D (Fullea & Afonso 2009). The key advantage of LitMod3D lies in its ability to simultaneously address the thermal and compositional state of the lithosphere. Within LitMod3D, physical properties in the lithospheric mantle are determined based on pressure, temperature, and bulk composition. This is achieved by solving equations related to heat transfer, thermodynamics, rheology, geopotential, and isostasy. Through iterative computations, we can estimate density, temperature, and heat flow by finding the best fit between the modeled and observed gravity and topography.
For a comprehensive understanding of LitMod3D and its theoretical foundation, we refer to Afonso et al. (2008) and Fullea & Afonso (2009).
The main parameters that have to be set are shown in Table 1. The densities for the crust and sediments initial values and in situ density are calculated in dependency on the pressure coefficient. Thermal parameters are, in absence of local data, based on global and previous studies (Globig et al. 2016, Puziewicz et al. 2019). The density structure of the mantle is based on the chosen composition, in turn based on PerPle_X (Connolly 2005; Connolly 2009).

The geometry of the model and the observables used to validate the model are based on the data sets described in the following section.

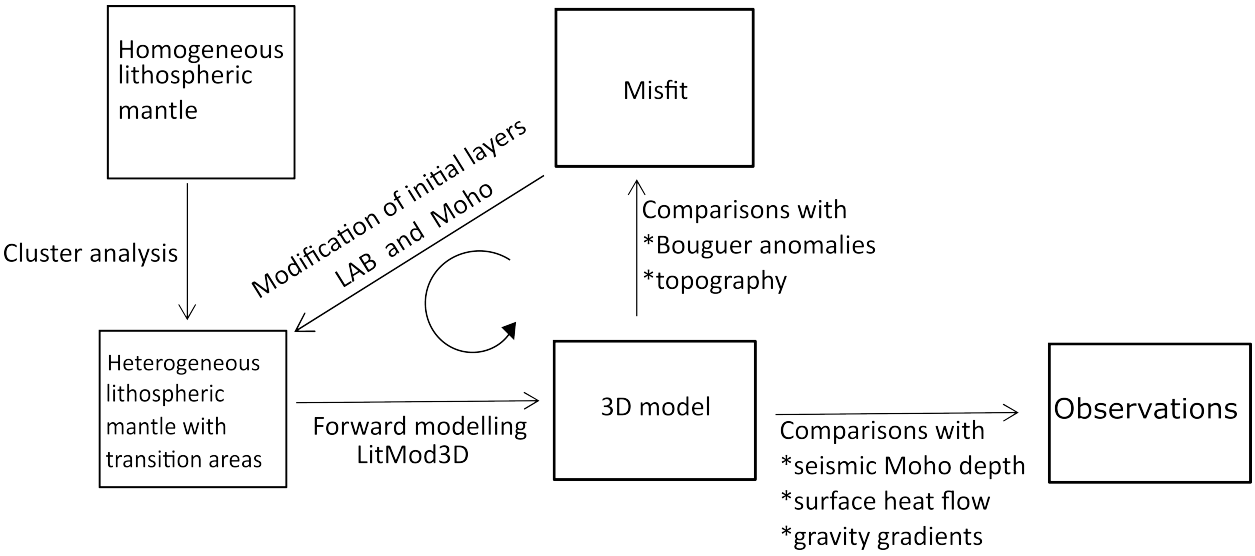

Figure **3-7**: Flowchart of the integrated study carried out in this work

Table **3-2**: Layers' thermophysical properties. The top mantle's density is directly computed by the code PerPle_X, the pressure coefficient for the mantle and the Grueneisen parameter for sediment and crust layer are negligible.

layers	Density $Kg.m^{-3}$	Thermal conductivity $W.m^{-1}.K^{-1}$	Heat production rate $W.m^{-3}$	Pressure coefficient	Grueneisen parameter
Sediments	2500	2.0	$9 * 10^{-6}$	$8.5 * 10^{-10}$	/
Crust	2670	2.5	$9 * 10^{-6}$	$1.5 * 10^{-10}$	/
Mantle	/	3.2	10^{-8}	/	1.25

3.5 Results

3.5.1 Seismological Regionalization

The regionalization was carried out disregarding the offshore area. Choosing the number of clusters is somewhat arbitrary. We tested between 2 to 6 clusters and found that 3 clusters effectively represent the known geology of the region. The velocity were considered between 50 and 300 km depth to prevent any skewed results from near-surface heterogeneities.
The cluster findings (Figure 8) indicate that the continental region of the study area can be distinctly divided into three primary blocks, which roughly correspond to the expected tectonic units.
Within each cluster, the vertical velocity profiles are broadly similar. Cluster 1 profiles exhibit an increase of seismic velocity from 50 km to 150 km, followed by a decrease until reaching approximately 220 km. Subsequently, there is an increase until around 240 km, after which the velocity remains relatively constant until reaching 300 km.
Cluster 2 consists of profiles that remain relatively constant between 50 km and around 70 km. From there, they experience a gradual decrease in seismic velocity until approximately 80 km, followed by a slight increase until reaching around 210 km. Finally, there is another increase as they progress towards 300 km.
Lastly, cluster 3 comprises profiles that demonstrate an increase from 50 km to 80 km, followed by a gradual decrease throughout the entire range until reaching 300 km.
Comparing the clustered blocks with the tectonic map of the region, it becomes apparent that cluster 1 corresponds to the Congo craton in the southeast and the West African craton in the northwest. Cluster 3 coincides with the WCARS, cluster 2 lies between the two other clusters and is identified as a transitional area between craton and rift zone. It exhibits a consistent velocity at the beginning. A notable dissimilarity between the expected geological distribution (Figure 1) and the clustering result (Figure 8) is the absence of the southern part of the Saharan metacraton in the cluster analysis output (northeastern section of the study area).

3.5.2 Model

Model setup

To conduct a comprehensive analysis of the WCARS and its surroundings using our model, we considered an area of 3800 km x 3800 km with a depth of 300 km. In order to ensure numerical accuracy, we have employed a lateral discretization of 50 km and a smaller vertical discretization of 2 km.
To establish the initial model geometry, we have utilized elevation, sediment thickness, interpolated Moho as well as the LAB presented in the data section.
To account for the diverse lithospheric characteristics present within the region, we have

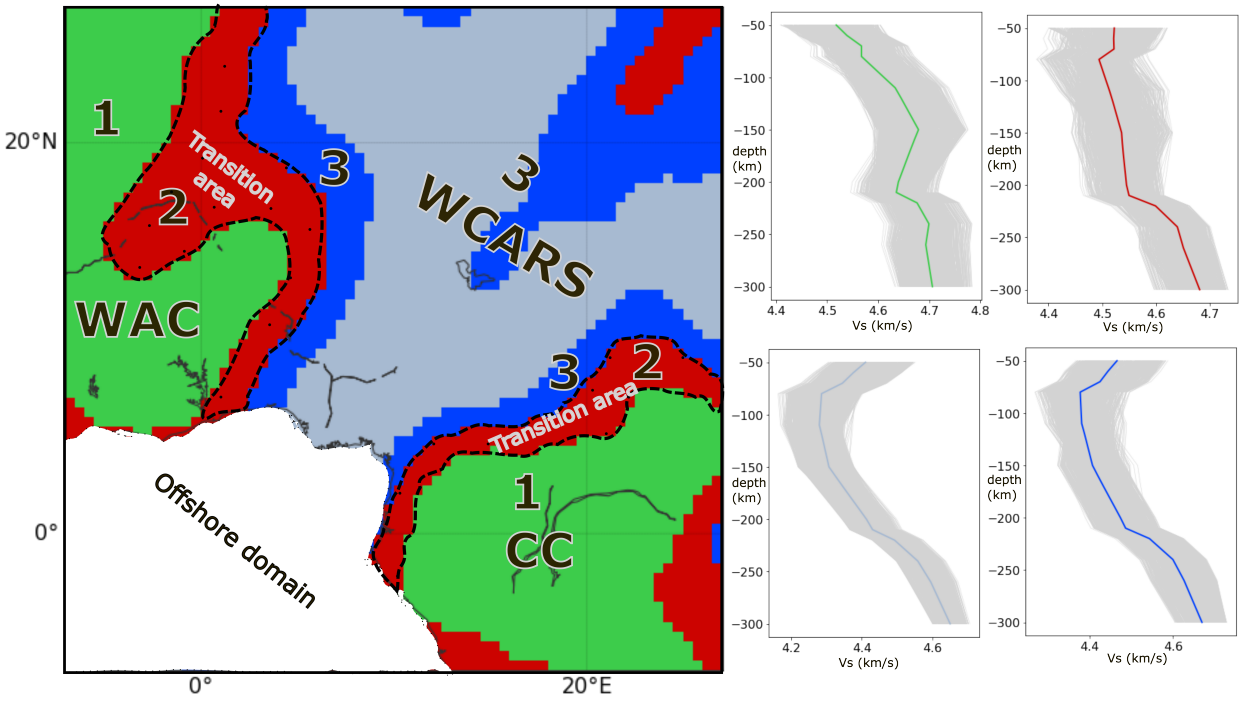

Figure **3-8**: Clusters of tectonic domains and corresponding velocity depth profiles. WAC: West African craton, CC: Congo craton, WCARS: West and central African rift systems. The number 1 to 3 represent groups of clusters. The four velocity-depth profiles in highlighted colors represent different centroids around which all the other velocity profiles (in grey) are clustered. Each profile group describes the corresponding coloured zone on the tectonic map. Because of their similarity, the two lower velocity-depth profiles have been considered as describing the same tectonic unit.

incorporated global geophysical and petrophysical properties that have been adjusted based on specific domains identified through cluster analysis. The obtained clusters are implemented as a combination of Proterozoic-Phanerozoic-Primitive Mantle types for cratons - rift - offshore areas respectively.

Lithospheric mantle composition

At this stage of our study, we made a number of sensitivity tests to determine the ideal type of the lithospheric mantle composition in the study area. We first considered the lithospheric mantle to be homogeneous, and tested the Archean, Proterozoic and Phanerozoic types respectively. The models show that a reasonable fit could be achieved for the Proterozoic and Phanerozoic types, while for the Archean type no satisfying fit to the observed topography and gravity anomalies can be achieved, without an unreasonable geometry. For Proterozoic lithospheric mantle, the modeled Moho is much shallower than the seismic Moho in rift zones, and for Phanerozoic lithospheric mantle, it is rather too deep under cratons. A similar observation can be made by comparing the model to heat flow data. The model with a Proterozoic lithospheric mantle results in reasonable heat flow values for the cratonic areas, while in the rift area the values are rather low. For the model with the Phanerozoic lithospheric mantle, heat flow values for the rift area appear to be reasonable, but they are too high for the cratons. Details of this sensitivity test are available in the appendix, Figure 18. Based on these observations and the results of the clustering exercise, we considered the lithospheric mantle as made of Proterozoic and Phanerozoic domains. More specificly, we introduced Phanerozoic-type lithospheric mantle under the WCARS surrounded by Proterozoic lithospheric mantle under the CC and WAC. The transition area between the cratons and the rift area is modelled as a gradual change leading to an intermediate, mixed composition (see Figure 9a). This model has shown the best fit between modelled and observed values. In the following, we will concentrate on the discussion of the best fit model.
Figure 10 shows the fit to the observed data of our preferred model. The modelled elevation closely matches the measured elevation shown in Figure 2a. In areas of high topography the misfit (Figure 10a1) displays some noticeable variations between modelled and measured elevation. These short-wavelength differences are related to small-scale structures, which our lithospheric-scale model is not intended to reproduce. In general, the reasonable data fit is confirmed by the statistical distribution showing an error close to zero for most of the area, with an RMS value of 137 meters.

The trend observed in the modelled Bouguer anomaly (Figure 10b) closely matches the measured Bouguer anomaly (Figure 2d). However, the modelled anomaly appears to be smoother, for the same reason as mentioned above. The differences show RMS value of 23 mGal with a slight shift to positive values.

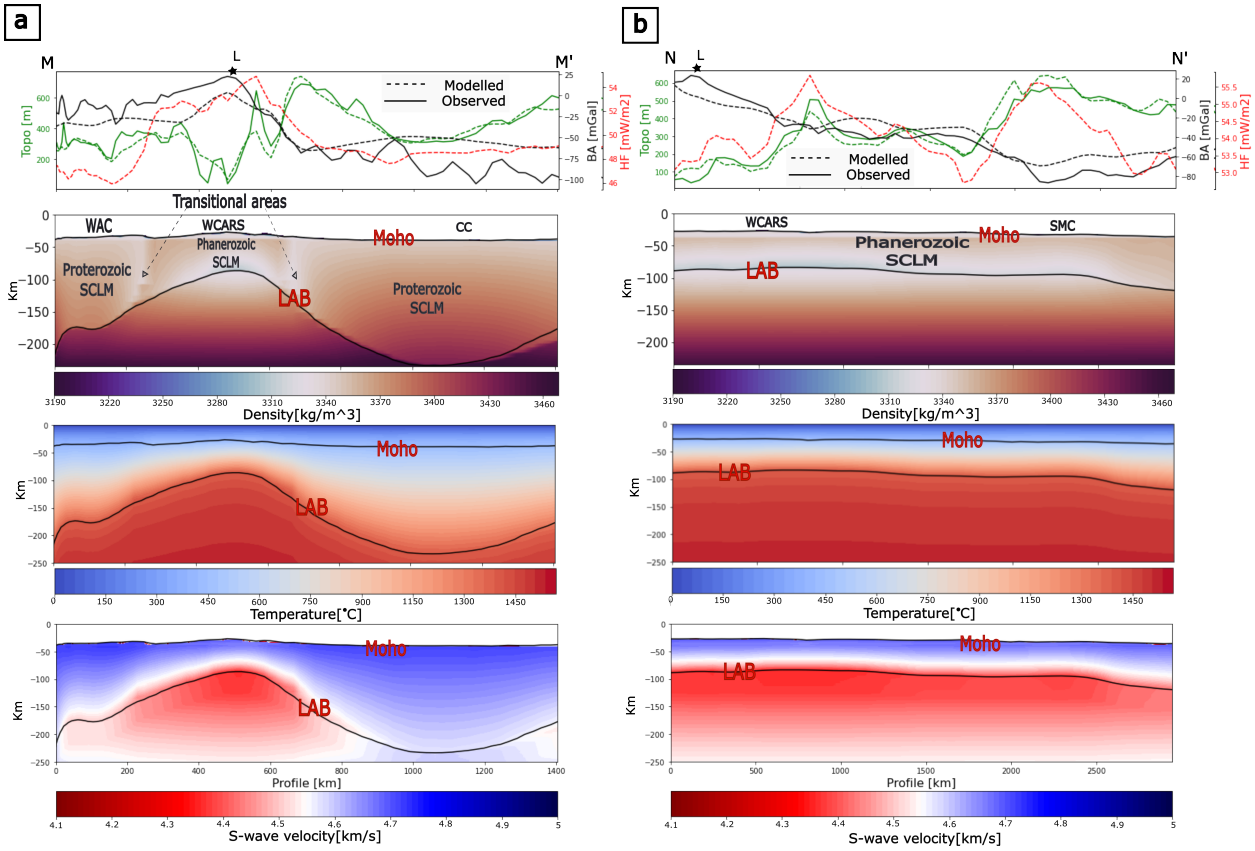

Figure **3-9**: This figure shows two cross sections through the modelled density, temperature and velocity. **a** represents the vertical cross section (MM', shown in Figure 1) crossing the WAC, the CC, the CVL and the Benue trough. **b** displays the vertical cross section (NN', shown in Figure 1) along the WCARS, going from the Benue trough toward the known north of the SMC. In opposition to **a** with large variations of LAB, **b** displays an almost constant LAB from the Atlantic coast to across the SMC. L is the junction point of the cross sections MM' and NN'. Solid and dashed black lines on top of the model respectively represent the observed and the modelled Bouguer anomaly. The solid and dashed green lines represent the observed and modelled topography. The dashed red line represent the modelled heat flow.

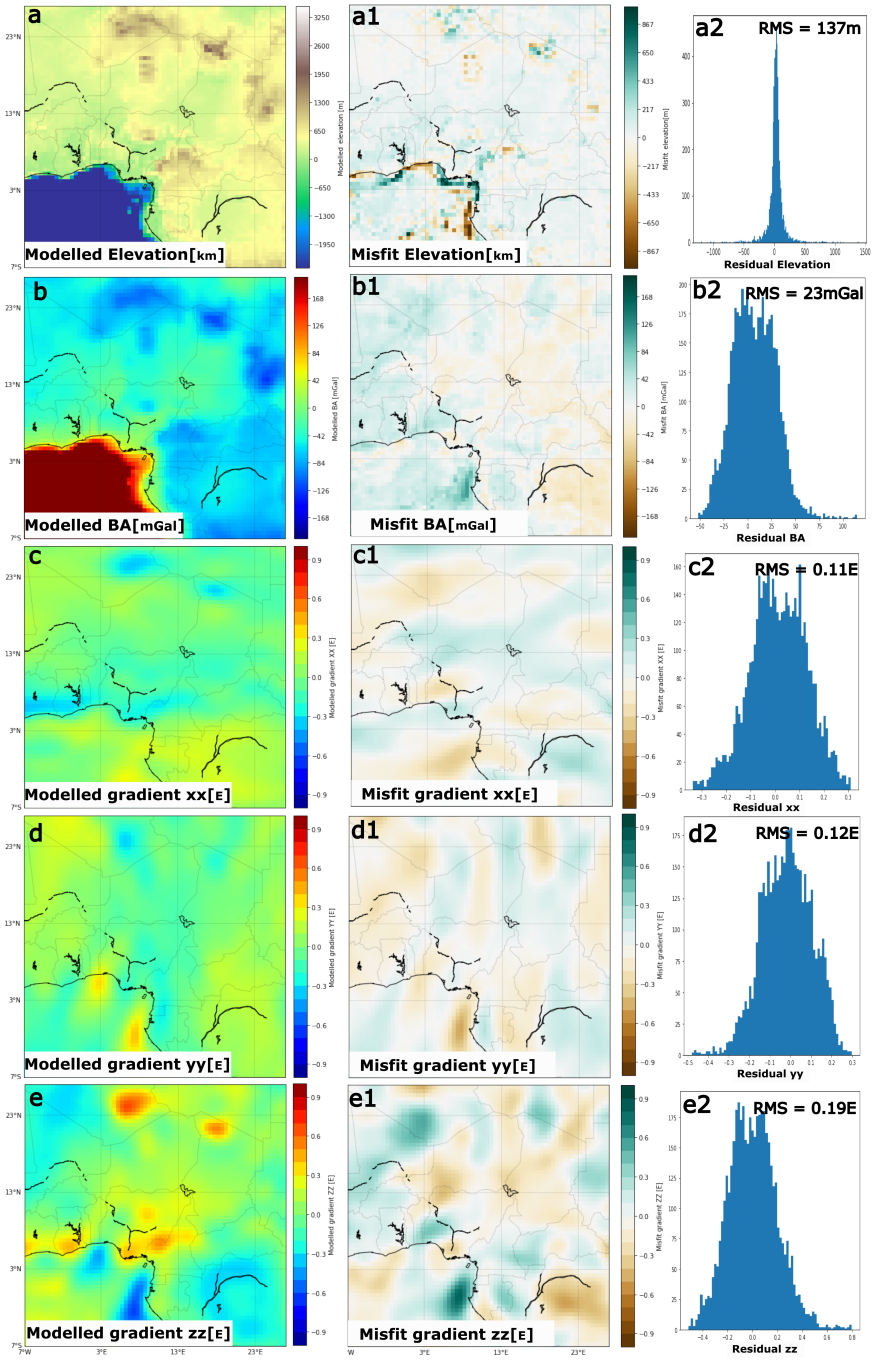

Figure **3-10**: Modelled Topography and gravity and their misfit in comparison to measured data shown in Figure 2 and Figure 3. **a** Topography, **a1** topography misfit, **a2** residual topography diagram, **b** Bouguer anomaly, **b1** Bouguer anomaly misfit, **b2** residual Bouguer anomaly diagram, **c** gravity gradient xx component, **c1** xx misfit, **c2** residual xx diagram, **d** gravity gradient yy component, **d1** yy misfit, **d2** residual yy diagram, **e** gravity gradient zz component, **e1** zz misfit, **e2** residual zz diagram.

Figures 10c, 10d, and 10e show the xx, yy, and zz components, respectively, of the modelled gravity gradient across the study area. The discrepancies observed are minimal, especially for the xx and yy components, which range between 0.3 E and -0.3 E. These components exhibit RMS values below 0.12 E. On the other hand, the misfit for the zz component (Figure 10e1) displays higher values compared to the other two. Upon closer examination, this misfit appears to follow the same pattern as the Bouguer anomaly misfit (Figure 10b1),
Moreover, the modelled Moho has been sampled at the available seismic Moho depth points. The comparison of both of them plotted on top of the modelled Moho (Figure 11a) shows a spatially variable but very low difference, indicating that the the final model is in reasonable agreement with the available data.

Crustal Thickness

Figure 11a shows that the WCARS's crust is thinner compared to adjoining cratonic crust. The thinnest crust is found in the Benue trough, propagating itself northeastward through northern Cameroon (Yola-Garoua basin), Lake Chad, and the middle north of Chad, as well as the Termit basin in Niger. Conversely, the thickest crust is found in the Tibesti region in the northwest of Chad and the Hoggar region in the Southeast of Algeria. While the CVL's crust is relatively thick, except in the coastal areas of Cameroon (Mount Cameroon area), a stark contrast can be observed between the CVL and the Benue trough along the Cameroon central-west border, as well as the contact between the Adamawa plateau and the Yola-Garoua basin.

Lithospheric Thickness

The modeled lithospheric thickness (Figure 11b) shows the expected difference between the cratons and the rift zone. Within the cratonic zone, the lithospheric thickness ranges from approximately 160 km to 240 km, and around 80 km to 140 km over the rifts. In the transition zones lithospheric thickness deepens from 140 km to 160 km. From the Benue trough to the Marrah region inside Sudan, the lithosphere is thin - as low as 80 km in certain regions like Marrah mountains. In the NE direction, there is no clear boundary between the rift zone and the SMC. On the east and west sides of the rift, we can clearly see the transitions that differ depending on whether we go towards the CC or the WAC. Unlike the transition towards the CC, which is horizontal over a short distance but with a sharp variation in depth, the transition towards the WAC takes place over a relatively long distance and evolves in the form of a staircase around a depth of 160 km. This results in an asymmetrical distribution of the two cratons in relation to the rift.

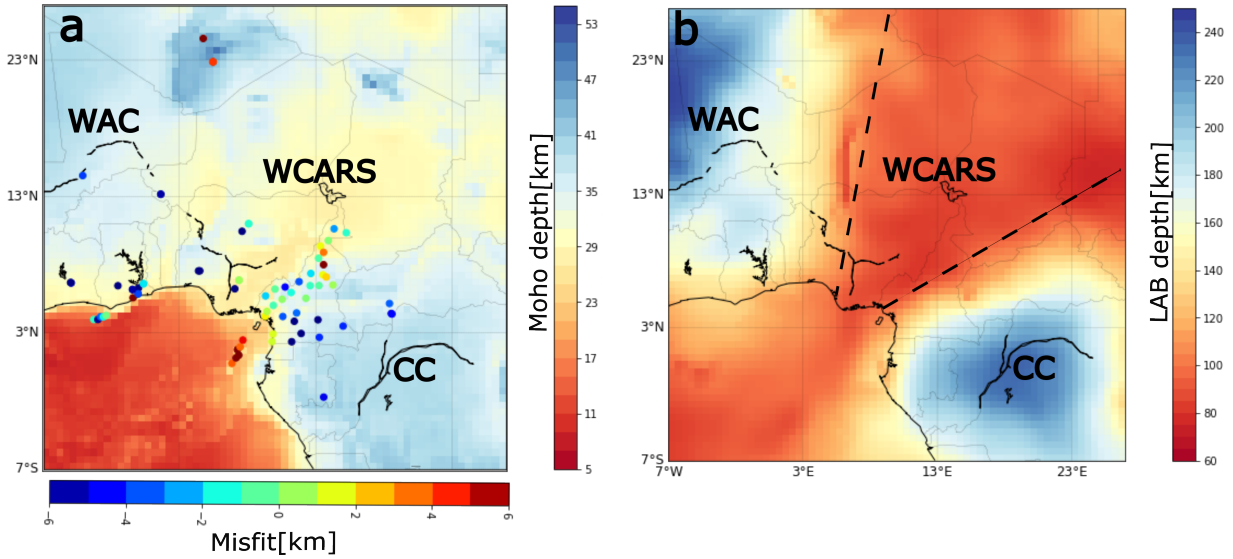

Figure **3-11**: **a** Modelled Moho depth and misfit (coloured points) in comparison to available seismic Moho depth; **b** Modelled LAB. The "V" shape of the opening of the lithosphere is highlighted by the dotted lines.

Heat flow

The modelled heat flow (Figure 12) follows the lithospheric thickness to a large degree and differs as well between the colder cratons ranging from (46 $mW \cdot m^{-2}$ to 54 $mW \cdot m^{-2}$) and the warmer rift zone with values ranging from 50 $mW \cdot m^{-2}$ to 64 $mW \cdot m^{-2}$. Additionally, the model indicates that the CVL, with an approximate value of 60 $mW \cdot m^{-2}$, experiences higher heat flow compared to the Benue depression, which has an approximate value of 54 $mW \cdot m^{-2}$. Furthermore, the sudden thinning of the lithosphere between the Adamawa plateau and the Garoua rift is causing a strong increase in heat flow in the direction of crustal thinning.

Density

Within the study area, there is a noticeable difference in the density distribution between the WCARS and the adjoining cratons, as well as internal heterogeneities inside the WCARS (Figure 13). Upon examining a horizontal section of the model at a depth of 50 km, the cratons exhibit a fairly constant density of around 3350 $kg.m^{-3}$, whereas the rift zone have highly variable density. The most prominent contrast of approximately -30 $kg.m^{-3}$) is observed in the Marrah Mountains region, which spans from western Sudan to crossing the border with Chad. This deficit in mass appears to extend in a northeast to southwest direction towards the Gulf of Guinea, passing through southern Chad where it is less pronounced, before eventually reaching the Adamawa Plateau in central-western Cameroon and the Jos Plateau in northeastern Nigeria, where the contrast is once again significant (around -20

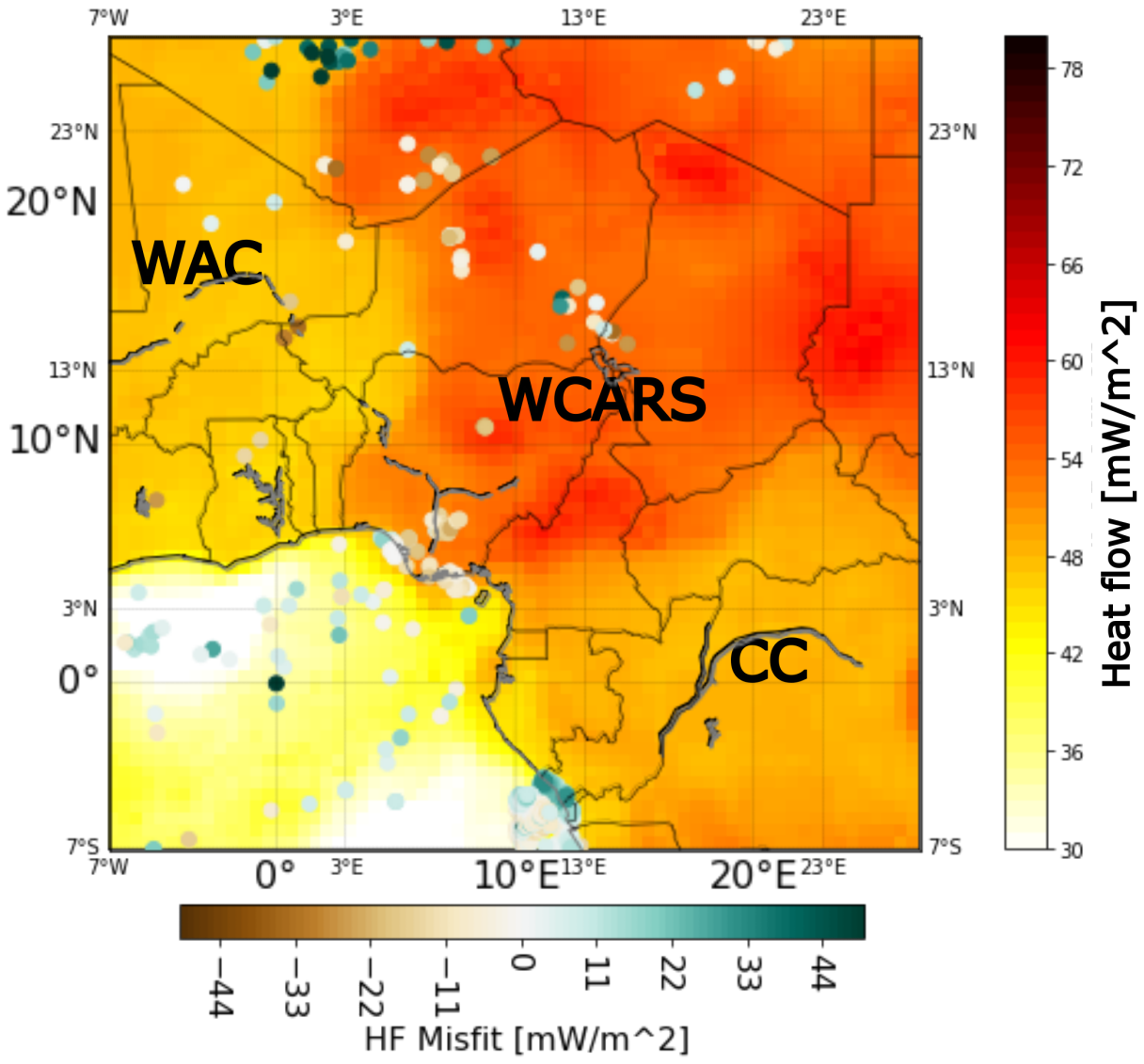

Figure **3-12**: Modelled heat flow and misfit (coloured dots) in comparison to available heat flow points in the region.

$kg.m^{-3}$).
Similar low densities are also identified in the Tibesti mountain region, albeit to a lesser extent in the Aïr (Niger) and Hoggar mountain regions. These areas with lower density correspond to regions with higher topography, which aligns with isostatic compensation. However, there are certain exceptions such as the Benue trough, Murzuq Basins, where a minor contrast of approximately -5 $kg.m^{-3}$ is observed.
At larger depths, the density distribution gradually becomes more uniform for both the WCARS and the cratons. However, at 150 km depth, a notable heterogeneity emerges in the south-western region of the WAC, segregating the south-western portion of this craton. That peculiar contrast in density is probably related to the variation of LAB depth. The gap of densities at the edge of the cratons, noticeable after 150 km are probably due to the compositional boundary (depleted = lighter) and the fact that the temperature near the LAB is similar to asthenospheric temperatures.
Figure 14 provides a 3D representation of the modelled density distribution, extending from the topographic surface down to a depth of 300 km. The vertical sections cross the CC, WAC, and WCARS regions. The model demonstrates a downward-oriented density gradient, except for the area below the WCARS. Below the WCARS, the density decreases from the middle of the lithospheric mantle towards the LAB, before increasing again inside the asthenosphere. That depletion is probably the consequence of the conflict between the high temperature due to the shallow asthenosphere and the relative low pressure due to the thin lithosphere in that area.
The 2D cross-section of the density distribution along MM' (passing trough the middle of the previous mentioned heterogeneity located in the southwest of the WAC, Figure 9a), emphasizes the transitional zone between the depleted Proterozoic lithospheric mantle beneath the WAC and the fertile Phanerozoic lithospheric mantle beneath the WCARS. It emphasizes as well the transitional zone between the fertile Phanerozoic lithospheric mantle beneath the WCARS and the Proterozoic lithospheric mantle beneath the CC. These transitional areas exhibit a significant reduction in mass compared to the adjoining blocks. On the other hand, the 2D cross-section along the NN' well shows that there is no clear boundary between WCARS and SMC in terms of LAB depth variation, but also density, temperature and velocity distributions (Figure 9b).

3.6 Discussion

3.6.1 Structure of the lithosphere

The thickness of the crust beneath the WCARS and its surroundings is highly variable. Isostatic compensation can explain most of these variations, especially in mountainous regions like Marrah (38 km), Tibesti (50 km), Hoggar (54 km), and the Adamawa plateau (40 km, similar to the findings of Ghomsi et al. (2022)). A stark lateral crustal thickness gradient is

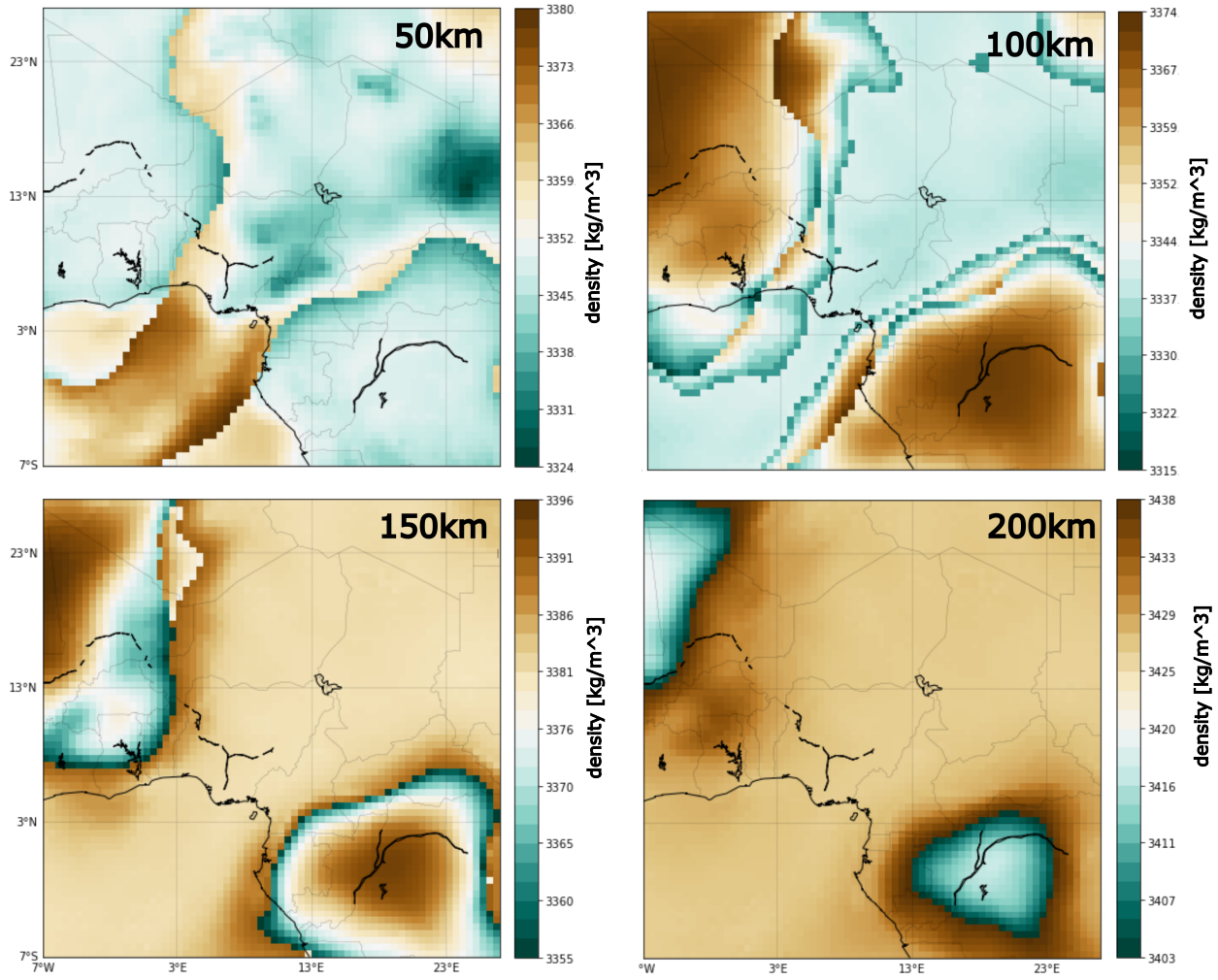

Figure **3-13**: Horizontal 2D sections of the modelled density distribution at 50 km, 100 km, 150 km and 200 km depth.

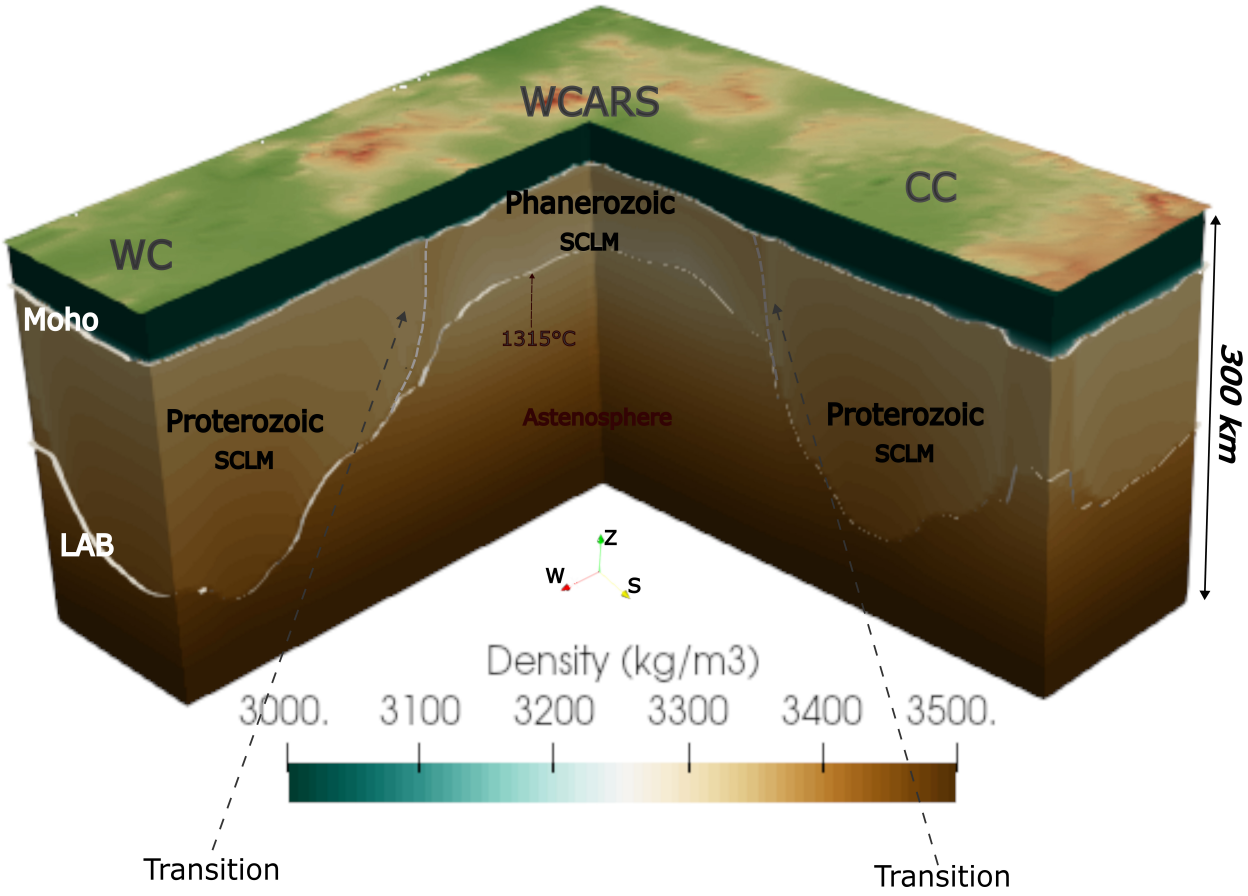

Figure **3-14**: Perspective view of the 3D density distribution, with geological block and layer boundaries. The depth has been exaggerated with factor of 7000.

located at the boundary between the oceanic domain and WCARS, reflecting the transition from oceanic to continental crust.
Despite their proximity, the CVL and the Benue trough exhibit significant differences in terms of Moho depth, as mentioned by Stuart et al. (1985). Our model suggests that the Benue trough has a Moho depth of approximately 27 to 30 km, while the CVL ranges from 37 to 40 km, consistent with the results of the shear wave velocity study conducted by Tokam et al. (2010). A similar variation in crustal thickness is observed on the western side of the Benue trough, extending from the Atlantic Ocean boundary to the Jos Plateau (approximately 33 km to 38 km). This indicates that the region likely experienced significant tectonic events, with the Benue trough maintaining the position of symmetrical axis during the rearrangement. Additionally, the crustal thinning observed in the Benue depression extends northeastward into the interior of the continent underneath sedimentary basins such as Yola, Garoua, and Chad, which occupy a substantial surface area and align with the findings of Globig et al. (2016), who also identified crustal thinning (ca. 28 km - 30 km) along the Mesozoic systems of the WCARS. In contrast, the depth of the Moho is slightly greater under the CC and WAC (ca. 33 km - 43 km).

The lithospheric thickness in the WCARS and its adjoining areas has a large range of variation, from approximately 80 km to 240 km. This aligns with previous findings (such as Globig et al. 2016) that the lithosphere-asthenosphere boundary exhibits significant spatial variability (ranging from 90 km to 230 km) within the region. The highest values are associated with the cratonic domains adjoining the WCARS, while the smallest values are related to the rift domains themselves during the Mesozoic period (Globig et al. 2016).

Furthermore, our model characterizes the lithospheric mantle beneath the West and Central African rift system and its surroundings as predominantly Phanerozoic and Proterozoic-type. It is important to note that the composition of the sub-continental lithospheric mantle is generally not homogeneous across a large area. With regard to WCARS, this is in agreement with other studies in the region (Bosworth 1992; Schull 1988 and Eyike & Ebbing 2015), which have described the majority of the inner portions of WCARS as Cenozoic and Mesozoic (Phanerozoic) in origin.

Corroborating these descriptions, Fairhead (1988) states that the opening of the Atlantic basins can be divided into four stages of development. These stages include the Jurassic opening of the Central Atlantic, the Early Cretaceous (approximately 130 - 119 Ma) opening of the South Atlantic with rifts spreading deeply into Africa via the Benue trough, the opening of the Equatorial Atlantic (119 - 105 Ma), the connection of these ocean basins, and the formation of the current mid-ocean rift system. Additionally, the WCARS underwent development until the end of the Cretaceous period. While the precise boundaries between WCARS and the adjoining units are not clearly defined, it is well known that WCARS

is adjacent to cratons. Therefore, the classification of the blocks neighboring WCARS as Proterozoic, as described in this study, aligns with Artemieva (2011), who concluded that Proterozoic cratons are surrounded by Phanerozoic belts.

We find no discernible difference between the lithospheric mantles under the WCARS and SMC (except in the far North-West part of the the SMC). In fact, the cluster analysis of seismic velocity in the study area clearly shows the distinction between WCARS, CC, and WAC. However, the SMC, as depicted in the geological map (Figure 1), remains inconspicuous. This implies that the SMC lacks any distinct characteristics of anomalous seismic velocities within the depth range of 50 km to 300 km. Additionally, our modeled LAB indicates no significant variation between the thin WCARS lithosphere and the SMC lithosphere (Figure 9b, Figure 11b). The density, temperature, and velocity distributions determined from our modelling efforts align with this observation, which concurs with the findings of Sobh et al. (2020), who also inferred a thin lithosphere beneath the SMC based on lithospheric modelling. Multiple geological events, including the partial delamination of the lithospheric mantle during the Neoproterozoic era, rifting during the Mesozoic-Cenozoic period, and the activation of the SMC during the Mesozoic (Sobh et al. 2020) likely facilitated the fertilization of the region through erosion of isolated lithospheric roots.

3.6.2 Origin of the WCARS

Our model suggests an asymmetry in the LAB geometry between the CC and WAC centres with respect to WCARS. The LAB under the WAC displays a step-like pattern towards its centre, which can indicate a stretching of the lithosphere in that region. Consequently, during the breakup of Gondwana, the western side of the current African continent experienced significant traction. However the traction was distributed differently within the continent, with the western block absorbing most of it. This explains the cascading form of the lithosphere observed under the eastern margin of the WAC lithosphere in contrast to the transition in one step between the rift and the northwest margin of the CC. Additionally, the "V" shape of the WCARS also extending across the SMC despite its pre-existing suggests that the pulling force that gave rise to the WCARS was most likely greater to the north, or simply multi-directional.

The findings of this work further support the characterization of WCARS as a passive rift system (Fairhead 2023), consistent with the extensional rift basin model proposed by McKenzie (1978).

Moreover, along the Benue trough to the Yola-Garoua basin, the stretching factor (see appendix B, stretching factor's section) is around 1.2 (which indicates a continental rift, Allen & Allen 2013), while to the northeast (South Sahara meta craton) it is reduced to 1.1 (closer to an intracratonic sag basin, Allen & Allen 2013). As expected, the cratonic areas

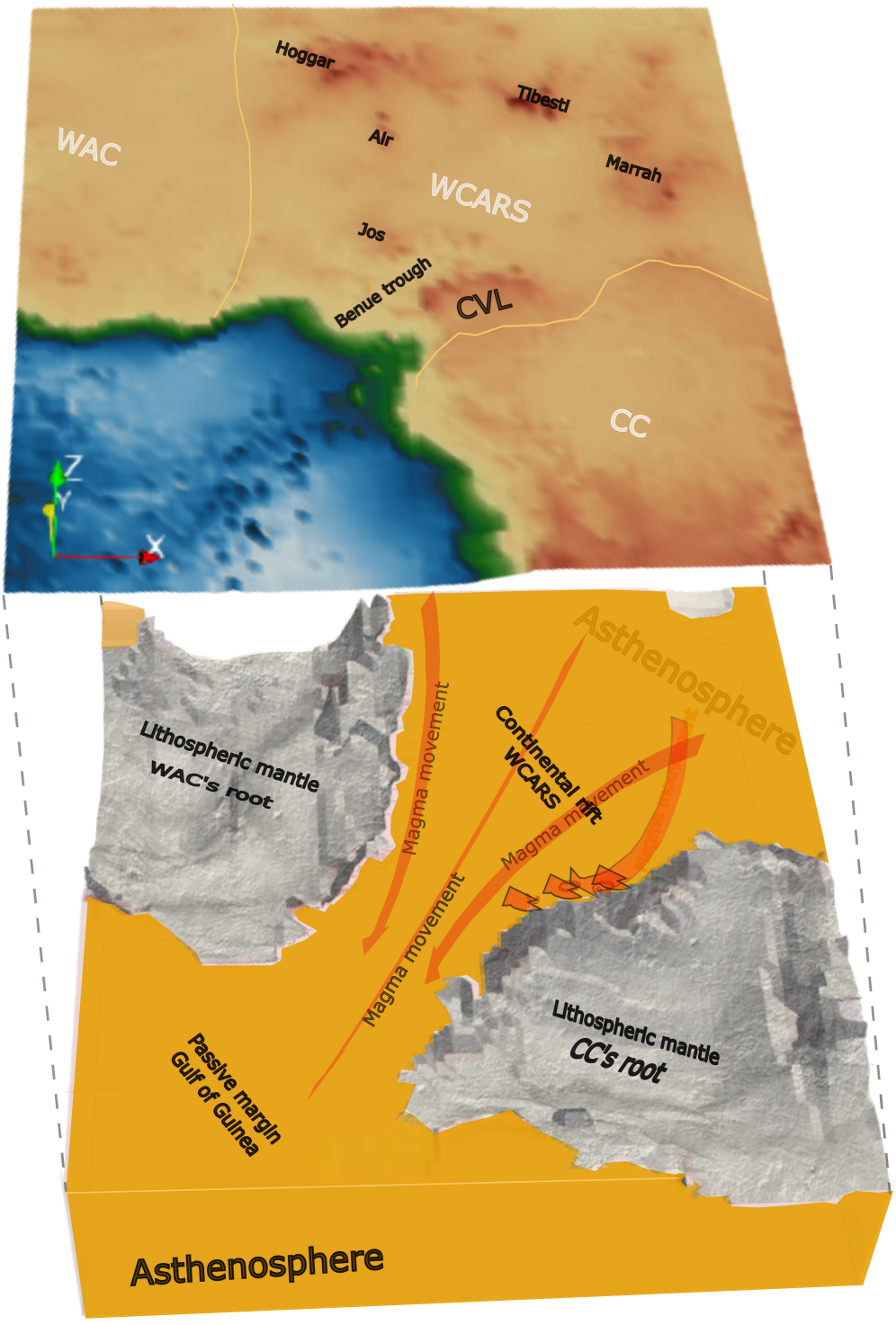

Figure **3-15**: Sketch showing magma movement between cratonic roots during the Atlantic's opening and the WCARS formation. The magma moving from the continent to the passive margin through the continental rift, and facing the northwestern border of the CC, leading to magma uploading inside the CVL's lithosphere.

have a stretch factor lower than 1 due to their stability in opposition to the Gulf of Guinea, with a stretch factor higher than 1.5.
In the case of an active origin of the WCARS, we expected to find the area of thinnest lithospheric mantle under the volcanic line, however the model shows that the LAB beneath the Benue trough is shallower than beneath the CVL.

3.6.3 Origin of the CVL

Previous research has already noted the connection between CVL and the Benue trough (Fitton 1980; Stuart et al. 1985). Our model indicates that the CVL could be connected with the CC, especially with the shape of the northwestern boundary of the CC where there is the most pronounced variation of the LAB (Figure 15) between the rifts and the cratons. According to our model, the origin of the CVL could be attributed to the opening of the WCARS in addition to the particular shape of the northwest margin of the CC, in agreement with the theory of edge convection mentioned by Milelli et al. 2012 and Koch et al. 2012 to describe the cause of the CVL. We suggest that during the break-up of the Gondwana supercontinent in the Jurassic-Cretaceous period, mantle material from the interior of the continent (current WCARS) started to flow towards the present-day Atlantic Ocean i.e. SW movement (Elsheikh et al. 2014), pulled in by the movement of the South American tectonic plate moving away from the African plate. The "V" shape of the lithospheric mantle opening caused the flow velocity to increase from northeast to southwest in relation to the Venturi effect phenomenon (Scheaua 2016). In addition, the northwestern margin of the CC has acted as a deep frontal barrier, resulting in convective movement, driven not by temperature gradients but by magma dynamics. This mechanism agrees with the study of King & Ritsema 2000, who based on numerical modelling to study the origin of intraplate volcanism in South America and Africa and concluded that the CVL is the consequence of edge-driving convection beneath the CC. Such a temporary event could have led to the formation of magma chambers along the known CVL. The pressure within each chamber varied depending on factors such as the amount of water present and the quantity and quality of minerals being melted, causing the equilibrium between magmatic pressure and lithostatic pressure to be effectively random (well detailed in Gudmundsson 2012). This randomness could explain the absence of any age progression along the CVL (De Plaen et al. 2014).

3.7 Conclusions

This study examined the lithospheric structure of the West and Central African rift system and its surroundings and the link to the enigmatic Cameroon volcanic line, by applying integrated geophysical and petrological 3D modeling.
Cluster analysis of shear wave tomography grouped the study area into three main tectonic

blocks. Namely the rift zone, the northern part of the Congo craton and the east part of the West African craton. Furthermore, the clustering highlights the absence of any particular signature from the southern part of the Saharan meta craton. Initial models with a uniform mantle composition were not able to explain all observables simultaneously (topography, gravity, Moho depth, heat flow). Therefore, in our preferred model, a Phanerozoic-type lithospheric mantle under the West and Central African rift system is linked to the two adjoining cratons of Proterozoic-type by transitional areas of different size and shape. Further findings of this study confirm the wide range of variations in crustal (ca. 25 km to 50 km) and lithospheric (ca. 70 km to 250 km) thicknesses across the study area, with the shallowest LAB found under the region of the Benue trough-Cameroon volcanic line until the Marrah region, and the deepest under cratonic centres. They also confirms the absence of any cratonic characteristics of the Sahara meta-craton (particularly its southern part), suggesting that it has undergone long term fertilization facilitated by tectonic events.
In addition, our model confirms the suggestion that the WCARS is a passive rift system. This observation and the overall lithospheric structure suggests that the origin of the Cameroon volcanic line, specially its continental part, could be explained taking into account the V-shaped opening of the lithospheric mantle beneath the West-Central African rift system, along with the abrupt transition between the rift and the northwestern edge of the Congo craton. This potential development should be explored further in the future with geodynamic modelling, where also the interaction between mantle flow and the lithospheric structure is studied in more detail.

Appendices

3.A Homogeneous lithospheric mantle across the study area

This section presents the limits of the integrated 3D modelling across the study area, considering the lithospheric mantle as homogeneous, which means that the cluster analysis hasn't been processed and no particular blocs have been defined. The investigation focused on three types of mantle namely Archean, Proterozoic and Phanerozoic, described in Table 3.

Bouguer anomaly and topography

Figures 16 and 17 depict the best Bouguer anomaly and topography models for three different homogeneous mantle compositions, along with their respective misfits compared to the measured values.
By inspecting the Bouguer anomaly (Figure 16, A), it is evident that the datafit of the three compositions are more similar than different however, some variations can be observed

Table **3-3**: Mantle composition, Griffin et al. (2009),Fullea & Afonso (2009) and McDonough & Sun (1995). LM for lithospheric mantle.

wt percentage	Archean LM	Proterozoic LM	Phanerozoic LM
SiO_2	45.7	44.7	44.5
Al_2O_3	0.99	2.1	3.5
FeO	6.4	7.9	8.0
MgO	45.5	42.4	39.8
CaO	0.59	1.9	3.1
Na_2O	0.07	0.15	0.24

in their misfit maps. Particularly, the Archean compositions exhibit a large and positive anomaly towards the south-east of the study area (Congo basin). Apart from this discrepancy, the gravity anomaly does not display significant variations between the three mantle types.

Examining the topography, it becomes more evident that the Archean type (Figure 17, A) is not a suitable fit compared to the other two mantle types. This is evident as its modelled topography strongly underestimates the known topography, except for mountainous regions. Certain areas such as cratons and parts within the rifts are situated well below sea level, reaching depths of up to -600 meters in some locations, which is unrealistic. The corresponding misfits and statistical analysis reveal the significant disagreement of the Archean type with the observed topography, while also highlighting how well the Proterozoic (Figure 17, B) and Phanerozoic (Figure 17, C) types align with the observed signals.

From a technical standpoint, the gravity and topography results indicate that the Archean lithospheric mantle type should not be considered for further analysis.

Heat flow and Moho depth

Upon further analysis of parameters such as heat flow and Moho depth, significant differences were observed between the Proterozoic and Phanerozoic lithospheric mantle and the expected values.
Regarding the Proterozoic lithospheric mantle, the heat flow (see Figure 18, A) ranging from 48 $mW.m^{-2}$ to 52 $mW.m^{-2}$ in the cratonic zones was deemed reasonable. However, the heat flow across the rift area was very low and did not align with expectations, as displaying similar values across the Congo craton, except over the highland zones. On the other hand, the Phanerozoic (Figure 18, B) showcased a suitable range of heat flow (54 $mW.m^{-2}$ - 64 $mW.m^{-2}$) in the rift zone but unsatisfactory values across the cratons, which seemed generally warmer than the rift zone. As a result, this analysis indicated that the Proterozoic

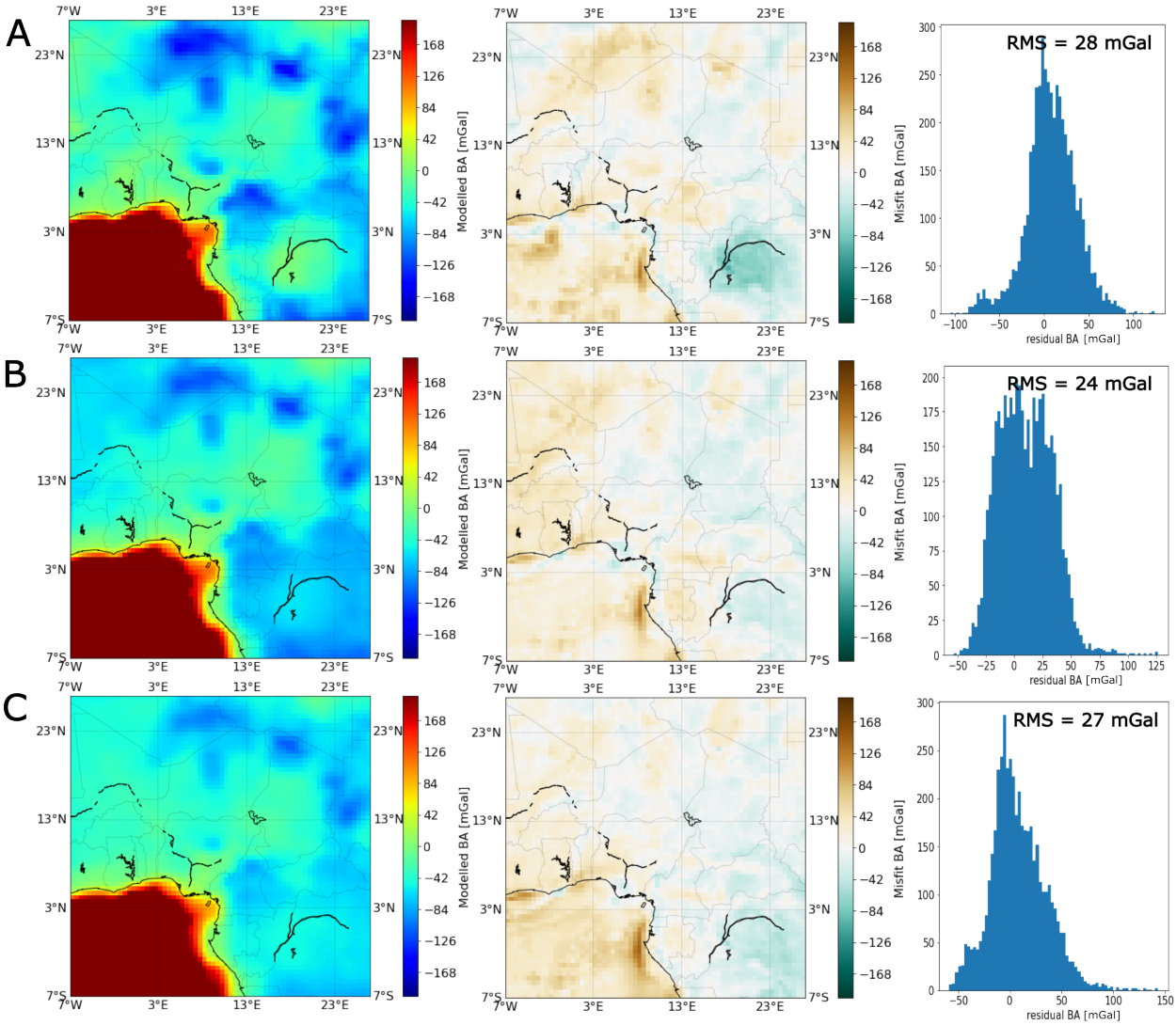

Figure **3-16**: Modelled Bouguer anomaly for homogeneous mantle, their misfit to the measured Bouguer anomaly (shown in Figure 2) and the associated residual diagram. **A** represents the result for the Archean type, **B** Proterozoic type, and **C** the Phanerozoic type.

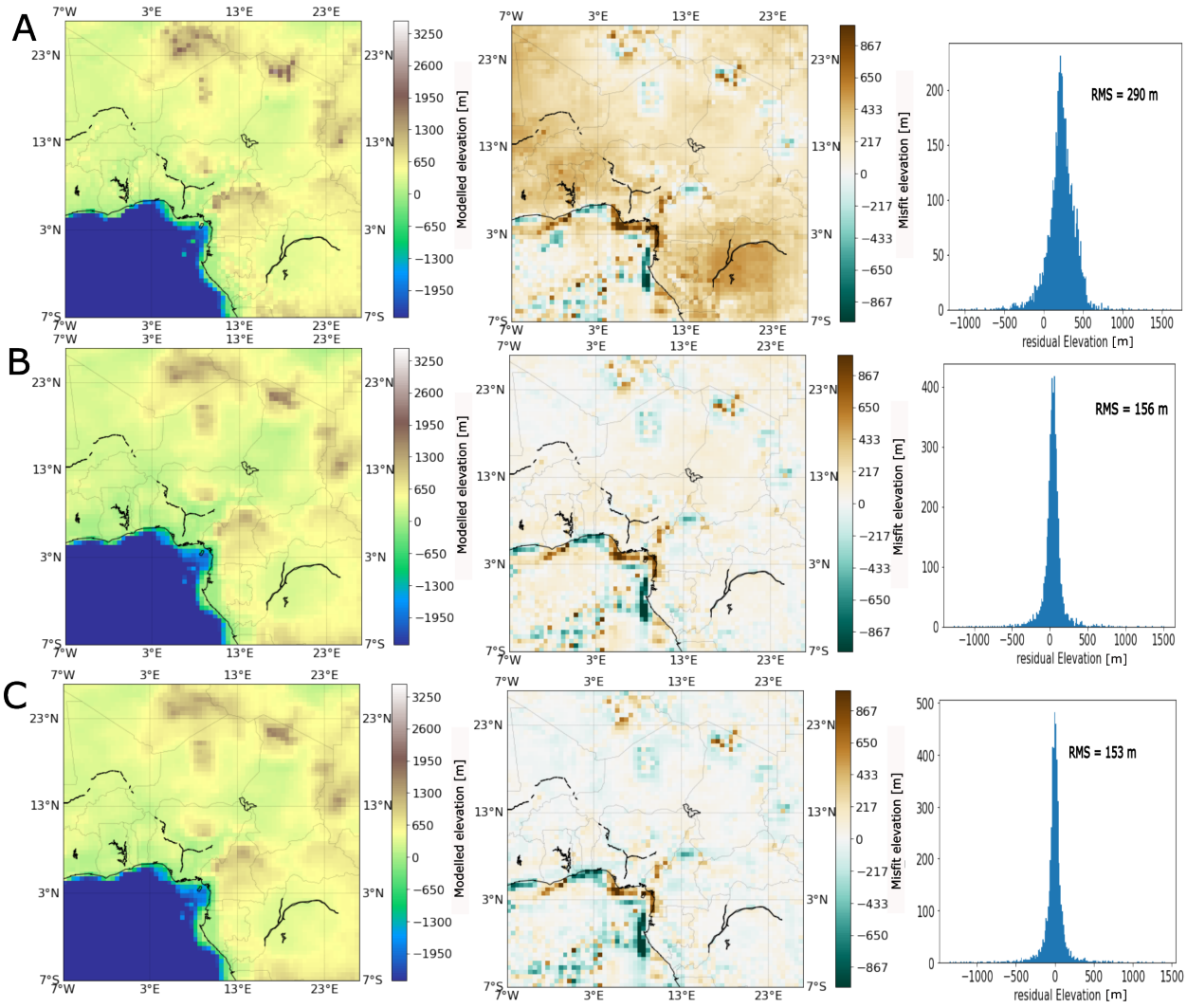

Figure **3-17**: Modelled topography for homogeneous mantle, their misfit to the measured topography (shown in Figure 2) and the associated residual diagram. **A** represents the result for the Archean type, **B** Proterozoic type, and **C** the Phanerozoic type.

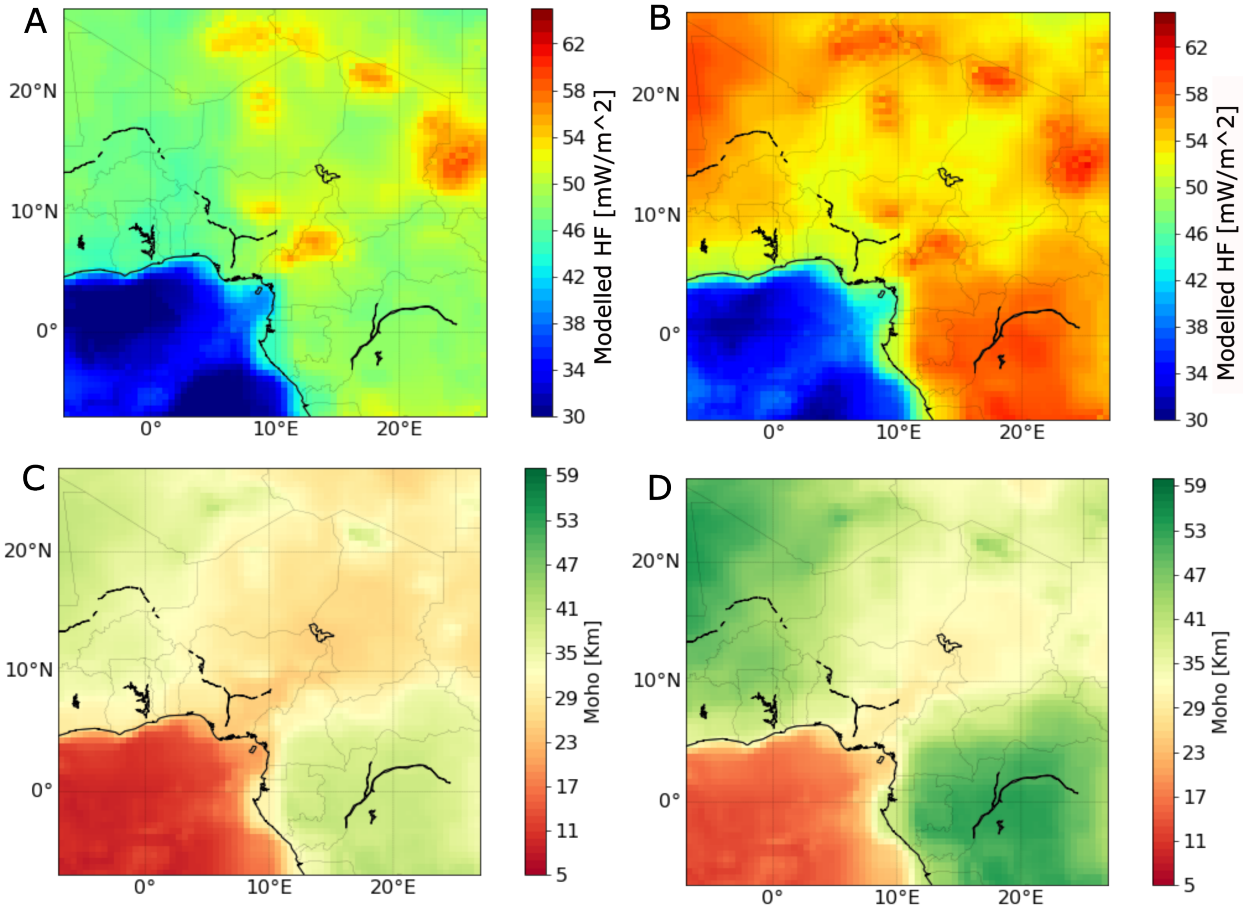

Figure **3-18**: **A** and **B** are the modelled heat flow in the case of Proterozoic and Phanerozoic types respectively, **C** and **D** represent the modelled Moho depth in the case of Proterozoic and Phanerozoic types respectively.

type was more suitable for the craton areas while the Phanerozoic type was better suited for the rift zone. Additionally, the Moho in too shallow range across the rifts for the Proterozoic lithospheric mantle and in too deep range across the cratons for the Phanerozoic lithospheric mantle, compared to the expected values, further reinforced the idea of dividing the study area based on the type of lithospheric mantle.
In summary, this case study has led to a reevaluation of the study area, no longer considering it as homogeneous but rather as heterogeneous, with Proterozoic type prevalent across the cratons and Phanerozoic type dominant across the rift zones.

3.B Stretching factor

As shown by Svartman Dias et al. 2016 and Allen & Allen 2013, the stretching factor s, $s = 30 * Moho^{-1}$ can help to investigate the deformations that faced the crust. We show

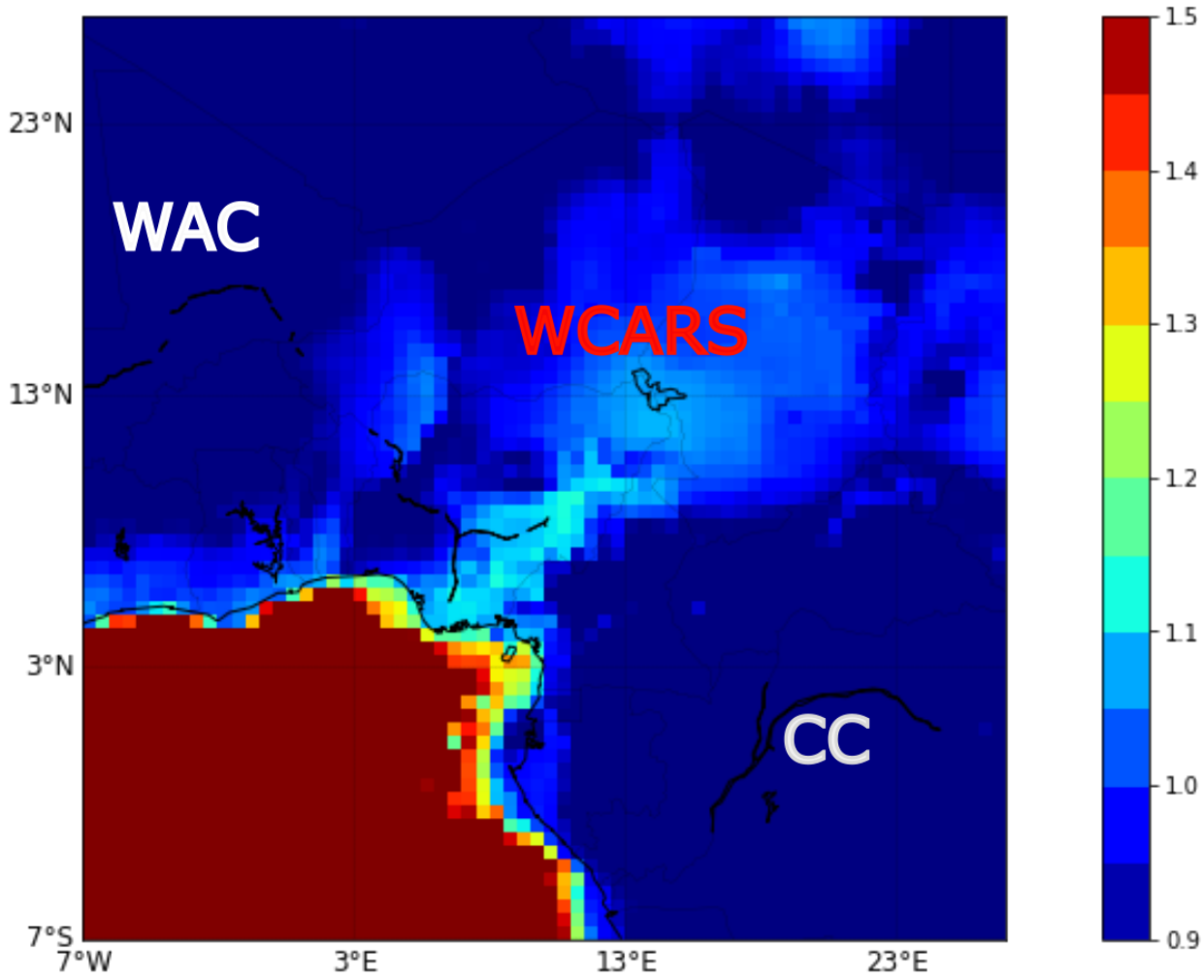

Figure **3-19**: Stretching factor

below the stretching factor of the crust over the study area. We can see that range of the stretching factor inside the WCARS is well in agreement with a passive origin (Figure 19).

Open research

The data and code files used in this paper are available at (Fosso Teguia M et al. 2023 and Fosso Teguia M et al. 2024*b*).

Acknowledgments

This study has been funded by the Deutsche Forschungsgemeinschaft (DFG, German Research Foundation) – 441292957. We thank the editors and the reviewers for their construc-

tive comments on the earlier version which has permitted to greatly improve the manuscript.

4 Crustal modelling across the west and central African rift system, based on gravity, magnetic and seismic data - Implications for the origin of the Bangui magnetic anomaly.

Estelle Eric Fosso Téguia M.; Jörg Ebbing; Eyike Albert; Alain Tokam; Gaelle Vanessa Nana; Matthew Tankersley
Tectonophysics, submitted

Abstract

The west and central African rift system (WCARS) extends over several geological domains, including shear zones, volcanic regions, and sedimentary basins, and is home to key geological features such as the Cameroon Volcanic Line (CVL) and the Bangui Magnetic Anomaly (BMA). Despite numerous studies, the detailed crustal structure of WCARS is yet to be fully understood. This work presents a comprehensive 3D crustal study that integrates gravity, magnetic, and seismic data, offering insights into the region's tectonic framework, rift dynamics and formation of the BMA. The coupled analysis of density, susceptibility, and topographic data reveals five distinct tectonic units, providing a refined understanding of

crustal composition and structure. Analysis of cross-sections along key transects over the study area demonstrates the impact of rifting and magmatic activity on crustal thinning and density distribution. The Central African Shear Zone (CASZ) and Kandi Shear Zone (KSZ) are identified as key reactivated fault zones that have influenced the spatial distribution and evolution of rift systems. The study also highlights the role of magmatism, driven by mantle upwelling, in modifying crustal properties, particularly in volcanic regions like the CVL and Benue trough. Our findings suggest a common tectonic origin for the CVL, Benue trough, and BMA, with felsic and plutonic intrusions contributing to the formation of the BMA. These results enhance our understanding of the tectonic and geodynamic evolution of the WCARS, emphasizing the role of preexisting structures and magmatism in shaping the region's rift architecture.

4.1 Introduction

The West and Central African Rift System (WCARS) has intrigued geophysicists and geologists for decades (Milelli et al. 2012; Eyike & Ebbing 2015; Eric et al. 2020; Fairhead 2023). This extensive rift system, which stretches from the Gulf of Guinea to the Sudanese border (Figure 1), has been a focal point for studies aiming to understand its formation, evolution, and the underlying crustal structure. The WCARS is characterized by complex tectonic processes and diverse geological structures including prominent rift basins such as the Benue trough, the Chad Basin, the Central African Shear Zone (CASZ), and the Kandi Shear Zone (KSZ). Additionally, many volcanic structures as the Cameroon Volcanic Line (CVL) but also the Bangui Magnetic Anomaly (BMA, Fairhead & Binks 1991) are part of the WCARS. The BMA is globally one of the most prominent magnetic anomalies (Girdler et al. 1992).

First insights into the lithospheric-scale architecture have been presented by Fosso Téguia M et al. (2024*a*), where a 3D density model of the WCARS with emphasis on the mantle structure was provided. The model, based on integrated geophysical-petrological modelling, revealed variations in the lithospheric density and composition from the rift to the surrounding cratons.

In this study, we aim to extend that previous model by studying density and magnetic susceptibility distribution across the WCARS, at the crustal scale. The new model is derived from a combination of gravity anomaly, magnetic anomaly, seismic velocity data and key geological information in order to provide a geological interpretation that aligns with the broader tectonic framework of the region.

To achieve our goal, we perform crustal density and susceptibility 3D modellings across the WCARS, and link the model outcomes to identify distinct geological structures and compare them with known geological features along 2D profiles.

4.2 2- Tectonic Setting and Earlier Geophysical Studies

The WCARS (Figure 1A) is a major geological feature that extends across several countries in Africa. The rift system is characterized by a complex interplay of tectonic processes that have shaped its evolution over millions of years (Fairhead & Binks 1991).
The WCARS comprises several rift segments, including the Benue trough, the Chad Basin, the CASZ and the KSZ. The Benue trough, a major component of the WCARS, extends from the Niger Delta inland and is divided into the Upper, Middle, and Lower Benue troughs (Guiraud & Maurin 1992; Obaje et al. 2009). The rift system is bordered by the Precambrian basement complexes of the West African Craton to the west and the Congo craton to the south. The sedimentary basins within the WCARS are filled with a thick sequence of Mesozoic to Cenozoic sediments, primarily deposited during phases of rifting and subsidence (Burke 1976; Fairhead & Binks 1991). However, the amount of sedimentary infill is not precisely known. It is generally accepted that the tectonic evolution of the WCARS is linked to the breakup of Gondwana and the opening of the South Atlantic Ocean. Early studies by Burke et al. (1973) and Whiteman (1973) and Burke (1976) suggested that the rifting began in the Late Jurassic to Early Cretaceous as a result of extensional forces associated with the separation of South America and Africa.
Fairhead & Green (1989) highlighted the role of preexisting structural weaknesses in the Precambrian basement in localizing the rift zones. During the Cretaceous, the WCARS experienced extensional tectonics, leading to the formation of deep rift basins and extensive volcanic activity. Djomani et al. (1995) and Guiraud & Maurin (1992) noted that the rifting was accompanied by crustal thinning and high heat flow, which influenced the thermal and mechanical properties of the lithosphere. This period also saw the development of major fault systems, the emplacement of igneous intrusions and the formation of the interconnected Benue trough, CVL and BMA (Fairhead & Binks 1991) which contributed to the complex geological architecture observed today.
The crustal structure of the WCARS has been previously studied using seismic, gravity, and magnetic datasets. For example, Tokam et al. (2010) used seismic data to map variations in crustal thickness and identified zones of high and low velocity, which correspond to different lithological and structural units.
Eyike & Ebbing (2015) used gravity data to model the crustal thickness and mapped its variations across Cameroon. Ghomsi et al. (2022) combined gravity and seismic data to explore the crustal configuration of the WCARS and identified regions of high-density mafic intrusions and lower-density sedimentary deposits, providing first order insights into the compositional heterogeneity of the crust. These earlier studies revealed lateral heterogeneity in the crust, with thinner crust beneath the rift basins and thicker crust beneath the surrounding cratons.

Studies like those by Ravat et al. (1992) investigated the BMA in the context of regional tectonics. The researchers suggested that the BMA might relate to ancient tectonic events,

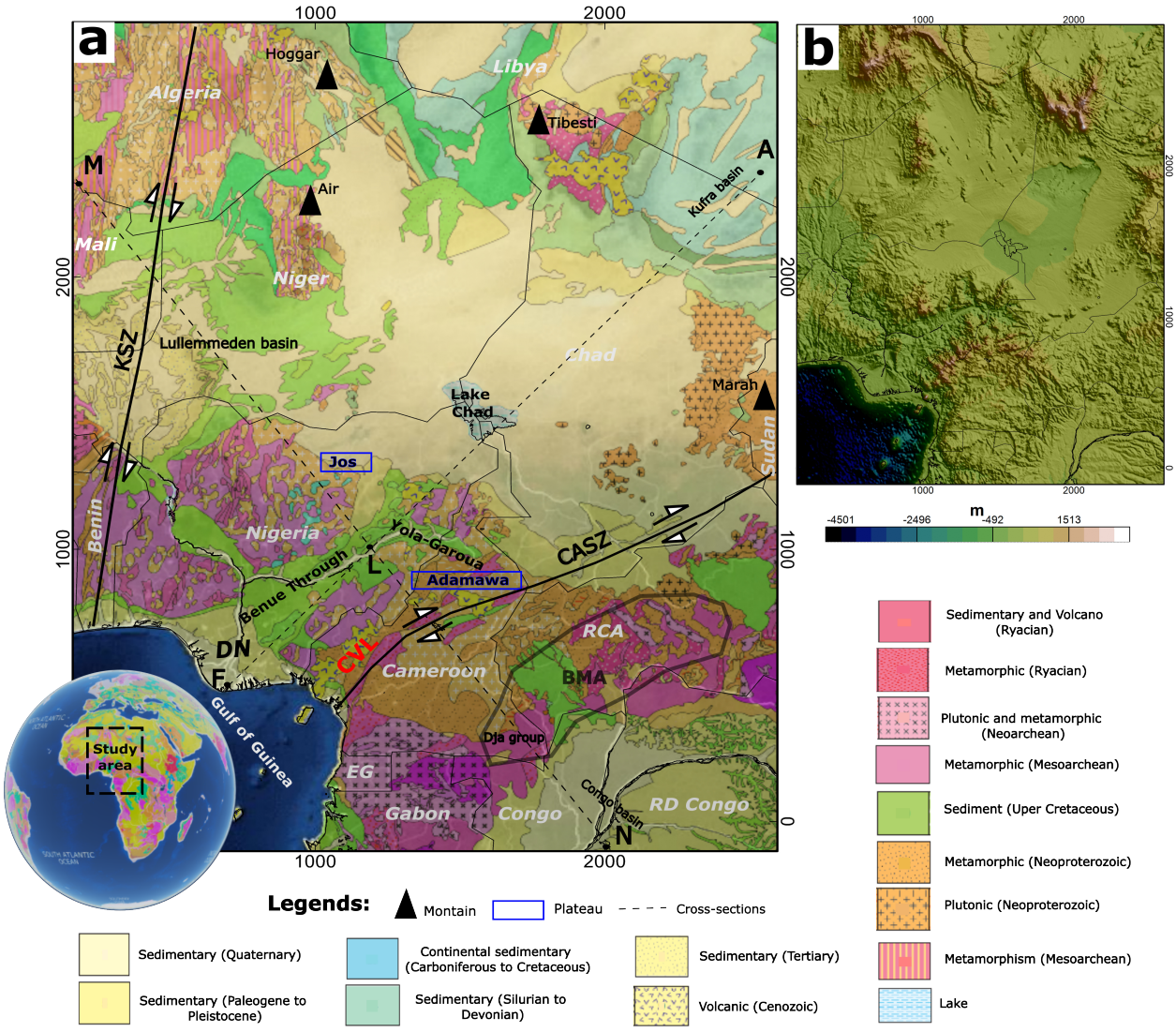

Figure **4-1**: **a** Geology of the study area modified from Onegeology (https://onegeology.org/), Fairhead (2023). DN: Delta of Niger, CVL: Cameroon volcanic line, CASZ: Central African shear zone, KSZ: Kandi shear zone, BMA: Bangui Magnetic Anomaly. FA and MN are the cross sections we will display from the model, and L their intersection. **b** Topography of the study area, from SRTM30 Plus v7 (Becker et al. 2009).

including the breakup of supercontinents like Rodinia and Gondwana. The anomaly is believed to be associated with a major crustal feature that possibly represents an ancient, stable cratonic area or the remnants of past tectonic interactions. In addition, Ravat et al. (2002) analyzed satellite magnetic data over the BMA using gradient analysis methods. They implemented Euler deconvolution and analytic signal techniques, and define the depth and orientation of magnetic sources within the BMA, although the depth resolution of these findings were limited by the high altitude of satellite data. Recently, Njiteu (2022) made the hypothesis that the origin of the BMA could have been influenced by tectono-magmatic events dating back to the Archean and Proterozoic eons, possibly linked to the Congo Craton's ancient lithospheric structures.
Fairhead (2023) compiled gravity and magnetic data over Africa to discuss the tectonic processes driving the evolution of the rift system. The Author presents a comprehensive analysis of the anomalies associated with the WCARS, where he interpreted these in terms of crustal structure and composition, revealing variations in crustal thickness, density, and magnetic properties across the region. However, given the complex and intricate tectonic history of the WCARS, the question of the density-susceptibility distribution in relation with the tectonic development of the WCARS, as well as the origin of the BMA and its relationship to other major features inside the region remain open.

Recently, Fosso Téguia M et al. (2024*a*) integrated geophysical and petrological data to produce a thermal and compositional 3D model of the lithosphere of the WCARS and adjoining cratons. They described the CVL's origin as the consequence of the V-shaped extension of the lithospheric mantle beneath the WCARS following the breakup of the Gondwana, and the lithosphere-asthenosphere boundary's variation at the transition from the WCARS to the Congo craton. They concluded that the CVL and the Benue trough were formed together during the same tectonic event. In this work we are going to refine that lithospheric model by describing the crustal layer in more details.

4.3 Data

The primary datasets include gravity, magnetic and seismic velocity. Furthermore, we make use of the thermal-compositional 3D lithospheric model presented in Fosso Téguia M et al. (2024*a*). The methodology allows us to integrate these data sets.

4.3.1 Gravity and Elevation Data

The topography is taken from the model SRTM30 Plus v7 (Figure 1B) of Becker et al. (2009). It contributes to the understanding of the tectonic evolution of the region, but also is used to calculate the topographic effect for gravity reduction. The gravity anomaly anomaly is taken from the global Earth model XGM2019e (Zingerle et al. 2020). From the model the free-air

anomaly at 5 km high is calculated (Figure 2a). With the tesseroid software package (Uieda et al. 2016) the gravity effect of the topography is calculated and subtracted to calculate the Bouguer anomaly (Figure 2b). The correction is performed considering densities of 2670 kg/m^3 for rock and 1030 kg/m^3 for water.

We also excluded the gravitational mantle contribution from the Bouguer anomaly by calculating the gravity effect of the mantle (Figure 2c) from the density model by Fosso Téguia M et al. (2024*a*). This was accomplished by taking the density distribution of the lithosphere, each density voxel inside the mantle was replaced by its density anomaly by considering 3300 kg/m^3 as reference value. Simultaneously, density voxels inside the crust were replaced by 0 kg/m^3 (Figure 3). Hence, it becomes possible to forward calculate the mantle's gravity anomaly. This was then subtracted from the Bouguer anomaly to give the residual anomaly attributed to crustal sources (Figure 2d).

4.3.2 Magnetic Data

Two different magnetic data sets have been used in this study. We have namely used the satellite model LCS-1 having a resolution of 110 km (Olsen et al. 2017) and the global magnetic anomaly model EMAG2 based on data from CHAMP, marine, airborne, and ground magnetic surveys, with an apparent resolution of 4 km (Maus et al. 2009) (Figures 4a and 4b). Please note, that while EMAG2 is provided on a 4 km grid, in parts of the study area no data or only data with larger point distance were available. To obtain a robust toolset for magnetic studies, LCS-1 was low-pass filtered, with a cutoff wavelength of 300 km, while the EMAG2 data was high-pass filtered using the same cut-off wavelength, and added to each other (Figure 5) (e.g. Hemant et al. (2007)). This synergy is particularly valuable for interpreting multi-scale geological features, reducing uncertainties, and improving the depth resolution of magnetic anomalies, suitable for understanding the interplay between shallow and deep structures over the WCARS' region.

The study region is close to the magnetic equator, but due to stability issues related to GY-MSYS 3D, the magnetic data have been reduced to the pole (RTP). This step corrects for the inclination (3.85°: inclination mean value over the study area) and declination (1.5°: declination mean value over the study area) effects of the Earth's magnetic field and simplifies the interpretation of magnetic anomalies. To make sure that no artefacts appear during the reduction to the pole, the final model has been tested by forward calculating not using the pole characteristics, but the exact field orientation. As we will see below, the resulting magnetic signal fits the original signal, implying that the meaning of the original data has not been altered by the reduction to the pole.

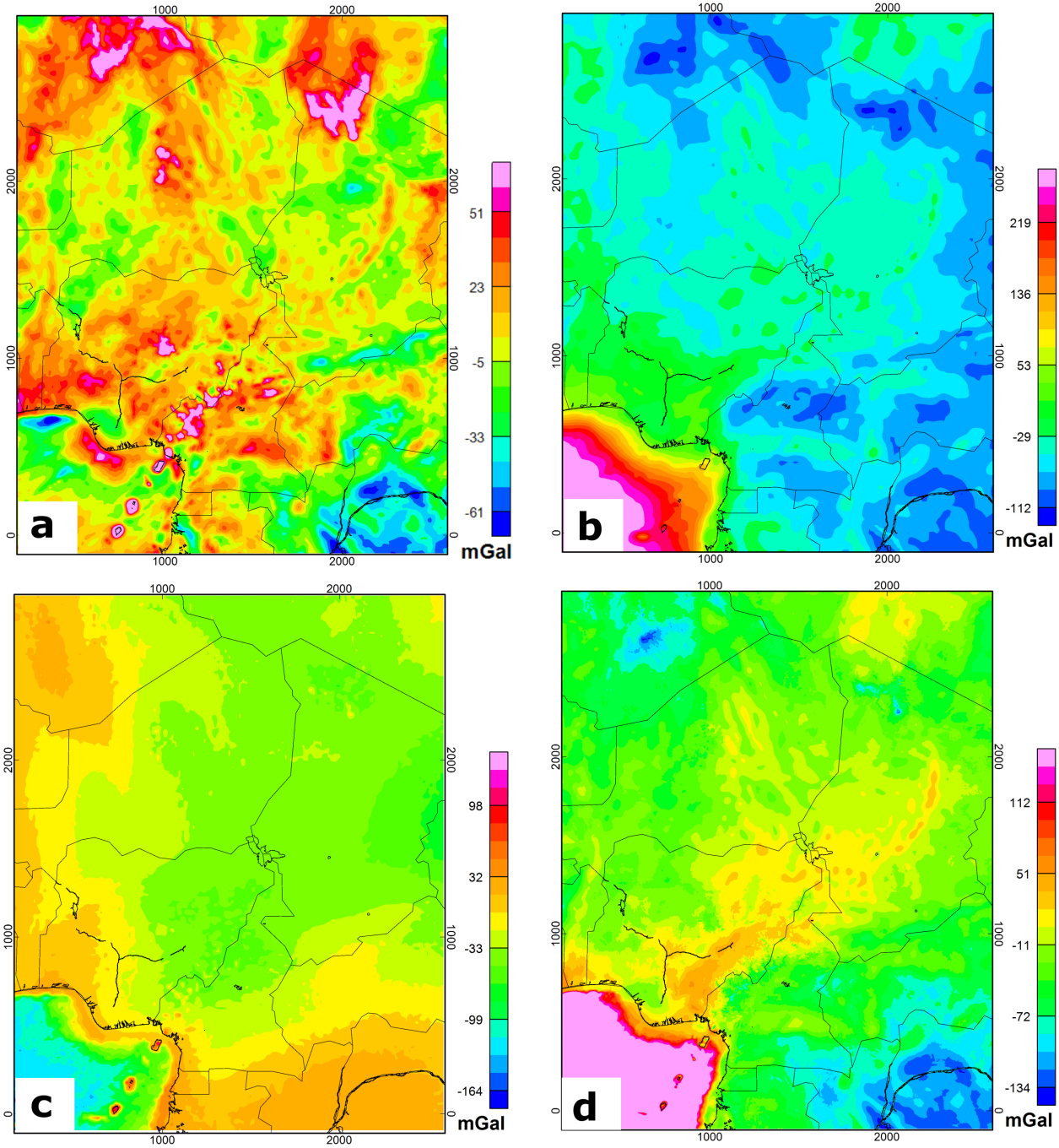

Figure **4-2**: **a** Free air anomaly from XGM2019e, **b** Bouguer anomaly, **c** Mantle gravity effect, **d** Crustal gravity anomaly, obtained by subtracting the mantle gravity effect from the Bouguer anomaly.

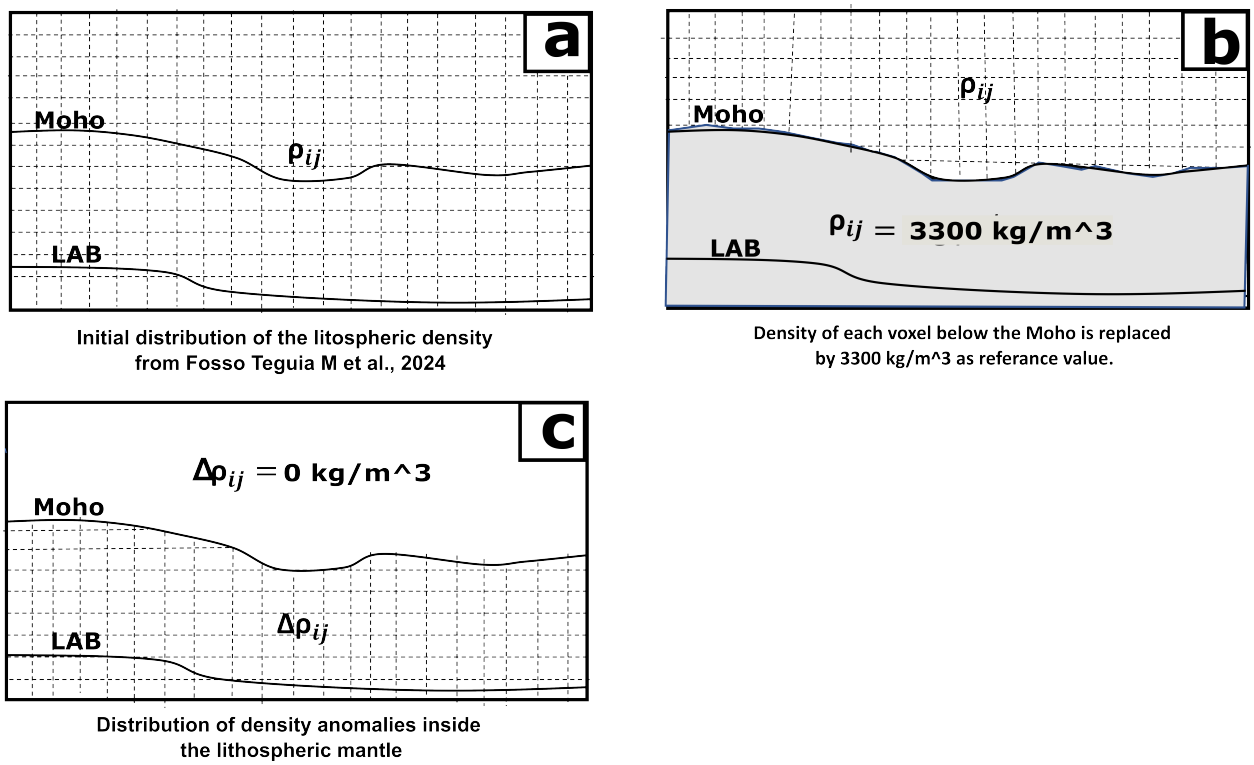

Figure **4-3**: Isolation of density anomalies located inside the lithospheric mantle. **a** The initial distribution of density voxels over the entire lithosphere from Fosso Téguia M et al. (2024*a*). **b** The reference values of density inside the mantle layer ($3300 kg/m^3$), and distribution of initial density voxels inside the crust. **c** The difference between a and b, providing the density anomalies located inside the mantle.

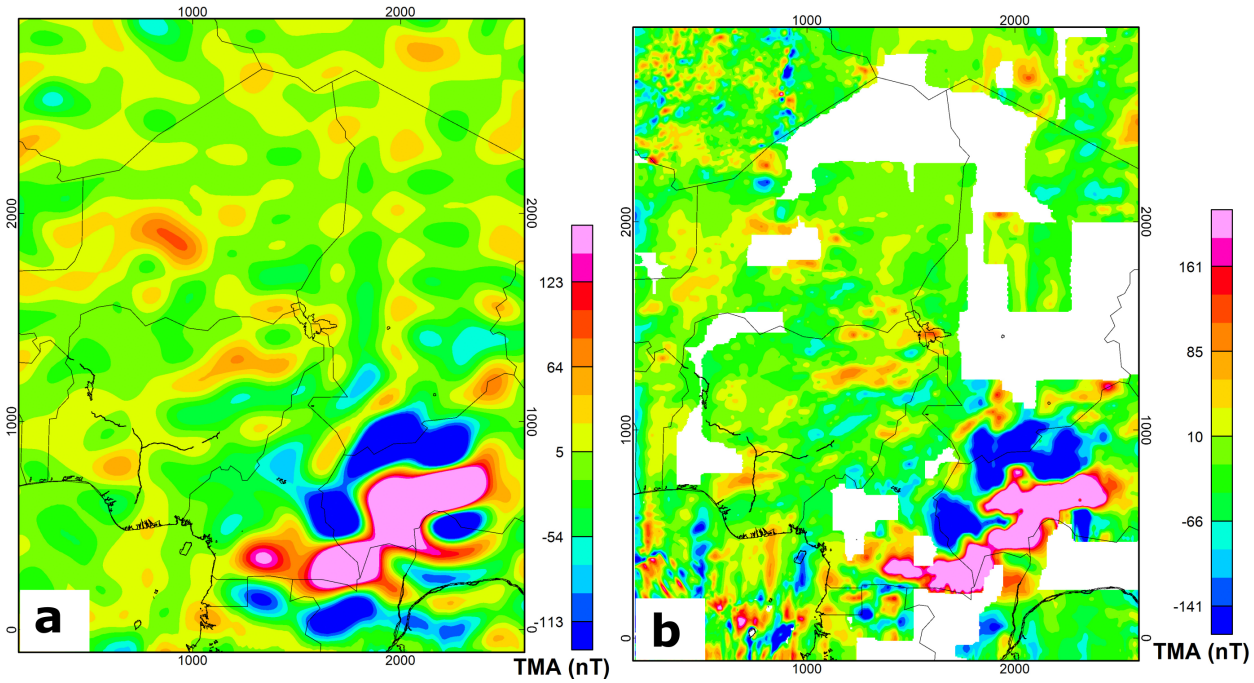

Figure **4-4**: RTP of magnetic datasets. **a** Satellite data (LCS-1), **b** Airborne data (EMAG2, version 3).

4.3.3 Structural Model and Additional Data

The Moho depth (Figure 6a) is from the integrated thermal-compositional 3D model by Fosso Téguia M et al. (2024*a*) and the sediments depth (Figure 6b) is from the model Crust1.0 (Laske et al. 2013).

To estimate possible density variations inside the lower crust (below 20 km) (Table 1. and Figure 10), the mean shear wave velocity (Vs) in that layer over the Cameroon area, provided by Tokam et al. (2010), have been converted to densities. The conversion process from seismic velocity to density has been done using the linear relationships between the density and the P-wave velocity (Equation 1) of Christensen & Mooney (1995). Coefficients a and b are depth dependent ($< 15km$, 15-25 km, 26-35 km, 36-45 km and 46 $km <$) and are given by Zoback & Mooney (2003). However, that relationship requires P-wave velocities and therefore the S-wave velocities from Tokam et al. (2010) have first been converted into P-wave velocities using Equation 2 (Sheriff & Geldart 1995) and assuming a Poisson's coefficient of $= 0.25$ (generally holds by more silica-rich materials like granitic compositions (Christensen 1996, Schön 2015), expected in the rift's lower crust).

(1)

$$\rho = a + b(V_{\mathrm{p}})$$

Where rho represents the density, V_{p} the P-wave velocity, a and b the regression coefficients for velocity-density relationship in crystalline rocks.

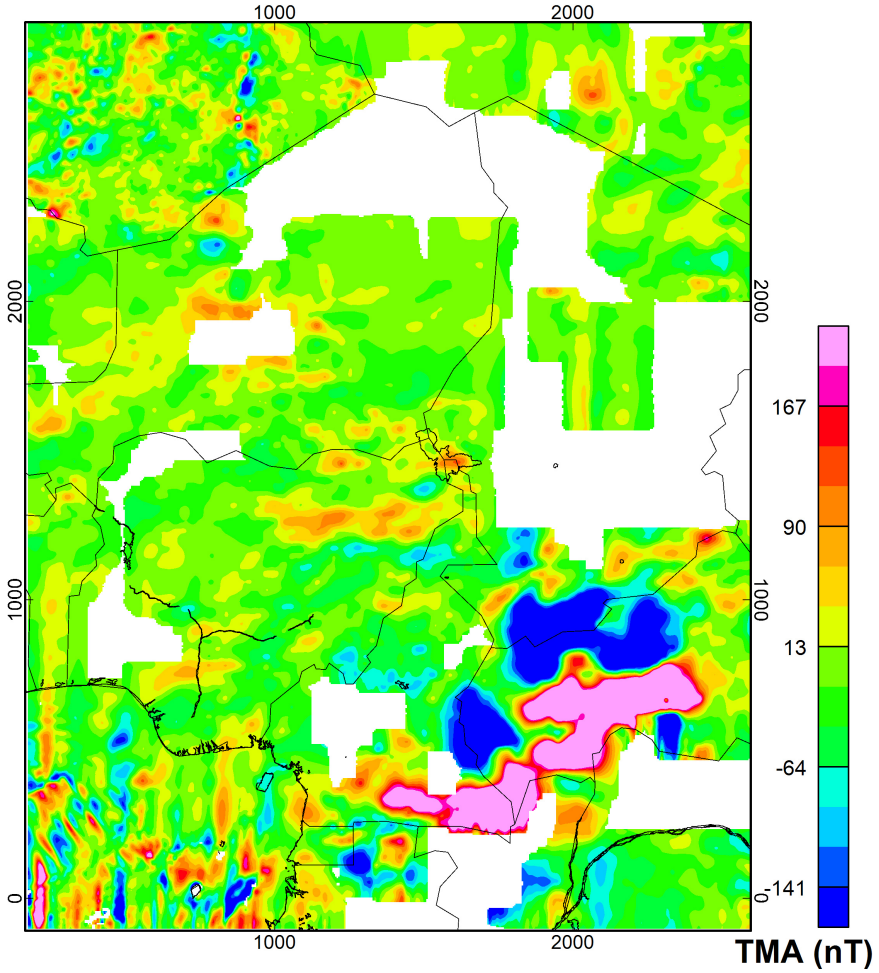

Figure **4-5**: RTP of LCS-1 and EMAG2 combined after low-pass and high-pass wavelength filtering respectively. We have kept gaps in the data to avoid the presence of resolution differences within the processed dataset.

(2)

$$V_{\mathrm{p}}V_{\mathrm{s}}^{-1} = \sqrt{2(1-\sigma)(1-2\sigma)^{-2}}$$

Where σ represents the Poisson's coefficient, V_{s} the S-wave velocity.
Moreover, that value of σ corresponds to $V_{\mathrm{p}}V_{\mathrm{s}}^{-1} = 1.73$ which is in agreement with the results of Gallacher and Bastow (2012), who obtained a mean value of $V_{\mathrm{p}}V_{\mathrm{s}}^{-1} = 1.74$ with possible error of 0.06 across the Cameroon area. In doing so, the variation of the shear wave velocity had been related to variations in the composition and thermal state of the lower crust and upper mantle, and attributed to regional tectonic processes, including rifting, magmatic activity, and the influence of the Cameroon Volcanic Line (Tokam et al. 2010). That study noted that areas with lower Vs values are likely associated with zones of partial melting or higher temperatures, while regions with higher Vs values may be characterized by cooler and more rigid lithosphere (Tokam et al. 2010).
As shown by Fosso Téguia M et al. (2024*a*), the north-western edge of the Congo craton extends into the south-eastern region of Cameroon (with a significant Moho depth), the Benue trough extends into the north (Yola-Garoua basin, with a shallow Moho depth), while the central zone of the country retains an intermediate Moho depth (see Figure 6a). We have used this tectonic diversity of Cameroon to extend the distribution of the lower crust density to the whole of the study area by following the depth of the Moho (Figure 7).

Table **4-1**: Lower crust density based on seismic velocity (Tokam et al. 2010) and Christensen & Mooney (1995) method to convert velocity to density.

Stations	Lon, Lat	Vs Tokam et al 2010	Vp	Md Tokam et al 2010	Md Fosso et al 2024	Sub-layers	Density	Mean density
01	9.8321, 2.3873	4.1	7.1	28	30	20-25	3109	3122
						26-30	3136	
02	13.2888, 2.6984	4.1	7.1	43	37	20-25	3109	3136
						26-35	3136	
						36-37	3136	
03	15.0344, 3.5190	3.9	6.7	43	37	20-25	2980	3001
						26-35	3002	
						36-37	3021	
04	11.9596, 2.9792	4.1	7.1	45.5	35	20-25	3109	3122
						26-35	3136	
05	9.9121, 2.9404	4.1	7.1	28	30	20-25	3109	3122
						26-30	3136	
06	11.2680, 2.3850	4.2	7.3	45.5	34	20-25	3174	3188
						26-34	3203	
07	11.4560, 3.8700	4.1	7.1	43	34	20-25	3109	3122

						26-34	3136	
10	10.6189, 4.2234	4.0	6.9	38	31	20-25	3044	3056
						26-31	3069	
11	13.1878, 3.9803	4.1	7.1	48	35	20-25	3109	3122
						26-35	3136	
12	11.6337, 4.4810	3.9	6.7	38	33	20-25	2980	2991
						26-33	3002	
13	9.4610, 4.5870	3.8	6.6	28	30	20-25	2914	2924
						26-30	2934	
15	9.9314, 5.0325	3.9	6.7	33	31	20-25	2980	2991
						26-31	3002	
16	10.5709, 5.4788	3.9	6.7	35.5	34	20-25	2980	2991
						26-34	3002	
17	12.3121, 5.5461	3.9	6.7	35.5	35	20-25	2980	2991
						26-35	3002	
18	9.3550, 5.7230	3.9	6.7	30.5	27	20-25	2980	2991
						26-27	3002	
19	11.2305, 5.9736	3.9	6.7	35.5	33	20-25	2980	2991
						26-33	3002	
20	10.0523, 6.2242	3.9	6.7	33	30	20-25	2980	2991
						26-30	3002	
21	12.6234, 6.4657	3.9	6.7	35.5	34	20-25	2980	2991
						26-34	3002	
22	13.2663, 6.4758	3.9	6.7	35.5	35	20-25	2980	2991
						26-35	3002	
23	10.7914, 6.3690	4.0	6.9	40.5	34	20-25	3044	3056
						26-34	3069	
24	14.2880, 6.5230	3.8	6.6	35.5	36	20-25	2914	2924
						26-35	2934	
25	11.8100, 6.7588	3.9	6.7	38	32	20-25	2980	2991
						26-32	3002	
26	13.5480, 7.2650	3.8	6.6	33	31	20-25	2914	2924
						26-31	2934	
27	12.6659, 7.3582	3.7	6.4	35.5	30	20-25	2849	2858
						26-30	2867	
28	13.2356, 8.4680	3.8	6.6	30.5	27	20-25	2914	2924
						26-27	2934	
29	13.3850, 9.3470	3.7	6.4	25.5	28	20-25	2849	2858
						26-28	2867	
30	13.9575, 9.7558	3.7	6.4	28	29	20-25	2849	2858

						26-29	2867	
31	15.2610, 10.3266	3.9	6.7	30.5	29	20-25	2980	2991
						26-29	3002	
32	14.3718, 10.6186	3.9	6.7	33	28	20-25	2980	2991
						26-28	3002	

4.4 Methodology

After description of data and data preparation in the previous section, this methodology section describes the work undertake in the results section. Our methodology consists of three main steps after data: 1) Upper crust density and susceptibility are individually inverted using GM-SYS 3D software. In the case of density inversion, the lower crust density is the one obtained by transformation of seismic velocity Vs. The background density for the inverted layer is set to 2670 kg/m3. The model itself incorporates several layers. From the top to the bottom, there are the sea level, the sedimentary's bottom provided by Crust 1.0 model, the upper-lower crust boundary (set at a constant depth of -20 km), and the Moho layer provided by Fosso Téguia M et al. (2024*a*). In the case of susceptibility inversion, the model configuration consists of a background magnetic susceptibility of 0 SI for the inverted upper crustal layer. The inducing magnetic field has a magnitude of 35253 nT, with an inclination of 90 degrees and a declination of 0 degrees. The model incorporates same boundary layers as in the density inversion.
2) Upper crust density, susceptibility and topography are coupled using Gaussian Mixture Model for clusters delimiting. Previous research has consistently demonstrated that Gaussian Mixture Models are highly effective for clustering combined geophysical data such as density and magnetic susceptibility within the Earth's crust (e.g. Lösing et al. (2023)). This approach allows for a better understanding of the subsurface, as it integrates multiple geophysical parameters to provide a more complex perspective. Such integration is particularly effective in resolving ambiguities that may arise when interpreting individual datasets, and it proves invaluable in regions with complex geological settings. The clustering process focused exclusively on the onshore domain.
3) Geological analysis performed with GM-SYS 2D software, considering the geological map, the clusters and the seismic density. At this step, a combination approach is adopted, where we superimpose information from the geological map (Figure 1A) accounting for the shallowest structures, from the clustering outcome (Figure 11) accounting for the intermediate layer, and from the density derived from velocity data (Figure 7) accounting for the deepest crust. This integration enables a more precise and constrained identification and description of geological blocks along cross-sections, FA and MN, which intersect at the Benue trough (point L), revealing not only lateral but also vertical heterogeneity.
Figure 8 gives a simplified overview of that workflow.

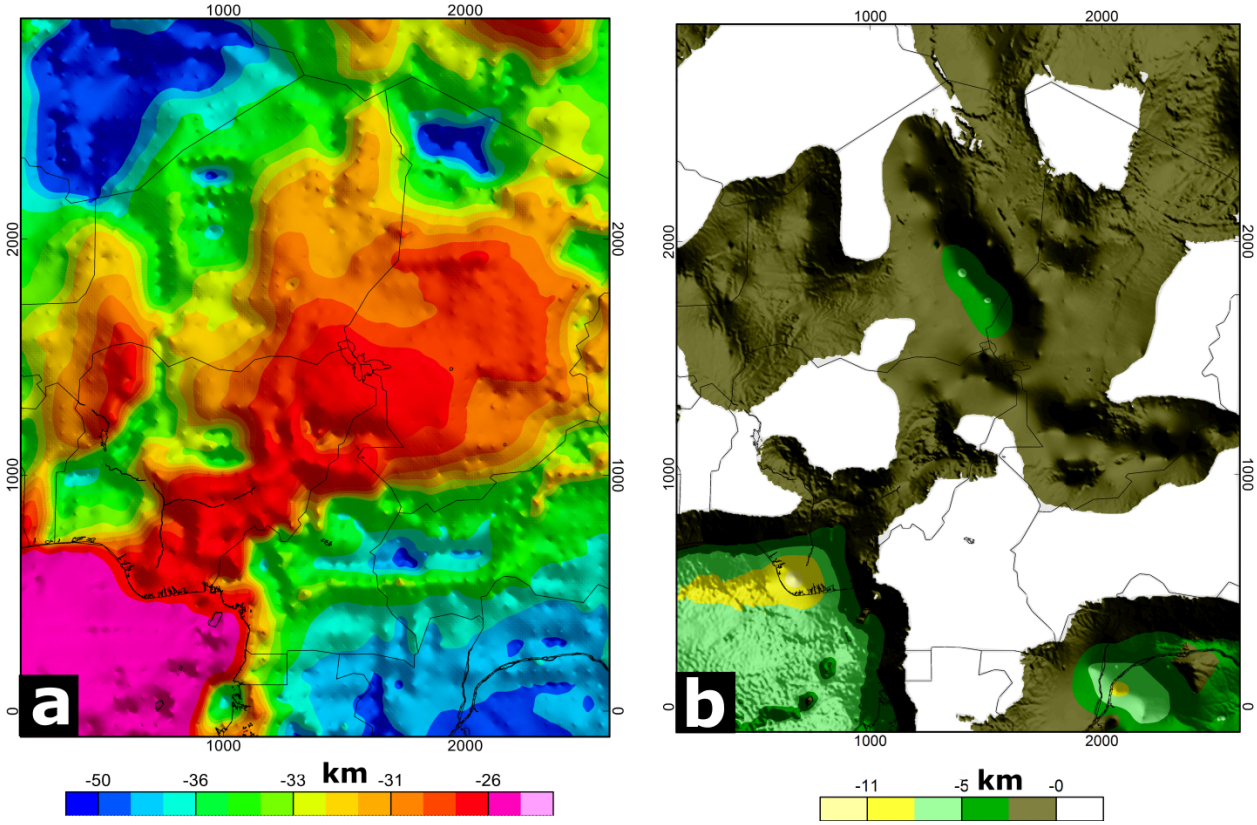

Figure **4-6**: a. Moho depth (Fosso Téguia M et al. 2024*a*), b. Sediment depth (after Crust 1.0, Laske et al. 2013) .

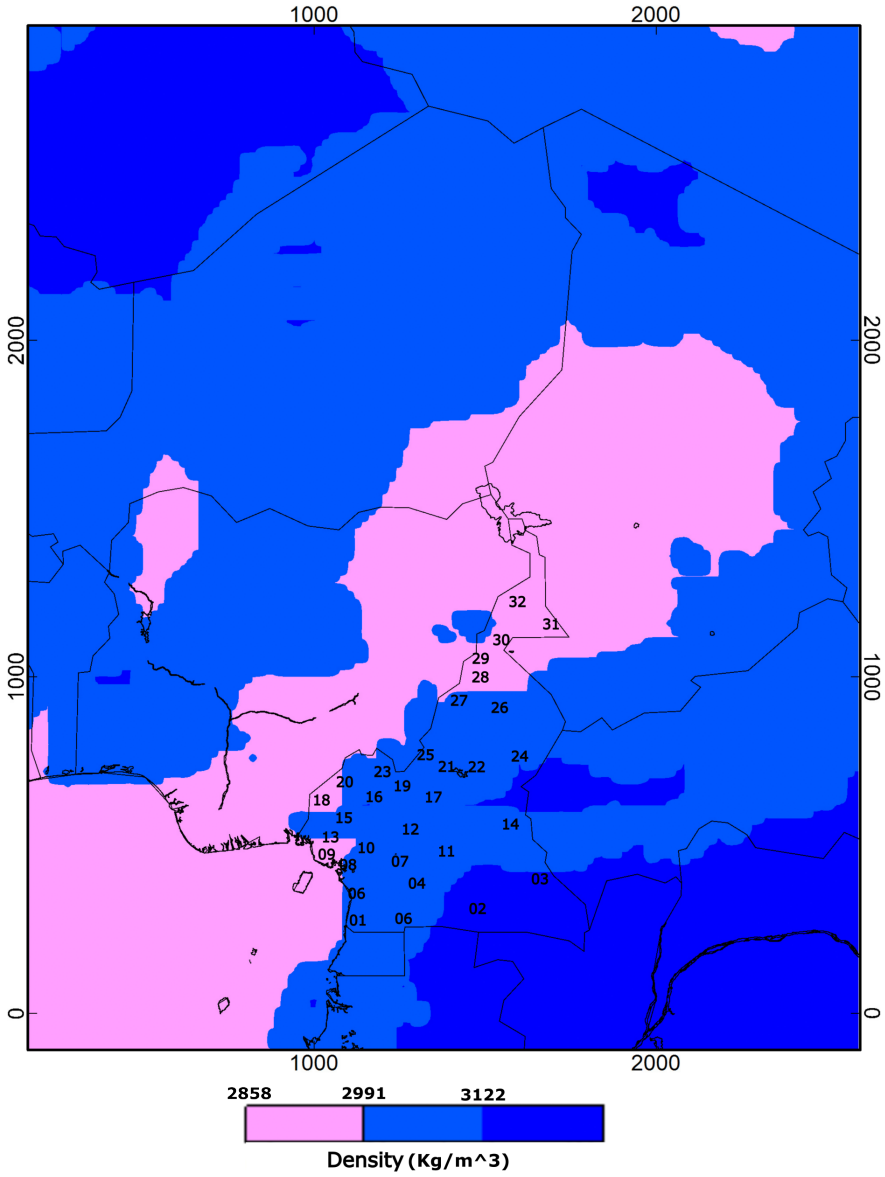

Figure **4-7**: Lower crust density. The interpolation of converted seismic velocity to density over the entire study area has been done in respect of the Moho depth sourced by Fosso Téguia M et al. (2024*a*).

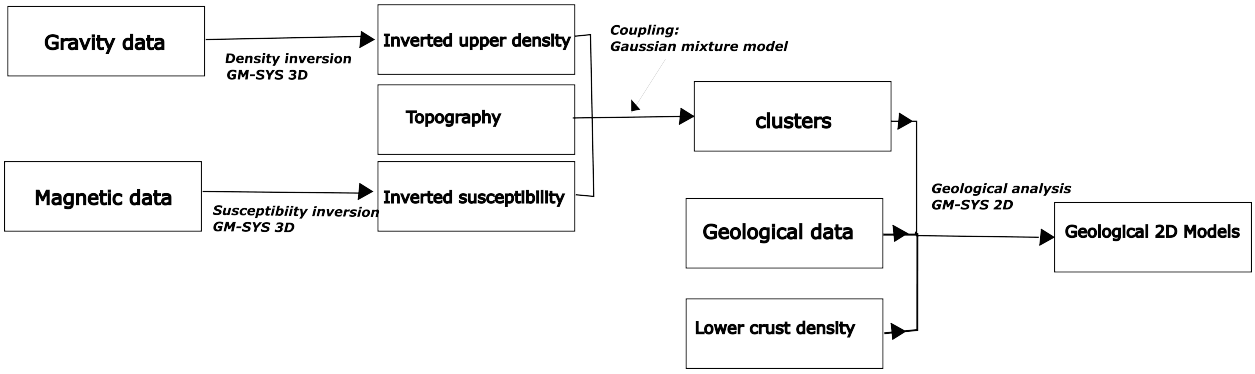

Figure **4-8**: Workflow

Table **4-2**: Statistic of the density inversion.

Gz	Minimum (mGal)	Maximum (mGal)	Mean (mGal)	Standard deviation
Observed	-140.68	524.48	-6.96	98.22
Forward calculated	-136.89	485.15	-6.95	97.52
Misfit	-116.90	97.14	0.13	3.66

4.5 Results

The 3D inversion of density and magnetic susceptibility has been conducted using GM-SYS 3D (Geosoft Inc., 2017). This approach yields delineations of lateral variations in the mean values of inverted parameters. Furthermore, integrated density-susceptibility 2D models have been produced using GM-SYS 2D, and aiming to give more realistic (not limited to lateral variations) interpretation of the WCARS' geological structure

4.5.1 Density Inversion

The crustal density modelling for the upper crust (from sediment's bottom to 20 km depth) offers a perspective on the lateral distribution of density across the study area (Figure 9). The corresponding gravity signal aligns well with the observed data, as evidenced by the minimal discrepancy between two of them (Table 2).
The inverted model is sufficiently able to reproduce the observed gravity data. The inverted upper crustal density variations reflect the tectonic and geological setting of the WCARS. Low upper crust density is found in the cratonic areas (stable and protected by the lithospheric mantle root), contrasted by high densities in the rift area, likely a result from crustal enrichment by magmatism during and after the WCARS stretching period.

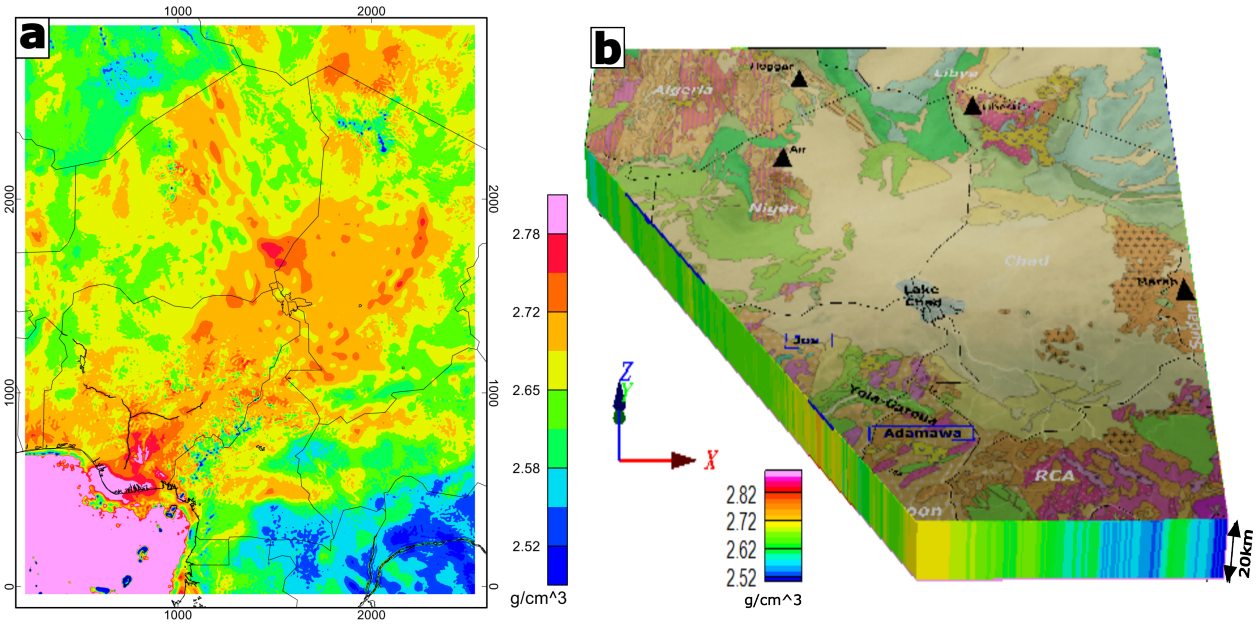

Figure **4-9**: Inverted 3D density of the upper crust. **a** is the 2D view of the model from the top, and **b** is the full 3D view. $\mathrm{Kg/m^3} = 1000 * g/cm^3$

Table **4-3**: Statistic of the susceptibility inversion.

B	Minimum (nT)	Maximum (nT)	Mean (nT)	Standard deviation
Observed	-581.4	1040.7	0.6	87.6
Forward calculated	-580.6	1042.1	3.6	77.8
Misfit	-116.85	142.90	-2.76	6.42

4.5.2 Susceptibility Inversion

Given that LCS1 encompasses the entire study area and exhibits more trusted quality compared to EMAG2 (Olsen et al. 2017; Thébault & Vervelidou 2015) in terms of consistency and reliability, the initial 3D modeling has been conducted using LCS1 as the target signal. The resulting inverted susceptibility model (Appendix A, Figure 1a) generated a Total Magnetic Anomaly (TMA) that closely aligns with the observed LCS1 data (Figure 4a), as evidenced by the favorable range of misfit between both of them (Appendix A, Table 1). However, the inversion results with only LCS1 notably lack short-wavelength information (Appendix A, Figures 1b and 1c). Hence, the combination of LCS1 and EMAG2 (Figure 5) has been used for the continued modeling process as target signal. The result of the susceptibility inversion (Figure 10), provides a corresponding signal in good agreement with the observed signal as displays inside Table 3.

The modeled susceptibility reveals prominent and positive values extending from the Re-

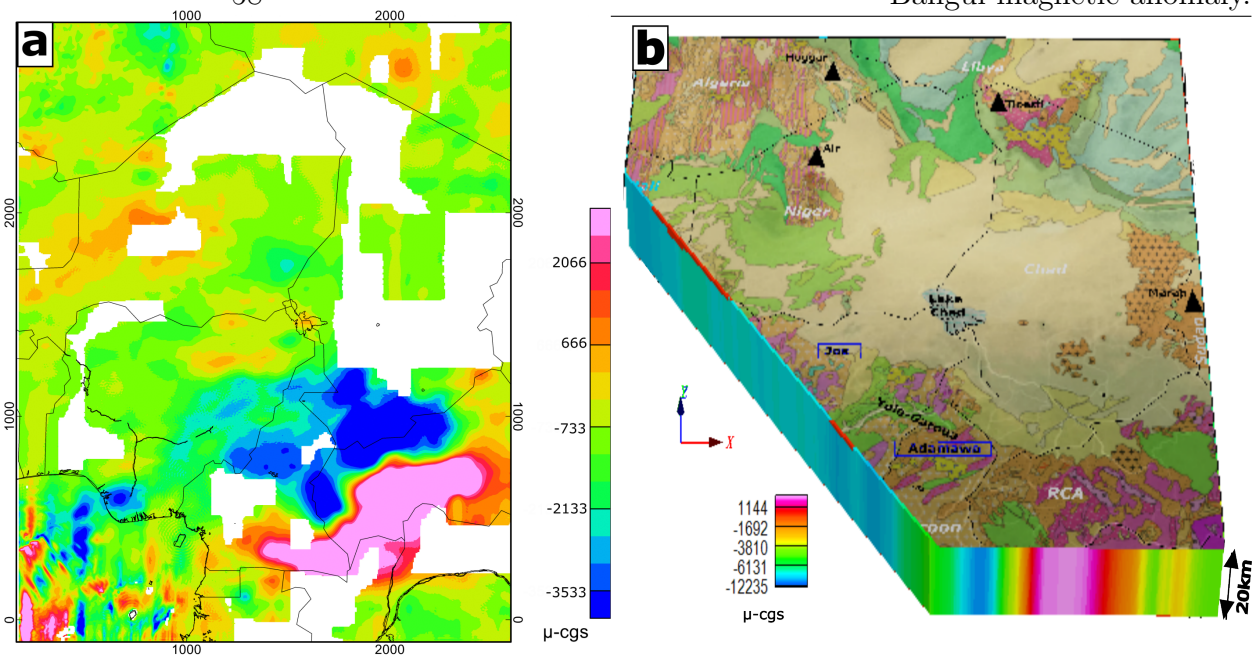

Figure **4-10**: Inverted 3D susceptibility of the upper crust. **a** is the 2D view of the model from the top, and **b** is its 3D view. μ-cgs $= 4 * 10^{-}6SI$

public of Central Africa (RCA) to southeastern Cameroon, aligning with the northern edge of the Congo craton.

4.5.3 Density and susceptibility coupling.

The clustering results, depicted in Figure 11, classify the upper crust of the WCARS into five distinct tectonic units, designated as C1 through C5, with their corresponding parameter values outlined in Table 3. Further details regarding the distribution of these clustering parameters can be found in Appendix B. The study area is predominantly characterized by cluster C4, which exhibits parameter values that are equal to or closely aligned with reference values. Cluster C5 aligns with the Benue trough, corresponding to the shallow Moho zone. C2 matches with high topography like the Adamawa plateau. C1 corresponds to the area of especial high magnetic anomalies (RCA-South Eastern Cameroon). C5 mainly covers the northern Congo basin.

4.5.4 Analysis and geological approach.

Cross-section FA.

Cross-section FA (Figure 12) traverses the longitudinal axis of the West and Central African Rift System (WCARS), intersecting structural features including the Benue trough, Lake Chad Basin, and Kufra basin. The lower crust beneath this profile exhibits relatively uni-

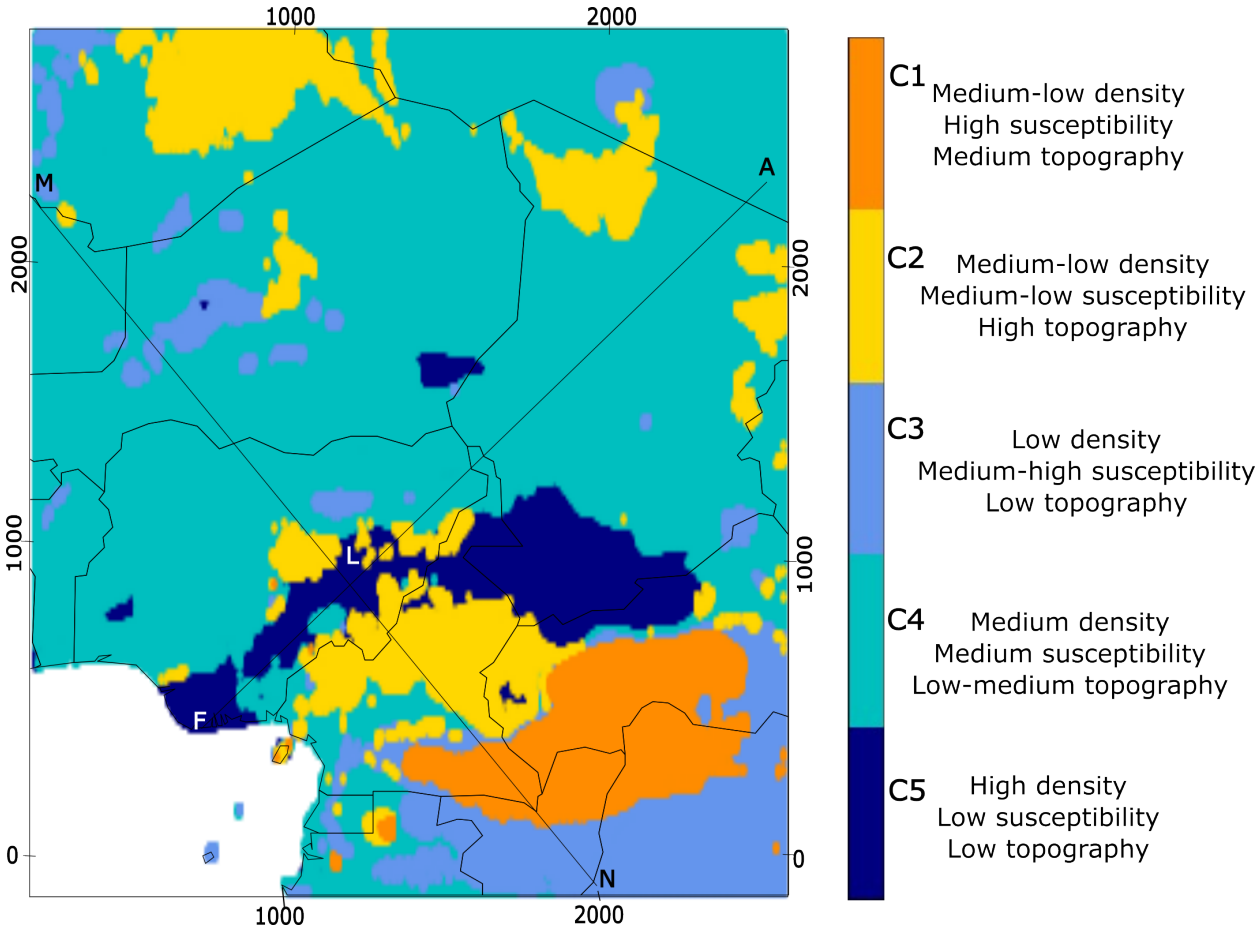

Figure **4-11**: Clusters. C1 to C5 represents the five possible groups delimited by the cluster analysis. MN and FA represent profiles for the next sections. L is their junction.

Table **4-4**: Average values of density and susceptibility for different clusters.

Cluster	Density [Kg/m3]	Susceptibility [SI]	Topography [m]
C1	2600	0.0754	450
C2	2630	-0.0251	1450
C3	2500	-0.0004	450
C4	2670	-0.0075	200
C5	2800	-0.0503	300

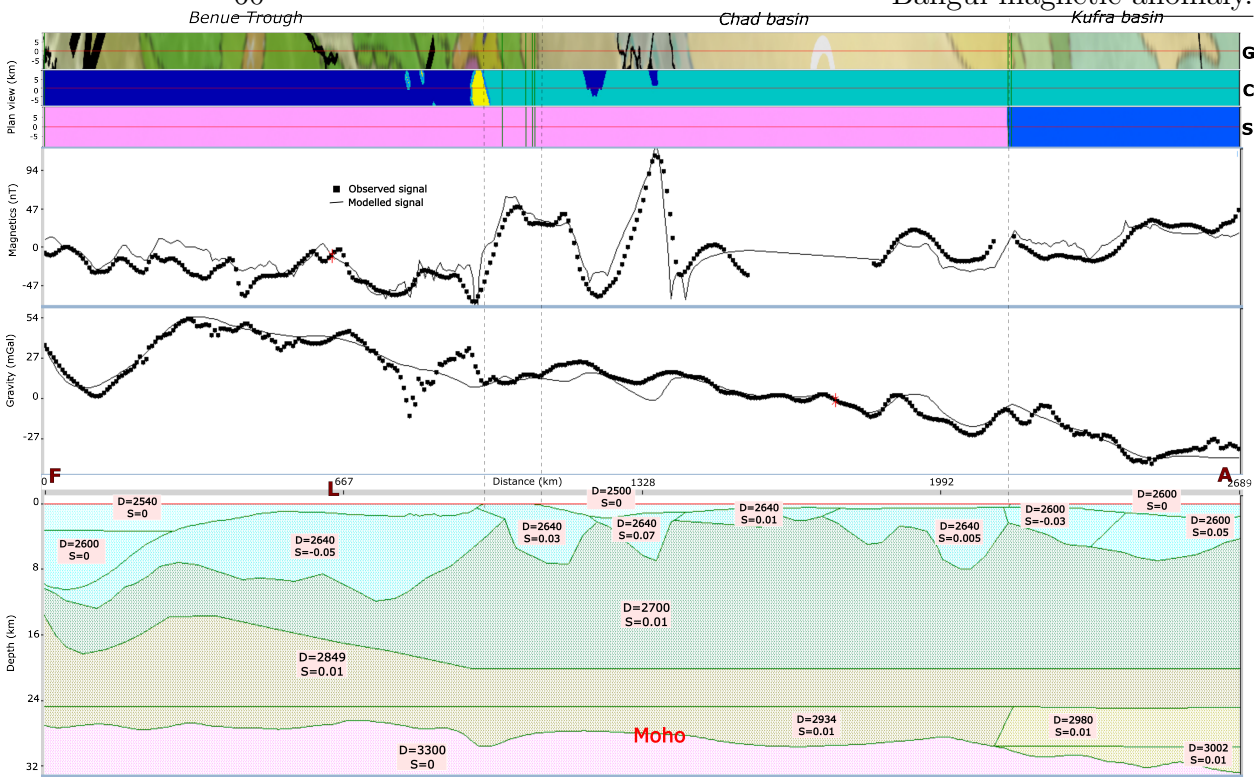

Figure **4-12**: Geological analysis along profile FLA (see Figures 1, 11 for location). From the top to the bottom the panels include, G: geological band (informing on the top layer), C: cluster band (informing on the upper crust), S: band of density from S-wave velocity (informing on the lower crust); Observed and modelled RTP combined magnetic signals, observed and modelled gravity signals, density-susceptibility model. Delimitation lines inside the lower crust have been guided by Table 1, based on Zoback & Mooney (2003).

form densities, with a notable increase observed in northeastern Chad. This density increase likely reflects the presence of the Saharan meta craton, which has been tectonically reworked and metamorphosed during the Pan-African orogeny (Abdelsalam et al. 2002, Sobh et al. 2020).

In the Benue trough, the presence of high-density material (2850 kg/m^3) extending from the lower to the upper crust suggests the existence of large igneous intrusions, aligning with Fairhead (2023), who described the Benue trough as a region shaped by Mesozoic rifting, which facilitated magmatic activity and crustal deformation.

The observed negative magnetic susceptibility (-0.05 SI) directly beneath the Niger Delta Basin and extending below the Benue trough through a structure with a density of 2640 kg/m^3, above the igneous intrusion, suggests re-magnetization following thermal demagnetization. This aligns with Ofoegbu (1984) who proposed re-magnetization processes in this

region. The magnetic fluctuations with opposite signs could indicate variations in the Curie depth, likely occurring between the Cretaceous and Cenozoic, which corresponds with the primary window of volcanism along the adjacent CVL. As that structure extends northeastward, it transits to a positive susceptibility (0.03 SI) before increasing in susceptibility (0.07 SI) and deepening beneath the Lake Chad Basin. According to our model, this progression of susceptibility appears to correspond with the decreasing volume of recent igneous material in the middle crust along the profile.
Beneath the Kufra Basin, the model identifies less dense (around 2600 kg/m^3) and magnetized structures with varying magnetic orientations, characterized by susceptibilities ranging between -0.03 and 0.05 SI. These structures likely represent an interplay of magnetized volcanic intrusions and remnant magnetized blocks, indicating a complex tectonic and magmatic history. In fact, beneath the sedimentary cover, the Kufra Basin is underlain by a Precambrian crystalline basement, which is typical of many North African basins (Coward & Ries 2003). This basement consists of ancient granitic and metamorphic rocks formed during earlier orogenic events (Le Heron et al. 2009). Furthermore, the basin also records episodic volcanic activity, though the extent and composition of the volcanic rocks are less well-documented (Luening et al. 1999). At the base of the Niger Delta Basin, the model shows dense sediments (2600 kg/m^3), indicative of deeply buried, compacted sedimentary sequences characteristic of passive margin settings, as also highlighted by Miall (2013). Given its considerable depth, these sediments may have undergone varying degrees of diagenetic alteration. Overall, the top layer of the crust along this profile is dominated by sedimentary basins, including the Benue Basin, Lake Chad Basin, and Kufra Basin, where sediment density ranges from 2500 to 2600 kg/m^3. These values align with typical densities for sedimentary rocks like shales, sandstones, and siltstones, as described by Reynolds (2011).

Cross-section MN.

Cross-section MN (Figure 13) reveals a complex structure with remarkable variations in both density and magnetic susceptibility throughout the crust.
The top layer along this profile exhibits an alternation of metamorphic, sedimentary, volcanic, and plutonic rocks as descripted by the geological map, reflecting the region's intricate tectonic and magmatic history. The lowest densities (2520 kg/m^3) are observed within sedimentary basins, including the Lullemmeden, Congo, and Benue basins. Moving from the northwest to the southeast, the transect crosses a metamorphic structure in eastern Nigeria, characterized by a density of 2640 kg/m^3 and a susceptibility of -0.03 SI, likely indicative of high-grade metamorphic rock. It also intersects a plutonic structure with a density of 2675 kg/m^3 and a susceptibility of -0.01 SI, possibly corresponding to granitic intrusions. In western Cameroon, the profile encounters another metamorphic structure with a density of 2600 kg/m^3 and a susceptibility of -0.02 SI, suggesting lower-grade metamorphism. Additionally, it passes through a plutonic structure in central Cameroon, with a density of 2675 kg/m^3

and a susceptibility of -0.04 SI, likely associated with the CVL. In southeastern Cameroon (over the Dja region), the profile reveals an intricate structure composed of sediments and volcanic rocks with a density of 2600 kg/m^3 and a susceptibility of 0.01 SI, likely Rhyacian-aged, covering the BMA.
High-density zones (more than 3000 kg/m^3) are found in the lower crust at the cross section's extremities, corresponding to the transitions into the West African and Congo cratons. This result agrees with Boukeke (1994) who, by using constraints from spectral analysis (focusing on gravity and magnetic anomalies) to define the depth of buried bodies, performed 2-dimensional modelling and suggested the emplacement of high-density material in the lower crust during the Pan-African collision over the northern border of the Congo craton. These areas are likely dominated by stable, high-density metamorphic rocks, as suggested by Toteu et al. (1994) and Ganne et al. (2014). These cratonic boundaries, known for their ancient and thick lithospheric roots (Fosso Téguia M et al. 2024*a*), isolate the crust from the asthenosphere, presenting a stark contrast to the more tectonically active regions of the WCARS.

Towards the rift axis, the density of the lower crust decreases, reaching its lowest value (2914-2934 kg/m^3) beneath the Benue trough. This reflects a more reworked, tectonically and thermally altered crustal lithosphere. The shallow Moho in this area, matching with the shallowest Lithosphere-Asthenosphere Boundary (LAB) of the WCARS (Fosso Téguia M et al. 2024*a*), suggests a regional connection between the Moho and the LAB, associated with reworking that occurred during and after the opening of the WCARS. Inside the middle crust, the presence of comparatively high density (2849 kg/m^3) structure only in the Benue's zone is characteristic of a tectonically thinned and rifted lithosphere, where mafic material from the mantle has intruded into the crust, as described by Fairhead & Binks (1991) and Reeves et al. (2004).
Apart from the Benue area, the intermediate crust is generally characterized by an average density of 2670 kg/m^3 and a susceptibility of 0.01 SI. Another remarkable contrast appears in southeastern Cameroon, in the Dja Group area, where the model shows structures with slightly lower density (2640 kg/m^3) and high susceptibilities, reaching 0.2 SI. While this density is consistent with a transition to a less dense cratonic intermediate crust, as highlighted by Djomani et al. (1995), the presence of a 0.2 SI susceptibility anomaly, corresponding to the Cameroonian part of the BMA, is intriguing.

4.6 Discussion

This study focuses on integrating seismic velocity, gravity and magnetic models to analyze crustal density and magnetic susceptibility variations across the WCARS. Through this approach, we aim to discus new insights into the region's tectonic framework, magmatic processes and rifting dynamics, and the origin of the BMA.

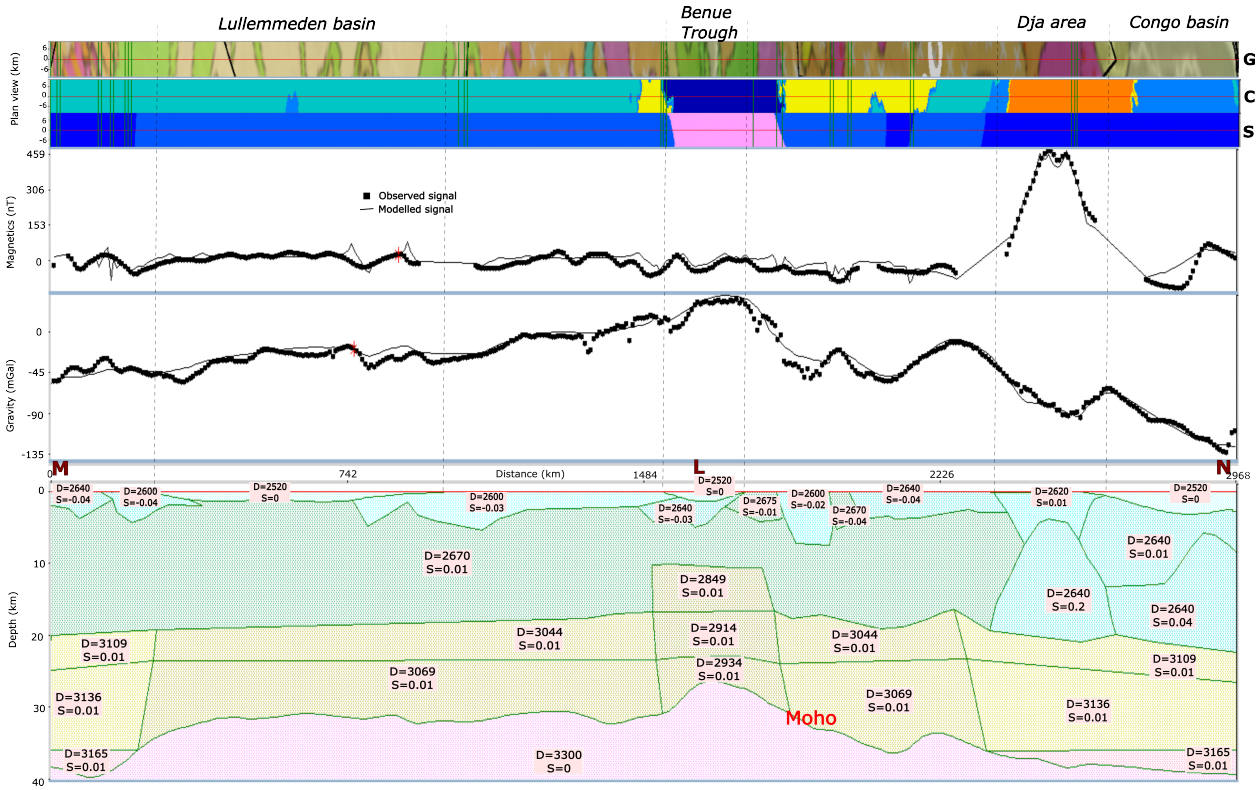

Figure **4-13**: Geological analysis along profile MLN (see Figures 1, 11 for location). From the top to the bottom, G: geological band (informing on the top layer), C: cluster band (informing on the upper crust), S: band of density from S-wave velocity (informing on the lower crust); Observed and modelled RTP magnetic signals; Observed and modelled gravity signals; Density-susceptibility model. Delimitation lines inside the lower crust have been guided by Table 1, based on Zoback & Mooney (2003).

4.6.1 Region's Tectonic Framework

By integrating 3D gravity and magnetic models (Figures 8 and 9), we mapped both crustal density and magnetic susceptibility variations, providing a detailed view of the structural boundaries between stable regions, such as the West African and Congo craton margins, and tectonically active zones, including the Benue trough, the CVL, the CASZ, the KSZ, and the Lake Chad Basin. The results reveal significant density contrasts, particularly in the lower crust, which delineate cratonic margins, transitional areas, and active rift zones. For instance, the MN profile clearly highlights boundaries between different blocks. The limit of the cratonic crust in the northwest (marked by lower crust density ¿ 3100 kg/m3) coinciding with the KSZ, while in the southeast it seems to be limited by the CASZ. Between these two shear zones, emerge areas marked by lower crust density between 3044 and 3069 kg/m3, which could be considered as transitional areas from cratons to the axis of the rift systems, marked by crustal thinning and a denser upper crust Extending from the KSZ to the west side of the Benue trough and from the CASZ to the surrounding of the CVL, the transitional area is larger by the West African craton side than by the Congo craton side. This assymmetry of the WCARS in respect of the Benue trough has been already highlighted by Fosso Téguia M et al. (2024*a*) at the lithospheric scale. These findings are consistent with earlier research suggesting that lithospheric discontinuities mark the boundaries between cratonic and rifted regions, guiding the tectonic and magmatic evolution of the WCARS (Fairhead et al. 2013; Abdelsalam et al. 2002).

Preexisting tectonic structures, such as the CASZ and KSZ, seem to play a key role in controlling the tectonic evolution of the WCARS. The CASZ and the KSZ appear to mark the end of the cratonic margins and the beginning of the transition to the rift zone. These ancient shear zones likely acted as zones of weakness, which were reactivated during the rifting process, guiding the development of rift systems (Fairhead & Binks 1991). This reactivation of faults and suture zones aligns with the concept of tectonic inheritance, where preexisting structures influence the spatial distribution of rifting and magmatism (Toteu et al. 2001; Burke 1976). Our density-susceptibility model further supports the idea that rift basins in the region often follow these ancient structures, emphasizing their significance in the region's tectonic evolution.

In sedimentary basins, such as the Lake Chad Basin, the relationship between tectonics, sedimentation, and crustal properties is complex but closely interconnected. Our model indicates that these basins are characterized by low-density crust, which reflects significant tectonic subsidence and sediment accumulation driven by crustal extension. This supports the notion that tectonics directly influence sedimentation patterns and rates in these basins. The subsidence in the Chad Basin, for example, is tied to ongoing rifting and crustal thinning, findings that are consistent with previous studies on basin evolution in rift settings (Le Heron et al. 2009). Together, these observations highlight the dynamic interplay between tectonics and sedimentation processes in shaping the WCARS.

4.6.2 Magmatic Processes and Rifting Dynamics

Our investigation into the role of magmatism, rift initiation, and crustal modification reveals the profound influence of volcanic and mantle processes in shaping the crust across the WCARS. High magnetic susceptibility anomalies observed along the Cameroon Volcanic Line (CVL) and the Benue trough point to significant magmatic intrusions, which have altered the local crust through thickening and compositional modifications. These magmatic processes, driven by mantle dynamics, not only modify the crust but also play a key role in accommodating rift extension, especially in regions of active volcanic activity (Burke 2001). The intrusions of mafic material have further stretched and restructured the crust, as seen in the Benue trough and Chad Basin.

Rift initiation and propagation are closely tied to crustal thinning, a process evidenced in both density and magnetic models. In regions like the Benue trough and Chad Basin, our models show high-density structures in the upper crust, decreasing toward the inner continent. This density gradient reflects the northeastward propagation of the WCARS, starting from the Atlantic and extending under the Benue trough and Chad Basin. Significant crustal stretching and subsidence, facilitated by mantle upwelling, create space for additional magmatic intrusions, reinforcing the connection between rifting and magmatism. This dynamic supports the theory that mantle processes, such as upwelling, promote lithospheric extension, driving rift systems and modifying the crust (Fairhead & Binks 1991; Guiraud & Maurin 1992).

Thermal processes, particularly mantle upwelling and post-rift cooling, also play a significant role in modifying crustal magnetization within the WCARS. Our susceptibility model reveals thermally demagnetized crust beneath the Benue trough and CVL, where high heat flow has likely altered the magnetic properties of the crust. For example, beneath the Benue trough basins, we observe negative susceptibility values (-0.05 SI), suggesting remagnetization linked to varying geomagnetic conditions during different post-rift periods. Ofoegbu (1984) supports this interpretation, noting bodies of variable magnetic polarity in the region. The thermal impact of mantle upwelling not only affects crustal magnetization but also weakens the crust's elasticity, facilitating further stretching and compression across the WCARS. This aligns with previous studies on the role of thermal processes in rifting, particularly the transition of lithosphere to continental margins (Sibuet & Tucholke 2013). Together, magmatism, rifting, and thermal processes form a cohesive system that governs crustal modification and tectonic evolution in the WCARS.

4.6.3 The Bangui Magnetic Anomaly

Several explanations can be proposed for the origin of the BMA. First, remnant magnetization from the ancient Congo craton lithosphere is one possibility. The Congo craton, with its stable Proterozoic structure, may retain strong magnetic signatures from past geomagnetic fields (Clark 1999; McEnroe et al. 2004). However, the BMA's location at the craton's

border, isolated from the main craton, makes this explanation less likely. Second, mafic and ultramafic intrusions during the Mesozoic rifting of the WCARS could explain the anomaly, as these rock types often show high magnetic susceptibility (Clark 1999; Rochette 1987). However, their typical densities (2800–3300 kg/m^3) differ from the BMA's modelled density (2640 kg/m^3), weakening this hypothesis. Third, tectonic reactivation and metamorphism at the craton's margins could have contributed, but the lack of correspondence between the shape of the CASZ and the BMA diminishes this idea. More plausibly, the BMA may result from felsic and plutonic intrusions. Felsic rocks, such as granite and rhyolite, often carry strong remnant magnetization and exhibit densities closer to that of the BMA (Telford et al. 1990). These intrusions likely cooled slowly in a stable geomagnetic field, contributing to the observed anomaly, especially considering that the WCARS is warmer than the Congo craton, as highlighted by Fosso Téguia M et al. (2024*a*). The block with lower magnetic susceptibility on the craton side of the BMA may be a result of these thermal differences during cooling.

Moreover, the alignment of the BMA with the Cameroon Volcanic Line (CVL) and Benue trough suggests a deeper lithospheric connection. These features likely share a tectonic origin, possibly related to the opening of the South Atlantic and the fragmentation of Gondwana (Fairhead & Binks 1991; Fosso Téguia M et al. 2024*a*). This structural correlation highlights the role of mantle processes in shaping Central and West Africa's geological landscape during the Mesozoic.

4.7 Conclusions

This study presents an integrated 3D crustal model of the West and Central African Rift System (WCARS), constructed using gravity, magnetic, and seismic data, offering insights into the region's tectonic framework, rifting dynamics and formation of the Bangui Magnetic Anomaly (BMA).

The crustal gravity anomaly has been isolated, the satellite and airborne magnetic models have been combined, and density and susceptibility inversions have been conducted across the upper crust after estimation of lower crust density from seismic velocity. The combined analysis of density, magnetic and topographic data allowed for the identification of five distinct tectonic units, offering a more nuanced understanding of the crustal configuration. That outcome combined to the distribution of the lower crust density and the geological map facilitated the analysis of two cross-sections covering key features over the region. Those two cross-sections reveal insights into the WCARS tectonic and geodynamic evolution. Key tectonic structures, including the Central African Shear Zone (CASZ) and Kandi Shear Zone (KSZ), mark the boundaries between cratonic margins and transition to rift zones, acting as zones of weakness reactivated during rifting. This tectonic inheritance has guided the spatial distribution of rift systems, with our model indicating that these shear zones played a crucial role in shaping the rift architecture of WCARS. The transitional areas between

stable cratonic regions and active rift zones exhibit progressive crustal thinning. Denser upper crust reflects the northeastward propagation of rifting from the Atlantic, through the Benue trough, and toward the Chad Basin. These findings are consistent with previous studies highlighting the role of preexisting structures in influencing rifting and magmatic processes in the region.
Magmatism, driven by mantle upwelling, has further modified the crust, particularly in areas of volcanic activity like the CVL and Benue trough. The possible thermal demagnetization and re-magnetization processes associated with tectonic activity during the Cretaceous and Cenozoic periods suggest significant heat flow, which has impacted crustal magnetization and elasticity, facilitating rifts propagation and WCARS stretching. Additionally, the BMA likely results from felsic and plutonic intrusions, supported by density values consistent with granite and rhyolite, and aligned with the CVL and Benue trough, indicating a shared tectonic origin

Acknowledgments

This study has been funded by the Deutsche Forschungsgemeinschaft (DFG, German Research Foundation) - 441292957. Open Access funding enabled and organized by Projekt DEAL.

Appendices

4.A Susceptibility inversion with LCS1

The 3D inversion is conducted using LCS1 as the target signal. The resulting inverted susceptibility model (Figure 14a) generated a TMA that closely aligns with the observed LCS1 data (Figure 6a), as displayed in Table 5.
Figures 14b and 14c display the superposition of EMAG (blue) and TMA from inverted susceptibility (purple), respectively along FA and MN. These results evidenced notably lacks short-wavelength information when LCS1 is used as target signal for the inversion.

4.B Clustering

Figure 15 presents details of the clustering results depicted in Figure 11. Readers can see how for each of the five clusters, cluster parameters are coupled.

Table **4-5**: Statistic of the susceptibility inversion using only LCS1.

B	Minimum (nT)	Maximum (nT)	Mean (nT)	Standard deviation
Observed	-421.77	731.34	1.48	69.73
Forward calculated	-413.70	715.73	1.46	68.03
Misfit	-47.955	63.799	0.00	4.905

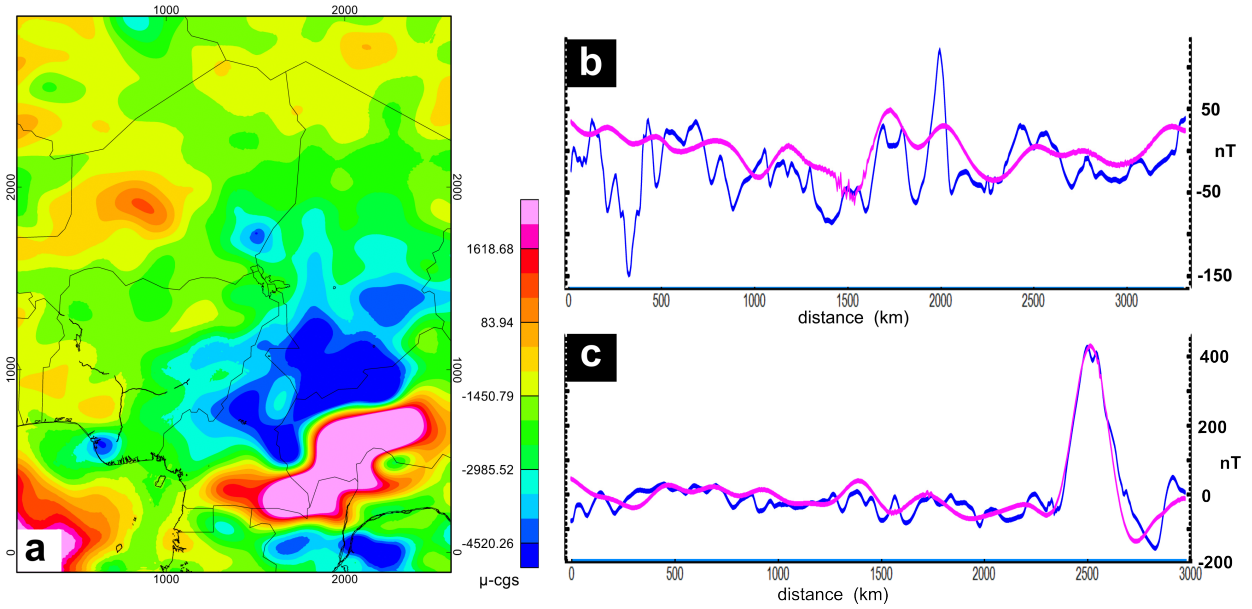

Figure **4-14**: a. Inverted susceptibility using LCS1 as targeted signal. b. Forward calculated from inverted susceptibility (Purple) and EMAG2 (Blue) signals along transect FA, c. Forward calculated from inverted susceptibility (Purple) and EMAG2 (Blue) signals along transect MN.

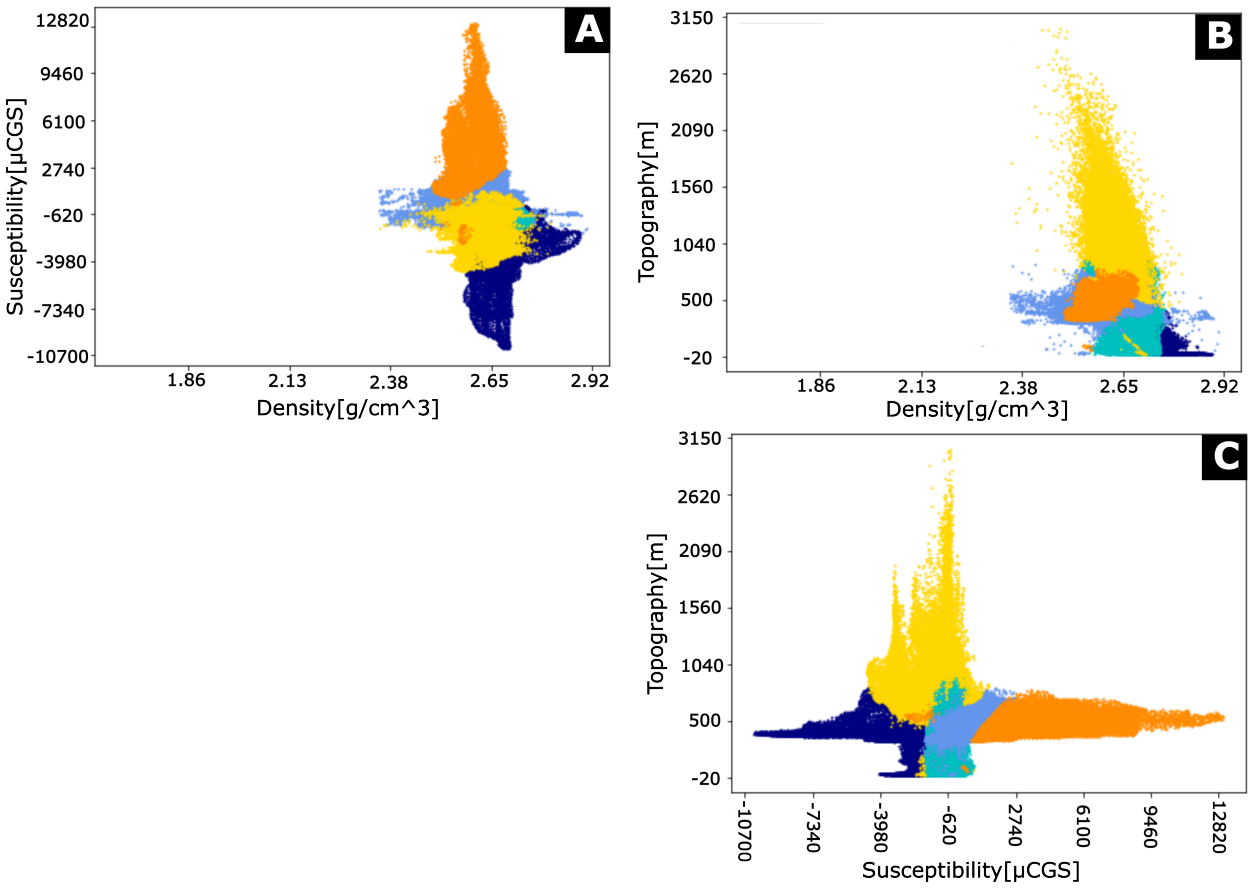

Figure **4-15**: Distribution of clustering parameters.

5 Surface Heat Flow Variations across the West and Central African Rift System

Abstract

This study investigates the lateral variations in surface heat flow (SHF) across the West and Central African Rift System (WCARS), along a transect extending from the eastern boundary of the West African Craton to the northern margin of the Congo Craton. Using an integrated approach combining crustal density and susceptibility models, lithospheric thermal structures, and radiogenic heat production data, we assess the SHF distribution and study its potential correlation with crustal heterogeneity and tectonic features. The results predict significant localized variations in SHF, particularly in the rift zones and volcanic regions, emphasizing the interplay between lithospheric thinning, crustal deformation, and the contribution of radiogenic heat production in the upper crust. These results illustrate the thermal structure and geodynamics of the WCARS, suggesting the movement of hot materials during rifting and the evolution of key geological structures such as the Benue trough and the Cameroon Volcanic Line. These results contribute to the advance of understanding crustal processes and regional tectonics, with implications for geothermal energy exploration and interpretation of geophysical anomalies in the region.

5.1 Introduction

The spatial distribution of heat flow across tectonic units provides critical insight into lithospheric structure, thermal evolution, and geodynamic processes, shedding light on the interactions between various tectonic and geological domains. Furthermore, understanding heat flow has direct applications in resource exploration, particularly in identifying geothermal energy and hydrocarbon potential (Song et al. 2013, Melouah et al. 2023). Despite these potential benefits, the West and Central African region remains significantly underexplored in terms of heat flow studies.
Recently, Fosso Téguia M et al. (2024*a*) developed a three-dimensional lithospheric thermal model and derived surface heat flow estimates for this region by integrating geophysical and petrological data. This model offered robust estimates of heat flow and its lateral variations, primarily attributed to compositional and thickness heterogeneities in the lithospheric mantle. Building on this model, the present study aims to assess surface heat flow by focusing on crustal-scale structures, particularly the lateral variations within the upper crust as recently described by the crustal gravity-magnetic model from Fosso Teguia M. et al (subm., Chapter 4). To achieve this, we couple lithospheric thermal modelling with the results from the crustal-scale modelling based on gravity and magnetic data.

5.2 Geological and Tectonic Setting

The West and Central African region (WCARS) represents a prominent geological domain extending across multiple African nations, characterized by a complex tectonic history and diverse structural elements. Its main components include the Benue trough, the Cameroon volcanic line (CVL), the Chad Basin, the Bangui Magnetic anomaly (BMA), the Central African Shear Zone (CASZ), and Kandi Shear Zone (KSZ) (Guiraud & Maurin 1992; Obaje et al. 2009). This rift system is bordered by the Precambrian basement complexes, namely the West African Craton to the west and the Congo Craton to the south (see Figure 1). The basins within WCARS are predominantly infilled with Mesozoic to Cenozoic sediments deposited during episodes of rifting and subsidence (Burke 1976; Fairhead & Binks 1991). The tectonic evolution of the region is intricately linked to the breakup of the Gondwana supercontinent and the subsequent opening of the South Atlantic Ocean during the Late Jurassic to Early Cretaceous. This extensional regime, driven by the separation of South America and Africa, was the primary force shaping the WCARS (Burke 1976). Pre-existing structural weaknesses in the Precambrian basement played a critical role in localizing rift zones, promoting the formation of deep basins and widespread volcanic activity during the Cretaceous (Fairhead & Green 1989).

Geophysical studies utilizing seismic, gravity, and magnetic datasets (e.g., Fosso Teguia M et al., subm., Chapter 4) have revealed significant crustal heterogeneity across the WCARS.

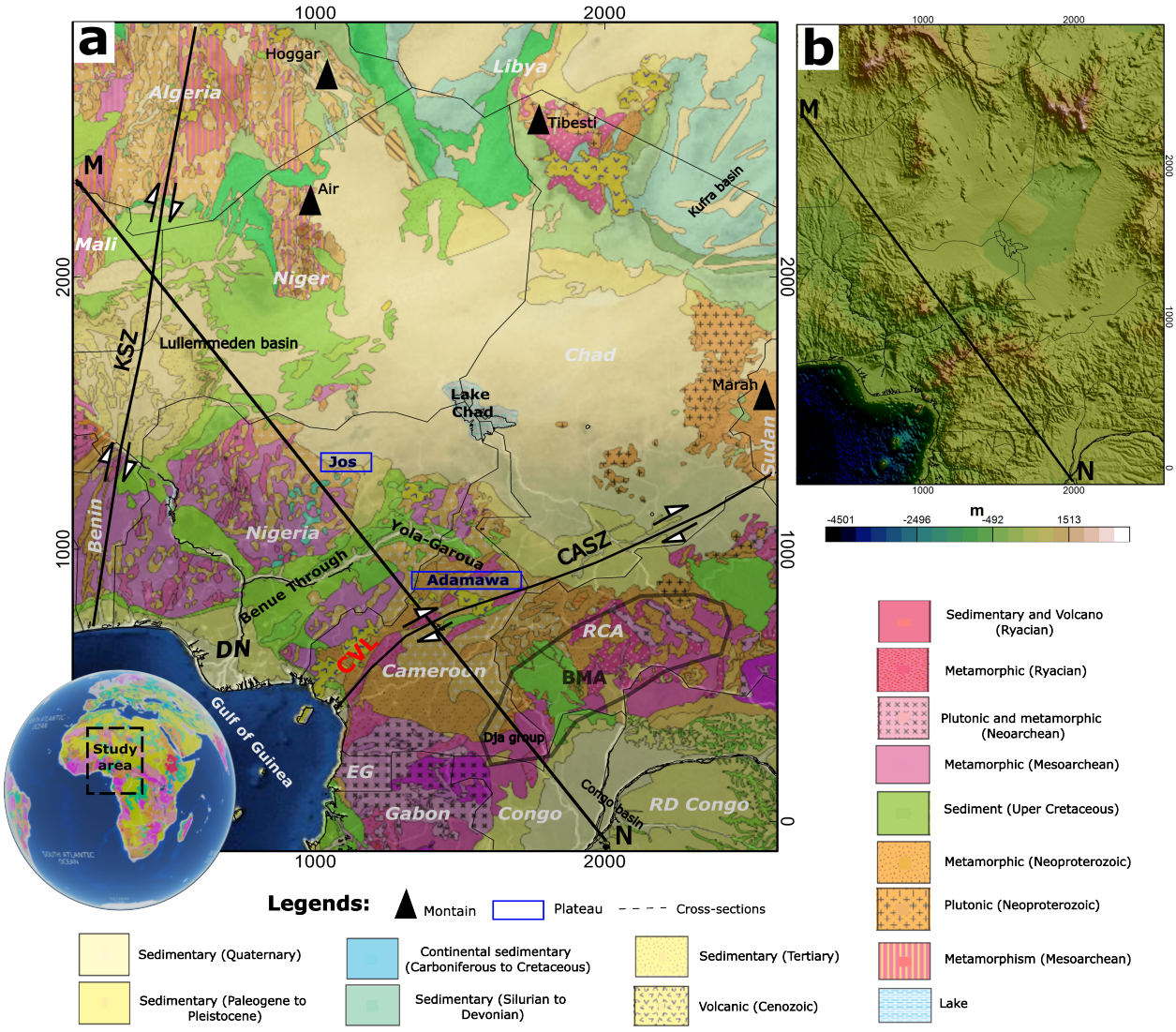

Figure **5-1**: Study area from Fosso Teguia M. et al (subm., Chapter 4). **a** The the West and Central African region. DN: Delta of Niger, CVL: Cameroon volcanic line, CASZ: Central African shear zone, KSZ: Kandi shear zone, BMA: Bangui Magnetic Anomaly. MN is the profile line along what the variation of the surface heat flow (SHF) is studied. **b** Topography of the study area, from SRTM30 Plus v7 (Becker et al. 2009).

Complementary petrological investigations have provided additional insights, particularly regarding radiogenic element distributions. Studies such as Dongmo et al. (2010), Tchouankoue et al. (2014), and Lemdjou et al. (2020) have documented the concentrations of uranium (U), potassium (K), and thorium (Th) in the region. Moreover, Gard et al. (2019) compiled a global whole-rock geochemical database, incorporating data from central and west Africa, and derived radiogenic heat production estimates for these elements.

The integrated geophysical and petrological 3D lithospheric model developed by Fosso Téguia M et al. (2024*a*) has provided a regional-scale understanding of the thermal structure and surface heat flow (SHF) across the WCARS (see Figure 3d). However, that model does not account for lateral and compositional variations within the crust or the influence of topography on SHF.

This study aims to refine the variations in SHF across WCARS structures traversed by the MN profile by integrating multiple datasets: (1) the recent crustal density and susceptibility model of Fosso Teguia M et al. (subm., Chapter 4), which offers a detailed characterization of crustal variability; (2) the temperature model of Fosso Téguia M et al. (2024*a*); and (3) radiogenic heat production from Gard et al. (2019). This integrated approach will enhance our understanding of crustal heterogeneity and its role in shaping the region's geological framework.

5.3 Data

The data used in this study are drawn from various well-established models and datasets. Geometry of the model: The Moho depth (Figure 2a) is derived from the integrated thermal-compositional 3D model developed by Fosso Téguia M et al. (2024*a*). The boundaries between the lower and intermediate crust, as well as the upper crust and its lateral variations (Figure 2d), are obtained from the crustal density and susceptibility model of Fosso Téguia M. et al. (subm., Chapter 4). The sediment depth information (Figure 2b) is based on the Crust1.0 model Laske et al. (2013), while topographic data (Figure 1b) are sourced from SRTM30 Plus v7 (Becker et al. 2009).

Geochemical and thermal data: Radiogenic heat production values (Figure 3a) are provided by Gard et al. (2019), calculated using point measurements of uranium (U), potassium (K), and thorium (Th) concentrations, and applying the relationship defined by Rybach (1988): $A(\mu W m^{-3}) = \rho(9.67 * U + 2.56 * Th + 2.89 * K) * 10^{-5}$, where rho is the density of the rock. The heat flow point values presented in Figure 3b represent the measured values surrounding the studied transect. They are provided and described by the International Heat Flow Group (Fuchs et al. 2021). As we do not have any point values exactly on the transect, we have projected (onto the transect) for this study those that are not more than 300 km from the

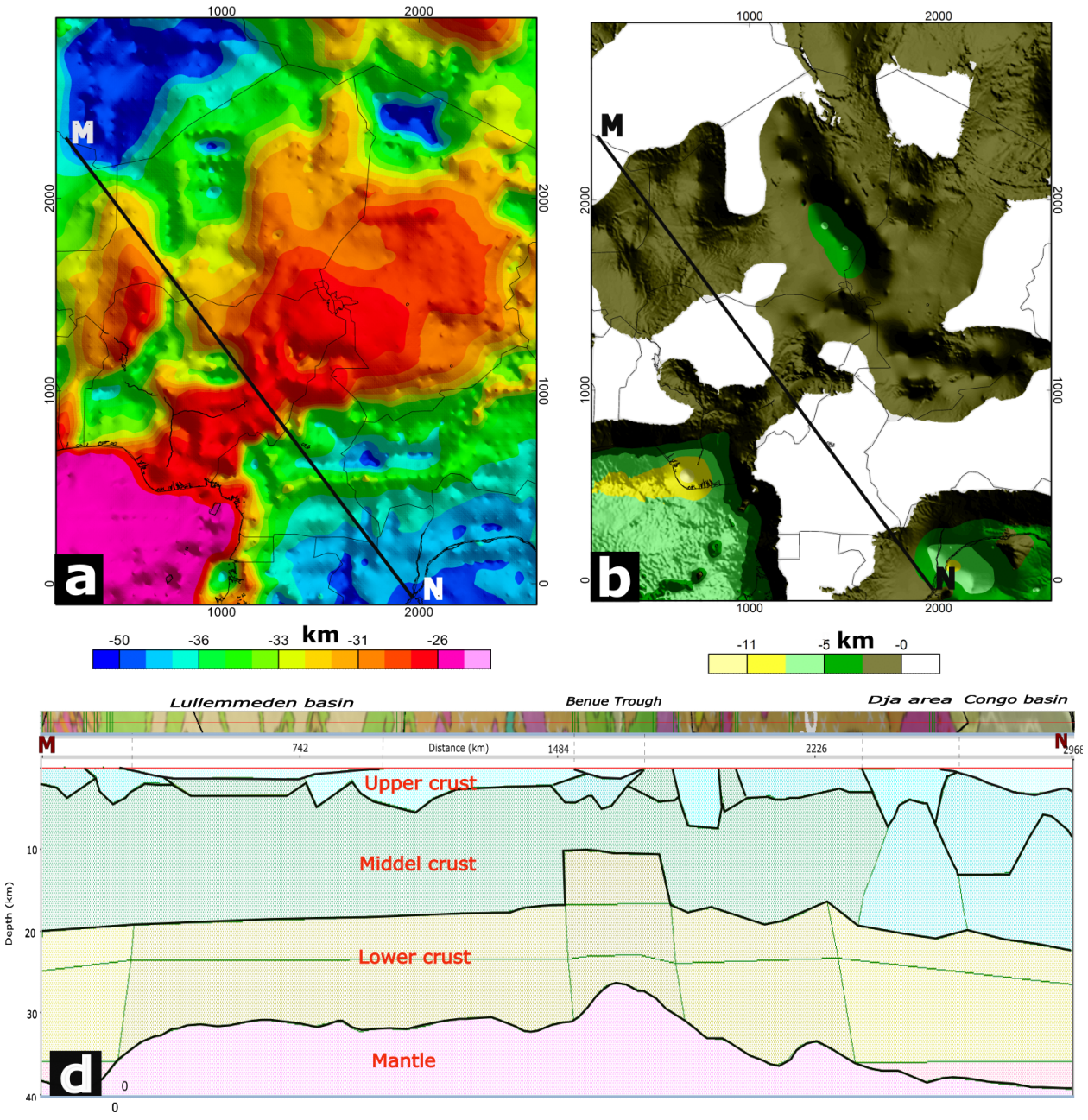

Figure **5-2**: **a** The Moho from Fosso Téguia M et al. (2024*a*), **b** the sediment depth from Laske et al. (2013), **c** the lower-intermediate crust boundary, upper crust and its lateral variation, Fosso Teguia M. et al (subm., Chapter 4).

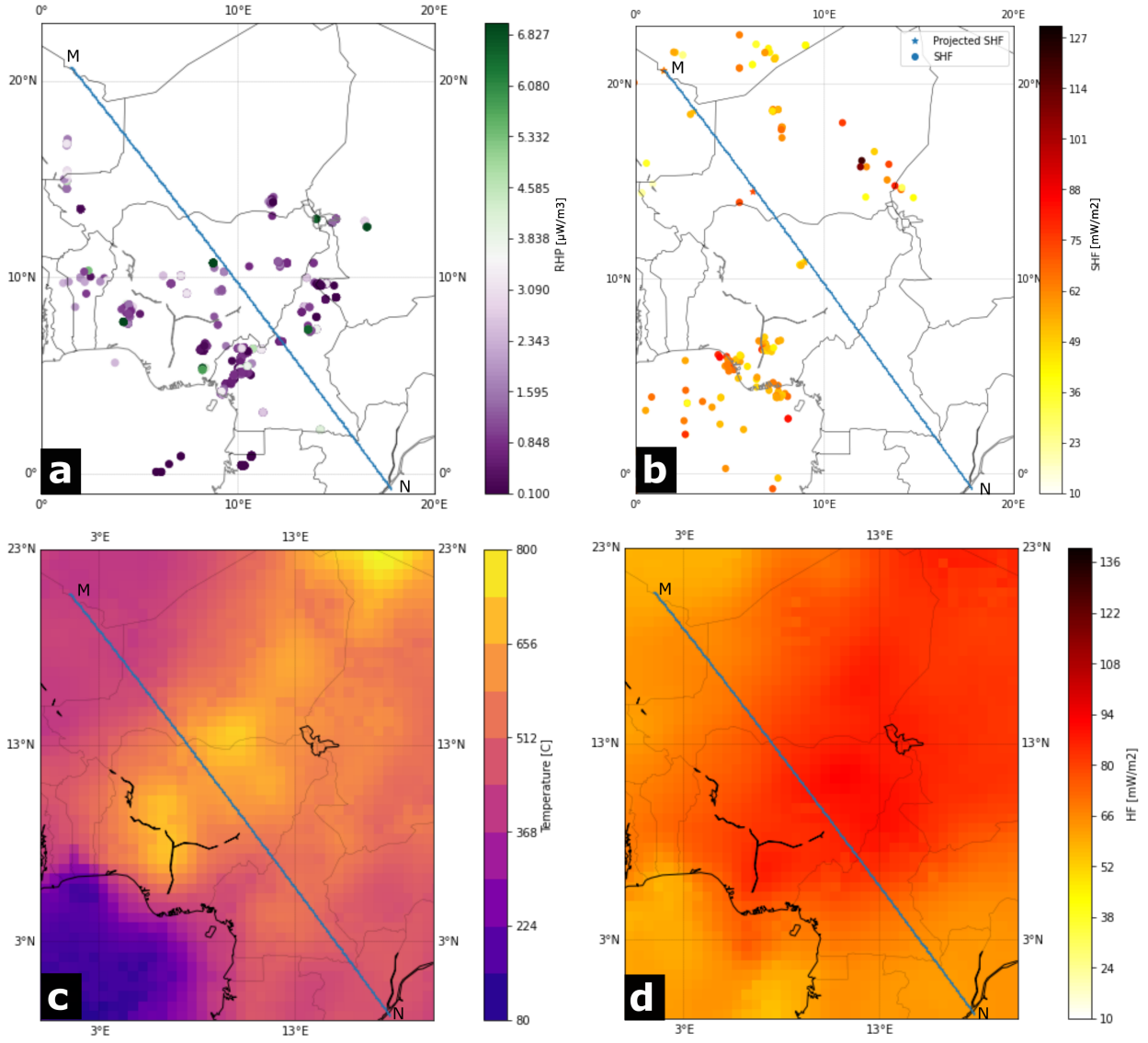

Figure **5-3**: **a** Radiogenic heat production values from Gard et al. (2019), **b** SHF observations from Lucazeau (2019). **c** The Moho temperature and **d** the SHF from the 3D lithospheric model of Fosso Téguia M et al. (2024*a*).

transect. Additionally, the temperature at the Moho surface (Figure 3c), provided by Fosso Téguia M et al. (2024*a*), is used as a boundary condition during the processing.

5.4 Methods

This study focuses on a transect (MN), defined by Fosso Téguia M. et al. (subm., Chapter 4), which extends from the eastern boundary of the West African Craton to the northern edge of the Congo Craton. Along the profile, key geological and tectonic features are intersected, including the Benue trough, the CVL, the Bangui Magnetic Anomaly, and various shear zones.

We use the open-source library PyGimli(Geophysical Inversion and Modeling Library) designed for geophysical modeling and inversion by Rücker et al. (2017). We calculate SHF in 2D by solving the steady-state heat equation, as has been demonstrated in Rücker et al. (2017), showcasing the library's capabilities in thermal modeling.

We make three study cases to study the effect of both the crustal structure and the radiogenic heat production (RHP), on the variation of the SHF along the transect.

5.5 Results

The RHP for the sediment layer has been set to $0W.m^{-3}$ and its thermal conductivity to $1W.m^{-1}.k^{-1}$ while the thermal conductivity of the crystalline crust has been set to $2.5W.m^{-1}.k^{-1}$. The three different cases explored during the processing are (1) homogeneous crystalline crust, (2) two-layer crystalline crust, and (3) three-layer crystalline crust (lower, middle and upper crust) as well as lateral blocks inside the upper crust. That last case is the one we call heterogeneous crust in the rest of this chapter. Figure 4 shows the temperature distribution of each study case. Differences are not easily noticeable with respect to the temperature, but the SHF gives us the following results:

Homogeneous crust (Figure 4a) We have considered the crust from the Moho to the base of the sedimentary basins as homogeneous with an RHP value of $10^{-7}W.m^{-3}$. The resulting SHF exhibits a trend similar to that derived from the lithospheric model of Fosso Téguia M et al. (2024*a*), which was also based on constant parameter values. Small-scale variations in that homogeneous model (also present in the two other cases) can be attributed to variations of the layer overlying the crystalline crust. Therefore, these variations reflect the combined influence of the mantle, sediments, and topography. However, the lower crust should be more depleted and therefore cannot have the same RHP as the rest of the crust

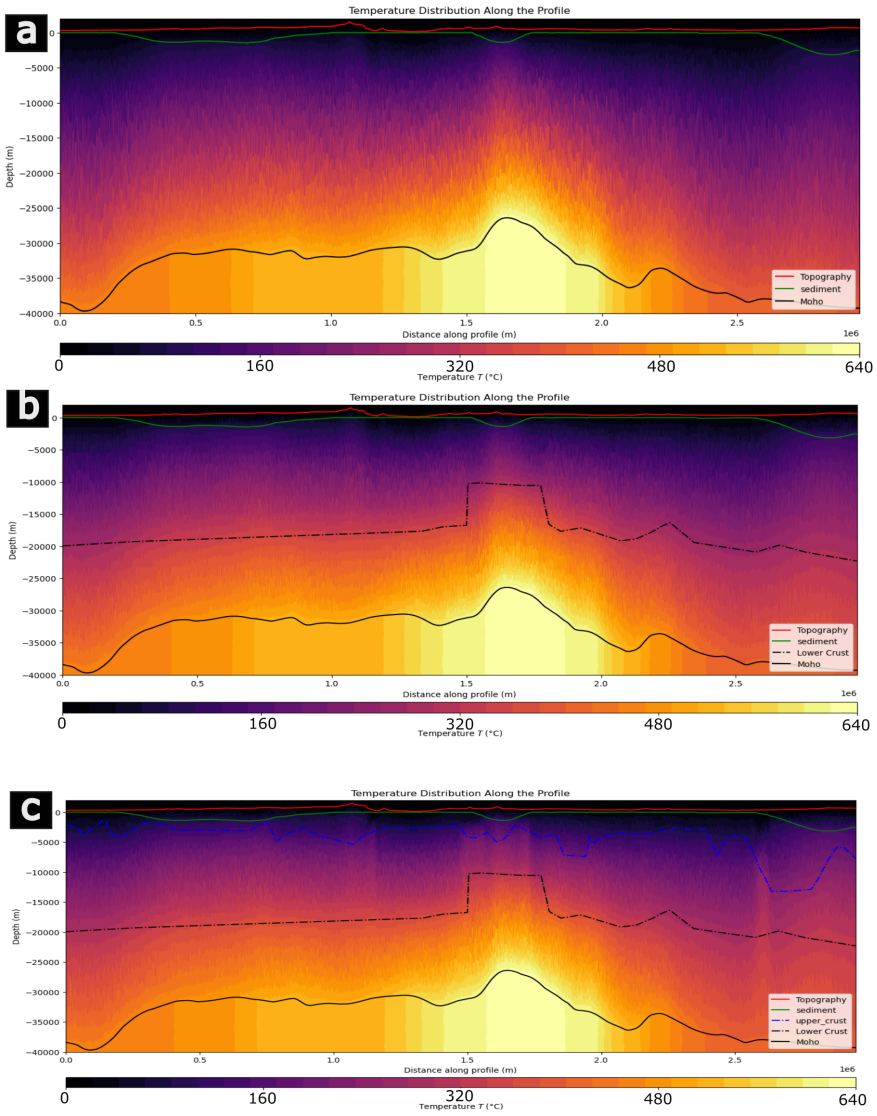

Figure **5-4**: Crustal distribution of temperature (in degree Celsius) along MN. The red line represents the topography, the green line the sediment depth, and the black line the Moho. **a**, the crust is set as homogeneous. **b**, The crust is divided in two part, the dashed black line represents the middle-lower crust boundary. **c**, the upper crust variations are added and the dashed blue line represents the upper-middle crust boundary.

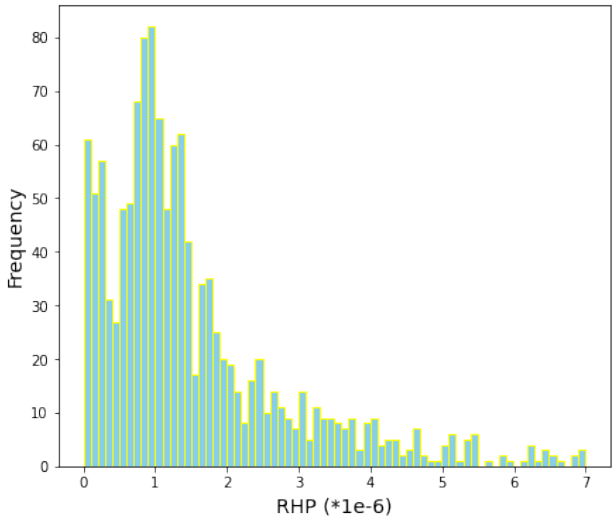

Figure **5-5**: Frequency of RHP across the WCARS

Two-layer crust (Figure 4b) In terms of RHP, $10^{-7}W.m^{-3}$ has been assigned to the lower crust and $10^{-6}W.m^{-3}$ to the layer above, leading to reduced SHF (Figure 6a). The difference of case one and two (Figure 6a) show the main structural-compositional effects in the rift axis (Benue trough area) and at the western extremity of the transect (next to the Lullemmeden Basin). The result of this second case reflects the influence of the middle-lower crust interface, the mantle, sediments, and topography on the SHF.

Heterogeneous crust (Figure 4c) In addition to $10^{-7}W.m^{-3}$ assigned to the lower crust, $10^{-6}W.m^{-3}$ to the middle crust, we have assigned different value of RHP ranging between $1.5 * 10^{-6}W.m^{-3}$ to $3 * 10^{-6}W.m^{-3}$ to the upper crust. The choice of values in the upper crust is based on the distribution of RHP values (Figure 3a, Figure 5). The resulting SHF (Figure 6a), which reflects contributions from the mantle and all of the crustal components, shows more contrast (Figure 6a) with the second case than with the second case with the first case, highlighting the structural-compositional effects of the upper crust. This SHF diverges from the lithospheric model in the northwest section (Lullemmeden Basin and adjacent areas), where it becomes warmer and achieves a good fit with the measured SHF in that region.

In the rift area, specifically between the Lullemmeden Basin and the Benue trough, this model and the lithospheric one converge despite local variation in this model. However, it has been challenging to reproduce measured SHF in the rift area with a purely layered RHP model. Rather, to reconcile these differences, the structural architecture of the upper crust of Fosso Téguia M. et al. (subm., Chapter 4) was adjusted by dividing the upper crustal block between the two basins into two distinct blocks with different RHP values: $3 * 10^{-6}W.m^{-3}$ for the western block and $1.5 * 10^{-6}W.m^{-3}$

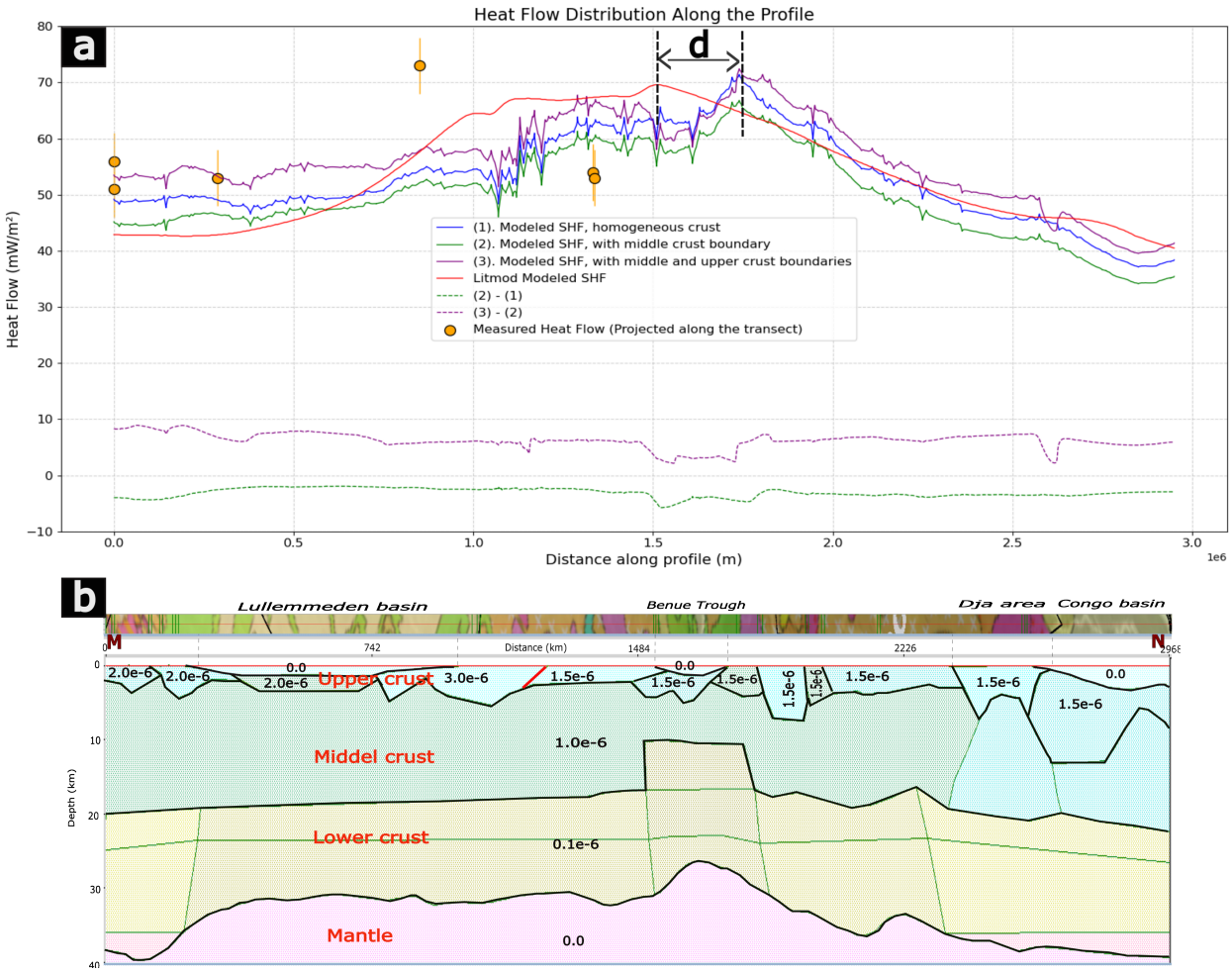

Figure **5-6**: **a**, Variation of SHF along MN. (1) The blue curve represents the modeled SHF, considering the crust as an homogeneous block. (2) The green curve represents the modeled SHF, considering the crust as made of two blocks separated by the middle-lower crust boundary. (3) The purple curve represents the modeled SHF, considering the lower, the middle and the upper crust variations (representing the heterogeneous crust and the final result of this study). The red curve represents the modeled SHF from the lithospheric model of Fosso Téguia M et al. (2024*a*). *d* represents the distance between lithospheric and new modeled peaks. The yellow circles represent projected values of the measured SHF on the profile. they have a tolerance of more or less $5mW.m^{-2}$. The dashed green curve represents the difference (2) - (1), and the dashed purple (3) - (2). **b** gives the final distribution of RHP (in $W.m^{-3}$) for the heterogeneous crust along MN

for the eastern block. But in spite of that differences between modeled and measured SHF in the rift area remain high, up to $20mW.m^{-2}$ between both of them.
In the eastern segment of the study area, which includes the Benue trough and beyond, the absence of measured SHF data prohibits detailed assessement of the modeled SHF result. However, the modeled SHF trend remains consistent and slightly warmer compared to the lithospheric model. This result highlights that the highest and lowest SHF values along the transect are found in the eastern segment: exceeding $70mW.m^{-2}$ in the CVL area and around $40mW.m^{-2}$ in the northern Congo basin.

5.6 Discussion

5.6.1 Sensitivity of RHP distribution, based on the heterogeneous model

The relatively low SHF values at the ends of the profile align well with expectations, as these regions are influenced by stable the West African and Congo cratons, respectively. These cratons are typically characterized by low SHF values, ranging between 30 and 50 mW/m^2 (Lesquer & Vasseur 1992, Fosso Téguia M et al. 2024*a*). The slightly elevated SHF value of approximately 55 mW/m^2 at the western end is explained by the relatively high concentration of radiogenic elements ($2 * 10^{-6}W.m^{-3}$) compared to the eastern end ($1.5 * 10^{-6}W.m^{-3}$). Although the highest value of RHP ($3 * 10^{-6}W.m^{-3}$) is located in the area corresponding to the highest measured SHF point (the south east of the Lullemmeden basin), the gap between the modeled SHF and the measured values at that point remains significant ($10mW.m^{-2}$). This discrepancy maybe due to the sedimentary layer in the basin, which reduces the modeled SHF, while the measured values may have been influenced by sampling near the outcrops, as noted by Harlé et al. (2019) and Stål et al. (2022).
In contrast, the two measured SHF values west of the Benue trough, approximately $55mW.m^{-2}$, are unexpectedly low for a rift setting and even lower than the modeled SHF, which is slightly above $65mW.m^{-2}$. Despite the steep RHP gradient from $3 * 10^{-6}W.m^{-3}$ to $1.5 * 10^{-6}W.m^{-3}$, it was not possible to reconcile these measured values with the modeled result, which remains consistent with the one from the lithospheric model. These low measured SHF may be related to the quality of the measurement process, and do not accurately reflect the broader rift area. Moreover, these points are projections onto the study transect of the nearest available SHF data points.
Unfortunately, no measured SHF data are available for the eastern portion of the study transect, making it more challenging to constrain this area. However, the modeled SHF trend closely follows that of the lithospheric model, which aligns with the regional tectonic structure as described by Fosso Téguia M et al. (2024*a*). Furthermore, the new modeled SHF effectively captures the signatures of known geological structures along this section of the transect: a decrease in SHF across the Benue trough, a peak exceeding $70mW.m^{-2}$ across

the CVL, and another significant decrease in the northern Congo basin near the eastern transect extremity.
The geothermal heat flow model for Africa by Al-Aghbary et al. (2022), which employed a random forest approach, also supports the validity of the results of this study. Their model indicates that SHF values in the WCARS generally range from 40 to 70 mW/m^2, with localized anomalies exceeding 80 mW/m^2. That agreement in the SHF range supports the quality of this study's results, highlighting the utility of lateral SHF variations in advancing our understanding of the geodynamic and tectonic relationships among geological structures along the transect.

5.6.2 Tectonic and Geodynamics

The high concentration of radiogenic heat producing elements in the western section of the transect, including beneath the Lullemmeden basin, suggests that this region may have experienced significant tectonic activity, contrary to initial assumptions of cratonic stability. This could involve mantle-derived magmas migrating upwards and creating an upper crust enriched in radiogenic elements. This hypothesis is consistent with the findings of Jaupart & Mareschal (2021) and Hofmann (1997), who discussed the contribution of mantle-derived magmas to the enrichment of radiogenic elements such as uranium (U), thorium (Th), and potassium (K) in the crust.
SHF values in the rift center, are generally higher than those at the transect extremities. This observation is consistent with lithospheric thinning during rifting, characterized by significant magmatic intrusions and elevated crustal temperatures. These processes have been described by Fairhead (2023) and Fosso Téguia M et al. (2024*a*) as indicative of passive rifting.
Localized SHF variations within the rift zone, which are also present in the homogeneous and semi-heterogeneous crust scenarios, reflect crustal deformation from the Moho to the surface. These variations highlight the intensity and "chaotic" nature of forces that shaped the WCARS.

The comparison of the lithospheric model and the homogeneous model, which includes crustal structures, indicates that although the highest value in both models is located within the rift system, the peaks are not positioned at the same location but are separated by a measurable distance d (see Figure 6a). The peak of the lithospheric model is vertically aligned with the point of greatest crustal thinning corresponding to the Benue trough at the surface. In contrast, the new model presents a peak situated farther to the east, aligning at the surface with the Cameroon Volcanic Line (CVL). This discrepancy reveals the direction of movement of hot materials during and after the rifting process.
This observation serve as an additional support to the theory proposed by Fosso Téguia M et al. (2024*a*) regarding the origin of the enigmatic CVL. We suggested the occurrence of

edge-driven convection between the WCARS and the Congo Craton during the formation of the CVL, which facilitated the formation of magma chambers beneath the CVL. However, it did not explicitly determine the source or direction of the hot material that supplied these magma chambers. This study suggests that the hot material ascended in an eastward direction, originating from the mantle beneath the Benue trough and migrating to the upper crust below the CVL.

These results also contribute to improved localization and characterization of one of the reactivated pre-existing weaknesses identified by earlier studies, such as those of Guiraud et al. (1992) and Fairhead & Green (1989), in their descriptions of the development of the WCARS.

Based on the crustal structure of the West and Central African Rift System (WCARS) as modeled by Fosso Téguia M. et al. (subm., Chapter 4), this new model predicts a significant decrease in surface heat flow on the eastern side of the Bangui Magnetic Anomaly, particularly in the Dja area. This decrease is closely associated with the geometry of the source structure responsible for generating the magnetic anomaly.

5.7 Conclusions

This study investigated surface heat flow variations along a transect inside the West and Central African Rift System (WCARS), using crustal and lithospheric data to illuminate the thermal variation and geodynamic processes underlying the region. The model demonstrates notable variations compared to previous lithospheric-scale studies by incorporating the effects of radiogenic heat production and crustal heterogeneity.

The study shows significant variations in the SHF, particularly within the rift zones, where values are increased due to lithospheric thinning and magmatic intrusions, as well as in volcanic regions such as the Cameroon Volcanic Line (CVL). The comparison between the lithospheric and new models suggest new details about the possible movement of hot materials during rifting, providing support for existing theories regarding edge-driven convection and the origin of the CVL.

Key localized anomalies, such as the SHF decrease east of the Bangui Magnetic Anomaly and the sharp variations across the rift system, underscore the role of pre-existing crustal weaknesses and structural complexity in shaping the thermal regime. Despite the challenges posed by limited and low-quality SHF measurements in certain areas, the model aligns well with the available data and expands our understanding of the tectonic and thermal history of the region.

This topic is not only intended to enhance our knowledge of the thermal evolution of WCARS but also to have broader implications for geothermal resource assessment and the interpretation of geophysical anomalies. Future studies should incorporate more data and further refine the understanding of regional heat flow dynamics and their various implications.

6 Conclusion

This thesis has presented a comprehensive investigation into the lithospheric and crustal structure, thermal evolution, and geodynamic framework of the West and Central African Rift System (WCARS). By integrating geophysical, petrological, and thermal data, it has addressed critical knowledge gaps regarding the region's tectonic history and processes. Below, the findings are synthesized in relation to the research questions posed in Chapter 2.

Lithospheric and Crustal Structure
The integrated 3D geophysical-petrological model confirmed the passive origin of the WCARS, and reveals substantial lateral variations in lithospheric thickness and composition. These variations highlight the role of tectonic inheritance and rifting in shaping the WCARS.
The lithospheric mantle beneath the WCARS is predominantly Phanerozoic in composition, transitioning sharply to Proterozoic lithosphere under the adjoining cratons. Transitional zones of varying sizes and geometries connect these lithospheric domains, reflecting the region's complex tectonic evolution.
Crustal thickness varies significantly across the region, ranging from approximately 25 km in rift zones to over 50 km beneath cratonic regions. This heterogeneity underscores the influence of both tectonic extension and magmatic activity on lithospheric architecture.

Origin of the Cameroon Volcanic Line
The origin of the Cameroon Volcanic Line (CVL) is attributed to edge-driven convection facilitated by the V-shaped opening of the lithospheric mantle beneath the WCARS. This dynamic process has created magma chambers aligned with pre-existing lithospheric weaknesses, further emphasizing the importance of tectonic inheritance.

Origin of the Bangui Magnetic Anomaly
The Bangui Magnetic Anomaly is linked to felsic and plutonic intrusions associated with Mesozoic rifting and mantle upwelling. These intrusions likely carry strong remnant magnetization, consistent with density and susceptibility values identified in the crustal model.
Reactivated shear zones, such as the Central African Shear Zone (CASZ), have played a crucial role in localizing magmatic activity and shaping both the BMA and CVL. These findings align with hypotheses linking these anomalies to deep-seated tectonic processes.

Surface Heat Flow Variations

Surface heat flow variations across the WCARS are closely linked to crustal heterogeneity, radiogenic heat production, and lithospheric thinning. Elevated heat flow values in rift zones, such as the Benue Trough and Cameroon Volcanic Line, reflect the influence of lithospheric thinning and magmatic intrusions.
The study reveals the orientation of hot materials movement beneath the Benue Trough and the CVL, providing new insights into the mechanisms that led to the formation of the CVL. Nevertheless, this is just a first order study and much more remains to be done about this topic as we have been limited by the data coverage especially with measured HF points.

Collectively, these findings advance our understanding of WCARS's geodynamic evolution. The thesis underscores the interconnectedness of tectonic, magmatic, and thermal processes in shaping rift systems. By linking geophysical signatures to underlying geological mechanisms, it provides a robust framework for studying similar regions worldwide.

Future research should focus on high-resolution geodynamic simulations to further refine the interaction between mantle flow and lithospheric structures. Additionally, expanding the database of geophysical and geochemical observations across WCARS would enhance the accuracy and resolution of regional models.

In conclusion, this thesis not only resolves long-standing questions about WCARS's structure and evolution but also offers valuable insights for resource exploration and geohazard assessment. Its methodological approach and findings have broad implications for the study of rift systems and lithospheric dynamics, contributing to the global understanding of Earth's tectonic processes.

Bibliography

Abdelsalam, M. G., Liégeois, J.-P. & Stern, R. J. (2002), 'The saharan metacraton', *Journal of African Earth Sciences* **34**(3-4), 119–136.

Afonso, J. C., Fernandez, M., Ranalli, G., Griffin, W. & Connolly, J. (2008), 'Integrated geophysical-petrological modeling of the lithosphere and sublithospheric upper mantle: Methodology and applications', *Geochemistry, Geophysics, Geosystems* **9**(5).

Al-Aghbary, M., Sobh, M. & Gerhards, C. (2022), 'A geothermal heat flow model of africa based on random forest regression', *Frontiers in Earth Science* **10**, 981899.

Allen, P. A. & Allen, J. R. (2013), *Basin analysis: Principles and application to petroleum play assessment*, John Wiley & Sons.

Amante, C. & Eakins, B. (2008), 'Etopo1 1 arc-minute global relief model: Procedures, data sources and analysis, national geophysical data center, nesdis, noaa, us dept', *Commerce, Boulder, CO, USA* .

Artemieva, I. (2011), *Lithosphere: an interdisciplinary approach*, Cambridge University Press.

Asaah, A. N., Yokoyama, T., Aka, F. T., Usui, T., Wirmvem, M. J., Tchamabe, B. C., Ohba, T., Tanyileke, G. & Hell, J. (2015), 'A comparative review of petrogenetic processes beneath the cameroon volcanic line: Geochemical constraints', *Geoscience Frontiers* **6**(4), 557–570.

Becker, J., Sandwell, D., Smith, W., Braud, J., Binder, B., Depner, J., Fabre, D., Factor, J., Ingalls, S., Kim, S. et al. (2009), 'Global bathymetry and elevation data at 30 arc seconds resolution: Srtm30_plus', *Marine Geodesy* **32**(4), 355–371.

Bosworth, W. (1992), 'Mesozoic and early tertiary rift tectonics in east africa', *Tectonophysics* **209**(1-4), 115–137.

Boukeke, D.-B. (1994), *Structures crustales d'Afrique Centrale déduites des anomalies gravimétriques et magnétiques: le domaine précambrien de la République Centrafricaine et du Sud Cameroun*, ORSTOM.

Bouman, J., Ebbing, J., Fuchs, M., Sebera, J., Lieb, V., Szwillus, W., Haagmans, R. & Novak, P. (2016), 'Satellite gravity gradient grids for geophysics', *Scientific reports* **6**(1), 1–11.

Burke, K. (1976), The chad basin: an active intra-continental basin, *in* 'Developments in geotectonics', Vol. 12, Elsevier, pp. 197–206.

Burke, K. (2001), 'Origin of the cameroon line of volcano-capped swells', *The Journal of Geology* **109**(3), 349–362.

Burke, K. C. A., Whiteman, A. J. et al. (1973), 'Uplift, rifting and the break-up of africa'.

Celli, N. L., Lebedev, S., Schaeffer, A. J. & Gaina, C. (2020), 'African cratonic lithosphere carved by mantle plumes', *Nature communications* **11**(1), 1–10.

Christensen, N. I. (1996), 'Poisson's ratio and crustal seismology', *Journal of Geophysical Research: Solid Earth* **101**(B2), 3139–3156.

Christensen, N. I. & Mooney, W. D. (1995), 'Seismic velocity structure and composition of the continental crust: A global view', *Journal of Geophysical Research: Solid Earth* **100**(B6), 9761–9788.

Clark, D. A. (1999), 'Magnetic petrology of igneous intrusions: implications for exploration and magnetic interpretation', *Exploration Geophysics* **30**(2), 5–26.

Connolly, J. (2009), 'The geodynamic equation of state: what and how', *Geochemistry, geophysics, geosystems* **10**(10).

Connolly, J. A. (2005), 'Computation of phase equilibria by linear programming: a tool for geodynamic modeling and its application to subduction zone decarbonation', *Earth and Planetary Science Letters* **236**(1-2), 524–541.

Coward, M. & Ries, A. (2003), 'Tectonic development of north african basins', *Geological Society, London, Special Publications* **207**(1), 61–83.

De Plaen, R., Bastow, I., Chambers, E., Keir, D., Gallacher, R. & Keane, J. (2014), 'The development of magmatism along the cameroon volcanic line: evidence from seismicity and seismic anisotropy', *Journal of Geophysical Research: Solid Earth* **119**(5), 4233–4252.

Djomani, Y. P., Nnange, J., Diament, M., Ebinger, C. & Fairhead, J. (1995), 'Effective elastic thickness and crustal thickness variations in west central africa inferred from gravity data', *Journal of Geophysical Research: Solid Earth* **100**(B11), 22047–22070.

Dongmo, A. K., Nkouathio, D., Pouclet, A., Bardintzeff, J.-M., Wandji, P., Nono, A. & Guillou, H. (2010), 'The discovery of late quaternary basalt on mount bambouto: Implications for recent widespread volcanic activity in the southern cameroon line', *Journal of African Earth Sciences* **57**(1-2), 96–108.

Elsheikh, A. A., Gao, S. S. & Liu, K. H. (2014), 'Formation of the cameroon volcanic line by lithospheric basal erosion: Insight from mantle seismic anisotropy', *Journal of African Earth Sciences* **100**, 96–108.

Eric, F. T. M. E., Vanessa, N. G., Alain, L. T. S., Olivier, N. B. E., Albert, E. Y., Alain, Z. A., Bekoa, A. & Nfomou, N. (2020), 'Exploration of potential ore deposits along the cameroon volcanic line from gravity and magnetic studies', *Open Journal of Geology* **10**(10), 1009–1026.

Eyike, A. & Ebbing, J. (2015), 'Lithospheric structure of the west and central african rift system from regional three-dimensional gravity modelling', *South African Journal of Geology* **118**(3), 285–298.

Fairhead, J. (1986), 'Geophysical controls on sedimentation within the african rift systems', *Geological Society, London, Special Publications* **25**(1), 19–27.

Fairhead, J. (2023), 'The mesozoic west and central africa rift system (wcars) and the older kandi shear zone (ksz): Rifting and tectonics of north africa and south america and fragmentation of gondwana based on geophysical investigations', *Journal of African Earth Sciences* **199**, 104817.

Fairhead, J. & Binks, R. (1991), 'Differential opening of the central and south atlantic oceans and the opening of the west african rift system', *Tectonophysics* **187**(1-3), 191–203.

Fairhead, J. D. (1988), 'Mesozoic plate tectonic reconstructions of the central south atlantic ocean: the role of the west and central african rift system', *Tectonophysics* **155**(1-4), 181–191.

Fairhead, J. & Green, C. (1989), 'Controls on rifting in africa and the regional tectonic model for the nigeria and east niger rift basins', *Journal of African Earth Sciences (and the Middle East)* **8**(2-4), 231–249.

Fairhead, J., Green, C., Masterton, S. & Guiraud, R. (2013), 'The role that plate tectonics, inferred stress changes and stratigraphic unconformities have on the evolution of the west and central african rift system and the atlantic continental margins', *Tectonophysics* **594**, 118–127.

Fitton, J. (1980), 'The benue trough and cameroon line—a migrating rift system in west africa', *Earth and Planetary Science Letters* **51**(1), 132–138.

Fosso Teguia M, E. E., Ebbing, J., Haas, P. & Szwillus, W. (2023), 'Integrated geophysical-petrological 3d-modelling of the west and central african rift system and its adjoining areas (version 2)'.

Fosso Téguia M, E. E., Ebbing, J., Haas, P. & Szwillus, W. (2024*a*), 'Integrated geophysical-petrological 3d-modeling of the west and central african rift system and its adjoining areas', *Journal of Geophysical Research: Solid Earth* **129**(7), e2024JB029226.

Fosso Teguia M, E. E., Ebbing, J., Haas, P. & Szwillus, W. (2024*b*), 'Integrated geophysical-petrological 3d-modelling of the west and central african rift system and its adjoining areas (version 1)'.

Fuchs, S., Beardsmore, G., Chiozzi, P., Espinoza-Ojeda, O. M., Gola, G., Gosnold, W., Harris, R., Jennings, S., Liu, S., Negrete-Aranda, R. et al. (2021), 'A new database structure for the ihfc global heat flow database', *International Journal of Terrestrial Heat Flow and Applications* **4**(1), 1–14.

Fullea, J. & Afonso, J. C. (2009), 'Litmod3d users guide'.

Fullea, J., Lebedev, S., Martinec, Z. & Celli, N. (2021), 'Winterc-g: mapping the upper mantle thermochemical heterogeneity from coupled geophysical–petrological inversion of seismic waveforms, heat flow, surface elevation and gravity satellite data', *Geophysical Journal International* **226**(1), 146–191.

Ganne, J., Gerbault, M. & Block, S. (2014), 'Thermo-mechanical modeling of lower crust exhumation—constraints from the metamorphic record of the palaeoproterozoic eburnean orogeny, west african craton', *Precambrian Research* **243**, 88–109.

Gard, M., Hasterok, D. & Halpin, J. A. (2019), 'Global whole-rock geochemical database compilation', *Earth System Science Data* **11**(4), 1553–1566.

Ghomsi, F. E. K., Tenzer, R., Njinju, E. & Steffen, R. (2022), 'The crustal configuration of the west and central african rift system from gravity and seismic data analysis', *Geophysical Journal International* **230**(2), 995–1012.

Girdler, R., Taylor, P. & Frawley, J. (1992), 'A possible impact origin for the bangui magnetic anomaly (central africa)', *Tectonophysics* **212**(1-2), 45–58.

Globig, J., Fernàndez, M., Torne, M., Vergés, J., Robert, A. & Faccenna, C. (2016), 'New insights into the crust and lithospheric mantle structure of africa from elevation, geoid, and thermal analysis', *Journal of Geophysical Research: Solid Earth* **121**(7), 5389–5424.

Griffin, W., O'reilly, S. Y., Afonso, J. C. & Begg, G. (2009), 'The composition and evolution of lithospheric mantle: a re-evaluation and its tectonic implications', *Journal of Petrology* **50**(7), 1185–1204.

Gudmundsson, A. (2012), 'Magma chambers: Formation, local stresses, excess pressures, and compartments', *Journal of Volcanology and Geothermal Research* **237**, 19–41.

Guiraud, R., Binks, R., Fairhead, J. & Wilson, M. (1992), 'Chronology and geodynamic setting of cretaceous-cenozoic rifting in west and central africa', *Tectonophysics* **213**(1-2), 227–234.

Guiraud, R. & Maurin, J.-C. (1992), 'Early cretaceous rifts of western and central africa: an overview', *Tectonophysics* **213**(1-2), 153–168.

Haas, P., Ebbing, J., Celli, N. L. & Rey, P. F. (2021), 'Two-step gravity inversion reveals variable architecture of african cratons', *Frontiers in Earth Science* p. 1240.

Harlé, P., Kushnir, A. R., Aichholzer, C., Heap, M. J., Hehn, R., Maurer, V., Baud, P., Richard, A., Genter, A. & Duringer, P. (2019), 'Heat flow density estimates in the upper rhine graben using laboratory measurements of thermal conductivity on sedimentary rocks', *Geothermal Energy* **7**, 1–36.

Hemant, K., Thébault, E., Mandea, M., Ravat, D. & Maus, S. (2007), 'Magnetic anomaly map of the world: merging satellite, airborne, marine and ground-based magnetic data sets', *Earth and Planetary Science Letters* **260**(1-2), 56–71.

Hofmann, A. W. (1997), 'Mantle geochemistry: the message from oceanic volcanism', *Nature* **385**(6613), 219–229.

Jaupart, C. & Mareschal, J.-C. (2021), Radiogenic heat production in the continental crust, *in* 'Encyclopedia of Solid Earth Geophysics', Springer, pp. 1298–1303.

King, S. D. & Ritsema, J. (2000), 'African hot spot volcanism: small-scale convection in the upper mantle beneath cratons', *Science* **290**(5494), 1137–1140.

Koch, F. W., Wiens, D. A., Nyblade, A. A., Shore, P. J., Tibi, R., Ateba, B., Tabod, C. & Nnange, J. (2012), 'Upper-mantle anisotropy beneath the cameroon volcanic line and congo craton from shear wave splitting measurements', *Geophysical Journal International* **190**(1), 75–86.

Kolínskỳ, P., Schneider, F. M. & Bokelmann, G. (2020), 'Surface wave diffraction pattern recorded on alparray: Cameroon volcanic line case study', *Journal of Geophysical Research: Solid Earth* **125**(7), e2019JB019102.

Laske, G., Masters, G., Ma, Z. & Pasyanos, M. (2013), Update on crust1. 0—a 1-degree global model of earth's crust, *in* 'Geophysical research abstracts', Vol. 15, EGU General Assembly Vienna, Austria, p. 2658.

Le Heron, D. P., Howard, J. P., Alhassi, A. M., Anderson, L., Morton, A. & Fanning, C. M. (2009), 'Field-based investigations of an 'infracambrian'clastic succession in se libya and its bearing on the evolution of the al kufrah basin', *Geological Society, London, Special Publications* **326**(1), 193–210.

Lekic, V. & Romanowicz, B. (2011), 'Tectonic regionalization without a priori information: A cluster analysis of upper mantle tomography', *Earth and Planetary Science Letters* **308**(1-2), 151–160.

Lemdjou, Y. B., Zhang, D., Tchouankoue, J. P., Hu, J., Ngongang, N. B. T., Tamehe, L. S. & Yuan, Y. (2020), 'Elemental and sr–nd–pb isotopic compositions, and k–ar ages of transitional and alkaline plateau basalts from the eastern edge of the west cameroon highlands (cameroon volcanic line)', *Lithos* **358**, 105414.

Lesquer, A. & Vasseur, G. (1992), 'Heat-flow constraints on the west african lithosphere structure', *Geophysical research letters* **19**(6), 561–564.

Likas, A., Vlassis, N. & Verbeek, J. J. (2003), 'The global k-means clustering algorithm', *Pattern recognition* **36**(2), 451–461.

Lösing, M., Moorkamp, M. & Ebbing, J. (2023), 'Joint inversion based on variation of information—a crustal model of wilkes land, east antarctica', *Geophysical Journal International* **232**(1), 162–175.

Lucazeau, F. (2019), 'Analysis and mapping of an updated terrestrial heat flow data set', *Geochemistry, Geophysics, Geosystems* **20**(8), 4001–4024.

Luening, S., Craig, J., Fitches, B., Mayouf, J., Busrewil, A., El Dieb, M., Gammudi, A., Loydell, D. & McIlroy, D. (1999), 'Re-evaluation of the petroleum potential of the kufra basin (se libya, ne chad): does the source rock barrier fall?', *Marine and Petroleum Geology* **16**(7), 693–718.

Maus, S., Barckhausen, U., Berkenbosch, H., Bournas, N., Brozena, J., Childers, V., Dostaler, F., Fairhead, J., Finn, C., von Frese, R. R. et al. (2009), 'Emag2: A 2–arc min resolution earth magnetic anomaly grid compiled from satellite, airborne, and marine magnetic measurements', *Geochemistry, Geophysics, Geosystems* **10**(8).

McDonough, W. F. & Sun, S.-S. (1995), 'The composition of the earth', *Chemical geology* **120**(3-4), 223–253.

McEnroe, S. A., Langenhorst, F., Robinson, P., Bromiley, G. & Shaw, C. S. (2004), 'What is magnetic in the lower crust?', *Earth and Planetary Science Letters* **226**(1-2), 175–192.

McKenzie, D. (1978), 'Some remarks on the development of sedimentary basins', *Earth and Planetary science letters* **40**(1), 25–32.

Melouah, O., Ebong, E. D., Abdelrahman, K. & Eldosouky, A. M. (2023), 'Lithospheric structural dynamics and geothermal modeling of the western arabian shield', *Scientific Reports* **13**(1), 11764.

Miall, A. D. (2013), *The geology of fluvial deposits: sedimentary facies, basin analysis, and petroleum geology*, Springer.

Milelli, L., Fourel, L. & Jaupart, C. (2012), 'A lithospheric instability origin for the cameroon volcanic line', *Earth and Planetary Science Letters* **335**, 80–87.

Mooney, W., Romanowicz, B. & Dziewonski, A. (2010), '1.11 crust and lithospheric structure–global crustal structure', *Seismology and Structure of the Earth: Treatise on Geophysics* **1**, 361.

Njiteu, C. D. (2022), 'The origin of bangui magnetic anomaly-one of the largest magnetic anomalies in the world', *Preview* **2022**(216), 43–51.

Novianti, P., Setyorini, D. & Rafflesia, U. (2017), 'K-means cluster analysis in earthquake epicenter clustering', *International Journal of Advances in Intelligent Informatics* **3**(2), 81–89.

Obaje, N. G. et al. (2009), *Geology and mineral resources of Nigeria*, Vol. 120, Springer.

Ofoegbu, C. O. (1984), 'Interpretation of aeromagnetic anomalies over the lower and middle benue trough of nigeria', *Geophysical Journal International* **79**(3), 813–823.

Olsen, N., Ravat, D., Finlay, C. C. & Kother, L. K. (2017), 'Lcs-1: a high-resolution global model of the lithospheric magnetic field derived from champ and swarm satellite observations', *Geophysical Journal International* **211**(3), 1461–1477.

Plomerova, J., Babuška, V., Dorbath, C., Dorbath, L. & Lillie, R. (1993), 'Deep lithospheric structure across the central african shear zone in cameroon', *Geophysical Journal International* **115**(2), 381–390.

Puziewicz, J., Czechowski, L., Grad, M., Majorowicz, J., Pietranik, A. & Šafanda, J. (2019), 'Crustal lithology vs. thermal state and moho heat flow across the ne part of the european variscan orogen: a case study from sw poland', *International Journal of Earth Sciences* **108**, 673–692.

Ravat, D., Hinze, W. & Von Frese, R. (1992), 'Analysis of magsat magnetic contrasts across africa and south america', *Tectonophysics* **212**(1-2), 59–76.

Ravat, D., Wang, B., Wildermuth, E. & Taylor, P. T. (2002), 'Gradients in the interpretation of satellite-altitude magnetic data: an example from central africa', *Journal of Geodynamics* **33**(1-2), 131–142.

Reeves, C., De Wit, M. & Sahu, B. (2004), 'Tight reassembly of gondwana exposes phanerozoic shears in africa as global tectonic players', *Gondwana Research* **7**(1), 7–19.

Reynolds, J. M. (2011), *An introduction to applied and environmental geophysics*, John Wiley & Sons.

Rochette, P. (1987), 'Magnetic susceptibility of the rock matrix related to magnetic fabric studies', *Journal of Structural Geology* **9**(8), 1015–1020.

Rücker, C., Günther, T. & Wagner, F. M. (2017), 'pygimli: An open-source library for modelling and inversion in geophysics', *Computers & Geosciences* **109**, 106–123.

Rybach, L. (1988), 'Determination of heat production rate', *Handbook of terrestrial heat-flow density determination* pp. 125–142.

Schaeffer, A. & Lebedev, S. (2015), Global heterogeneity of the lithosphere and underlying mantle: A seismological appraisal based on multimode surface-wave dispersion analysis, shear-velocity tomography, and tectonic regionalization, *in* 'The Earth's heterogeneous mantle', Springer, pp. 3–46.

Scheaua, F. D. (2016), 'Theoretical approaches regarding the venturi effect', *Coefficient of Small Orifices* **69**.

Schön, J. H. (2015), *Physical properties of rocks: fundamentals and principles of petrophysics*, Elsevier.

Schull, T. J. (1988), 'Rift basins of interior sudan: petroleum exploration and discovery', *AAPG bulletin* **72**(10), 1128–1142.

Sheriff, R. E. & Geldart, L. P. (1995), *Exploration seismology*, Cambridge university press.

Sibuet, J.-C. & Tucholke, B. E. (2013), 'The geodynamic province of transitional lithosphere adjacent to magma-poor continental margins', *Geological Society, London, Special Publications* **369**(1), 429–452.

Sobh, M., Ebbing, J., Mansi, A. H., Götze, H.-J., Emry, E. & Abdelsalam, M. (2020), 'The lithospheric structure of the saharan metacraton from 3-d integrated geophysical-petrological modeling', *Journal of Geophysical Research: Solid Earth* **125**(8), e2019JB018747.

Song, R., Sheng-Biao, H., Chuan-Qing, Z., Xiao-Yin, T., Wei-Wei, L. & Ji-Yang, W. (2013), 'Characteristics of heat flow and lithospheric thermal structure in the junggar basin, northwestern china', *Chinese Journal of Geophysics* **56**(5), 661–673.

Stål, T., Reading, A. M., Fuchs, S., Halpin, J. A., Lösing, M. & Turner, R. J. (2022), 'Properties and biases of the global heat flow compilation', *Frontiers in Earth Science* **10**, 963525.

Stuart, G., Fairhead, J., Dorbath, L. & Dorbath, C. (1985), 'A seismic refraction study of the crustal structure associated with the adamawa plateau and garoua rift, cameroon, west africa', *Geophysical Journal International* **81**(1), 1–12.

Svartman Dias, A. E., Hayman, N. W. & Lavier, L. L. (2016), 'Thinning factor distributions viewed through numerical models of continental extension', *Tectonics* **35**(12), 3050–3069.

Szwillus, W., Afonso, J. C., Ebbing, J. & Mooney, W. D. (2019), 'Global crustal thickness and velocity structure from geostatistical analysis of seismic data', *Journal of Geophysical Research: Solid Earth* **124**(2), 1626–1652.

Tchouankoue, J. P., Wambo, N. A. S., Dongmo, A. K. & Li, X.-H. (2014), '40ar/39ar dating of basaltic dykes swarm in western cameroon: Evidence of late paleozoic and mesozoic magmatism in the corridor of the cameroon line', *Journal of African Earth Sciences* **93**, 14–22.

Telford, W. M., Geldart, L. P. & Sheriff, R. E. (1990), *Applied geophysics*, Cambridge university press.

Thébault, E. & Vervelidou, F. (2015), 'A statistical spatial power spectrum of the earth's lithospheric magnetic field', *Geophysical Journal International* **201**(2), 605–620.

Tokam, A.-P. K., Tabod, C. T., Nyblade, A. A., Julia, J., Wiens, D. A. & Pasyanos, M. E. (2010), 'Structure of the crust beneath cameroon, west africa, from the joint inversion of rayleigh wave group velocities and receiver functions', *Geophysical Journal International* **183**(2), 1061–1076.

Toteu, S., Van Schmus, W., Penaye, J. & Michard, A. (2001), 'New u–pb and sm–nd data from north-central cameroon and its bearing on the pre-pan african history of central africa', *Precambrian Research* **108**(1-2), 45–73.

Toteu, S., Van Schmus, W., Penaye, J. & Nyobe, J. (1994), 'U[U+E5F8] pb and sm[U+E5F8] n edvidence for eburnian and pan-african high-grade metamorphism in cratonic rocks of southern cameroon', *Precambrian research* **67**(3-4), 321–347.

Uieda, L., Barbosa, V. C. & Braitenberg, C. (2016), 'Tesseroids: Forward-modeling gravitational fields in spherical coordinates', *Geophysics* **81**(5), F41–F48.

Weatherill, G. & Burton, P. W. (2009), 'Delineation of shallow seismic source zones using k-means cluster analysis, with application to the aegean region', *Geophysical Journal International* **176**(2), 565–588.

Zingerle, P., Pail, R., Gruber, T. & Oikonomidou, X. (2020), 'The combined global gravity field model xgm2019e', *Journal of Geodesy* **94**(7), 1–12.

Zoback, M. L. & Mooney, W. D. (2003), 'Lithospheric buoyancy and continental intraplate stresses', *International Geology Review* **45**(2), 95–118.

Acknowledgments

I extend my heartfelt gratitude to my outstanding supervisor, Prof. Dr. Jörg Ebbing, whose rigorous scientific approach, patient leadership, and thoughtful guidance have made him the ideal mentor throughout this journey. I am deeply grateful for the incredible opportunity you have provided, for your unwavering support during my immigration challenges. I could not have expected a better Doktorvater, than you. I also express my sincere appreciation to Prof. Dr. Albert Eyike for introducing me to you.

I gratefully acknowledge the Deutsche Forschungsgemeinschaft (DFG, German Research Foundation)- 441292957 for funding this project.

I am deeply thankful to my home country for authorizing me to pursue my PhD abroad. Special thanks to:
- Mr. Joseph Le, Minister of the Public Service,
- Dr. Madeleine Tchuinte, Minister of Scientific Research and Innovations,
- Dr. Victor Hell, General Manager of the Institute for Mining and Geological Research, and
- Dr. Ateba Bekoa, Chief of the Center for Geophysical and Vulcanological Research.

My sincere thanks go to Dr. Wolfgang Szwillus and Dr. Peter Haas for their technical support during the early stages of my coding journey, for engaging discussions, collaborative spirit, and the enjoyable moments we shared throughout my PhD.

I extend my sincere gratitude to the esteemed members of the committee, Prof. Dr. Christian Winter, Prof. Dr. Thomas Meier, Prof. Dr. Carla Braitenberg, and Prof. Dr. Jörg Ebbing, for accommodating your schedules and kindly agreeing to evaluate my work on this date.

I am also deeply appreciative of the administrative support provided by the CAU International Center. My deep gratitude to Dr. Nancy Smith for her persistence and efforts in resolving immigration office issues, ensuring a smooth transition for me.

Many thanks to Dr. Mareen Lösing and Prof. Dr. Henriette Sudhaus for organizing my arrival in Kiel during the challenging period of the Covid-19 pandemic.

To all my colleagues in Ebbing's Group, especially Dr. Agnes Dakota, Dr. Dilixiati Yixiati, and Dr. Isaac Ran, I am truly thankful for your assistance and camaraderie.

A special thank you to Mrs. Vanessa Nana, who facilitated communication with the Cameroonian administration during my absence, ensuring seamless administrative processes.

Finally, I am profoundly grateful to my siblings and parents, the Fosso family, as well as the Sudhaus family of Felm, for their unwavering support and encouragement throughout this journey.

Estelle Eric Fosso Teguia M.
Kiel, January 2025